

# Local unitarity: cutting raised propagators and localising renormalisation

Zeno Capatti,<sup>a</sup> Valentin Hirschi<sup>b</sup> and Ben Ruijl<sup>a</sup>

<sup>a</sup>*Department of Physics, ETH Zürich,  
Rämistrasse 101, 8092 Zürich, Switzerland*

<sup>b</sup>*Department of Theoretical Physics, CERN,  
Espl. des Particules 1, 1211 Meyrin, Switzerland*

*E-mail:* [zeno.ca@gmail.com](mailto:zeno.ca@gmail.com), [valentin.hirschi@gmail.com](mailto:valentin.hirschi@gmail.com),  
[benruyl@gmail.com](mailto:benruyl@gmail.com)

**ABSTRACT:** The Local Unitarity (LU) representation of differential cross-sections locally realises the cancellations of infrared singularities predicted by the Kinoshita-Lee-Nauenberg theorem. In this work we solve the two remaining challenges to enable practical higher-loop computations within the LU formalism. The first concerns the generalisation of the LU representation to graphs with raised propagators. The solution to this problem results in a generalisation of distributional Cutkosky rules. The second concerns the regularisation of ultraviolet and spurious soft singularities, solved using a fully automated and local renormalisation procedure based on Bogoliubov's  $R$ -operation. We detail an all-order construction for the hybrid  $\overline{\text{MS}}$  and On-Shell scheme whose only analytic input is single-scale vacuum diagrams. We validate this novel technology by providing (semi-)inclusive results for two multi-leg processes at NLO, study limits of individual supergraphs up to N3LO and present the first physical NNLO cross-sections computed fully numerically in momentum-space, namely for the processes  $\gamma^* \rightarrow jj$  and  $\gamma^* \rightarrow t\bar{t}$ .

**KEYWORDS:** Automation, Higher-Order Perturbative Calculations, Renormalization and Regularization, Scattering Amplitudes

ARXIV EPRINT: [2203.11038](https://arxiv.org/abs/2203.11038)

---

**Contents**

<b>1</b>	<b>Introduction</b>	<b>1</b>
<b>2</b>	<b>Local Unitarity in the presence of raised propagators</b>	<b>2</b>
2.1	Local Unitarity for raised propagators (residue theorem approach)	3
2.1.1	Local Unitarity representation	8
2.2	Interference diagrams (distributional approach)	10
2.2.1	Generalised cutting rules	10
2.2.2	Example of application of the generalised cutting rules	12
2.3	Generalised cutting rules and truncated Green's functions	13
<b>3</b>	<b>The <math>R</math>-operation</b>	<b>15</b>
3.1	The $R$ -operation master formula	16
3.2	Constraints on the renormalisation operator $K$	18
3.3	IR-finiteness of the UV forest	19
<b>4</b>	<b>Subtraction operators</b>	<b>21</b>
4.1	The UV subtraction operator	21
4.2	Spurious soft divergences	23
4.2.1	Subtraction of spurious soft singularities	25
4.2.2	Embedding spurious soft subtraction within the UV $R$ -operation	27
4.3	On-shell counterterms for massive fermions	30
4.4	Summary: the $\mathbf{T}$ subtraction operator	31
<b>5</b>	<b>Localised renormalisation</b>	<b>33</b>
5.1	Integrated counterterms	34
5.1.1	Integrated UV counterterms	34
5.1.2	Integrated spurious soft subtraction counterterms	35
5.1.3	Integrated OS counterterms	36
5.2	Localised renormalisation in the hybrid $\overline{\text{MS}}$ + OS scheme	37
5.2.1	Field and coupling renormalization in the $\overline{\text{MS}}$ scheme	37
5.2.2	Summary: the $\bar{K}$ operator	39
5.2.3	Mass and gauge field renormalisation in the OS scheme	39
<b>6</b>	<b>Results</b>	<b>40</b>
6.1	Inclusive NNLO cross-section of $\gamma^* \rightarrow jj$ and $\gamma^* \rightarrow t\bar{t}$	41
6.2	Semi-inclusive NLO cross-section of $e^+e^- \rightarrow \gamma \rightarrow jjj$	48
6.3	(Semi-)inclusive NLO cross-section of $e^+e^- \rightarrow \gamma \rightarrow t\bar{t}H$	51
6.4	Numerical tests of the local UV subtraction of a three-loop nested self-energy	53
<b>7</b>	<b>Conclusion</b>	<b>55</b>

<b>A</b>	<b>Example application of the <math>R</math>-operation</b>	<b>56</b>
<b>B</b>	<b>Code performance and example of specific supergraphs up to N3LO</b>	<b>60</b>
B.1	Numerical tests of local LU cancellations on IR limits	64
<b>C</b>	<b>Dual number representations and efficient computation of derivatives</b>	<b>68</b>
C.1	Solving the distributional rules	71
C.2	Example use of multi-variate duals to compute partial derivatives	72

---

## 1 Introduction

The lack of clear evidence for physics beyond the SM within our current collider observations pushes High-Energy Physics into the high-intensity frontier and ushers in the Precision Era. In the context of hadronic collisions, one obstacle to precise comparisons between theory and experiment, is the limited accuracy of theoretical predictions. This limitation is for a large part driven by our (in)ability to compute higher-order corrections in the perturbative expansion of QFT coupling constants, which is made especially severe by the strength of QCD interactions.

This problem is well-studied, and several decades of efforts from the theoretical community have managed to postpone the point at which theoretical uncertainties of fixed-order origin become the main limitation to our ability to interpret collider data. Historically, and especially during the LEP era, these efforts have mostly pursued a fully analytical approach to the computation of (semi-)inclusive cross-sections. With the advent of parton showers and the need for supporting ever more complicated differential observables, phase-space integrals quickly became predominantly computed numerically, using slicing and/or subtraction approaches for regularising IR singularities [1–11]. Then, at NLO, the reduction of one-loop amplitudes also transitioned to numerical methods as soon as stable and fast numerical reduction algorithms became available [12–15]. Nowadays, traditional multi-loop computations welcome increasingly more numerical aspects, for example for the reduction through numerical reconstruction over finite fields [16–20], or solutions of systems of differential equations [21, 22] through series expansions [23–25], or also by direct numerical computation of amplitudes in momentum space [26–32].

This slow-moving transition to numerics still maintains the historical divide of the task of computing phase-space and loop integrals, with the important consequence that IR singularities must be regularised separately within each of these two classes of integrals. One notable exception is the method of reverse unitarity [33–36] since it turns phase-space integrals into loop ones in order to compute both together analytically. Although applications of reverse unitarity provided important N3LO fixed-order cross-sections for  $2 \rightarrow 1$  processes [37–42], it is as of now not possible to generalise this approach to higher multiplicity processes and arbitrary differential observables.

In general, the separate treatment of loop and phase-space integrals cannot take advantage of the inherent simplicity of the IR cancellation pattern featured in the proof of the KLN theorem [43–45]. Motivated by this realisation, we focused on establishing a fundamentally different framework for the computation of differential cross-sections whereby IR singularities cancel locally, without any subtraction procedure. We refer to the resulting formulation of the differential cross-section as its LU expression and we recently published its detailed construction in ref. [46], as well as the proof that it is free of any final-state IR singularities at any perturbative order and for any IR-safe observable. We also point the reader to the proceedings of ref. [47] for a more concise summary of LU. The objective of this construction is two-fold. First, we aim at discovering new theoretical aspects of perturbative expansions at fixed order in QFT, and with a particular attention towards new techniques for matching them to a (parton shower) resummation. Second, we want to apply the LU construction in order to build a competitive tool for the fully numerical computation of predictions of arbitrary collider observables.

In this work we address two key remaining challenges for practical higher-loop computations using LU. The first challenge is the identification of a universal treatment of raised propagators introduced from self-energy insertions that is more convenient than the procedure introduced in ref. [46]. The new treatment involves taking higher-order residues, which results in derivatives of amplitudes that are efficiently and automatically computed. The second challenge is the treatment of UV divergences. We use Bogoliubov’s  $R$ -operation and construct local UV subtraction terms that render any amplitude of any order UV-finite. We then modify our subtraction terms so as to also subtract spurious soft singularities and also automatically reproduce the OS mass renormalisation conditions. Next, we determine integrated level counterterms, consisting of only single-scale massive vacuum graphs, which are defined such that we obtain results directly renormalised in the commonly used hybrid  $\overline{\text{MS}}$  and OS scheme.

We validate this novel technology by providing (semi-)inclusive results for  $e^+e^- \rightarrow \gamma^* \rightarrow jjj$  and  $e^+e^- \rightarrow \gamma \rightarrow t\bar{t}H$  at NLO and the first physical cross-sections at NNLO fully computed in momentum-space, namely for processes  $\gamma^* \rightarrow d\bar{d}$  and  $\gamma^* \rightarrow t\bar{t}$ . We also verify the correct subtraction of IR and UV limits of specific individual supergraphs contributing up to N3LO.

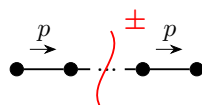
The outline of this work is as follows. We present the LU construction in presence of raised propagators in section 2. In section 3 we construct the  $R$ -operation for UV subtraction in LU. Next, we construct local counterterms for subtracting UV and spurious IR singularities in section 4. In section 5, we construct the integrated counterterms so as to automatically produce results renormalised in the hybrid  $\overline{\text{MS}}$  and OS scheme. In section 6 we provide numerical results supporting the validity of our construction. Finally, we present our conclusion in section 7.

## 2 Local Unitarity in the presence of raised propagators

Perturbative cross-sections generally include the effect of self-energy corrections to particles participating in the process. Diagrammatically, self-energy corrections amount to the in-

sertion of a 1PI graph on an edge which, in turn, results in a doubling of the edge itself. Repeated edges correspond to (raised) propagators with powers higher than one after substituting the Feynman rules. As the LU representation requires taking residues stemming from propagator poles, the question then arises of what is the correct residue-taking procedure in the case of raised propagators. This question has already been studied within the context of the LTD representation of Feynman integrals in ref. [48], and more recently for particular types for a single nested self-energy in ref. [49], together with its interplay with mass renormalisation. We are interested here in generalising these considerations and understanding how they fit in within LU. Ordinary Cutkosky rules, for example, cannot account for the correct contribution. Moreover, one wonders what is the effect of taking residues of such raised propagators on the local IR cancellations guaranteed by the LU representation.

The discussion of and solution to this problem, given in the proof of ref. [46] is correct, but difficult to apply in practice and is opaque in its interpretation. The underlying idea is that the LU representation associated with a forward-scattering diagram with raised propagators should equal the LU representation of the same forward-scattering diagram in which fictitious momenta are introduced to eliminate raised propagators, and only at the end the limit to zero of such fictitious momenta is taken. While convenient for the purpose of the proof, taking limits numerically is notoriously cumbersome, and we seek a more direct expression of the LU representation in the presence of raised propagators. In other words, we wish to identify the correct generalisation of the Cutkosky rule which yields the right expression when taking the cut of a repeated edge, that is:



In this section, we will show how to achieve this. Such a generalisation of the LU representation is based on a conceptual understanding of the relationship between raised propagators and the residue formula for higher-order poles. This, in turn, provides a clear candidate for the generalisation of the Cutkosky distributional rule.

Our discussion will leverage many of the key results presented in ref. [46], as well as employ a similar notation. We therefore refer the reader to that work for more details on the quantities manipulated in this section. We also refer the reader to ref. [50] for a comprehensive review of the modern treatment of IR singularities and to refs. [51–53] for a recent and original approach to the topic of Cutkosky cuts and cutting rules in general. The reader only interested in the final expression for the generalised cutting rules applicable to raised propagators can proceed to section 2.2.

### 2.1 Local Unitarity for raised propagators (residue theorem approach)

We now give a summary of the LU representation. Let us start with a three-dimensional representation  $f_{3d}(G)$  of a graph  $G$ . In the following, we will call  $G$  a supergraph, in anticipation of it being identified with the parent diagram from which interference diagrams are constructed. One may use LTD [54–57], cLTD [31, 53, 58, 59] or TOPT [60–63] to obtain

such a three-dimensional representation from the four-dimensional one, since the three formulations are locally equivalent. In other words, these local representations are just different mathematical expressions of the same integrand, which is obtained from the sum over all residues arising when considering the integration over the energy components of all loop momenta. Importantly, this also implies that the physical threshold structure coincides in all three representations. We note that LTD, or rather the closely related Feynman-Tree Theorem [64, 65], has recently been used [66] in the context of a Parton Shower Monte Carlo program, also in order to more easily characterise and address IR divergences.

Assume that  $G$  is a connected supergraph, corresponding to a couplet  $G = (\mathbf{v}, \mathbf{e} = \mathbf{e}_{\text{ext}} \cup \mathbf{e}_{\text{int}})$ , where  $\mathbf{v}$  is the set of vertices of the graph and  $\mathbf{e}$  is the set of edges. We assign to the external, on-shell, particles the edges in  $\mathbf{e}_{\text{ext}} = \mathbf{a}_{\text{in}} \cup \mathbf{a}_{\text{out}}$ . The particles in  $\mathbf{a}_{\text{in}}$  are incoming and those in  $\mathbf{a}_{\text{out}}$  are outgoing, and the sign of their on-shell energy is fixed accordingly. For forward-scattering diagrams,  $G$  has the same incoming and outgoing particles, and each incoming particle has an outgoing partner with same momentum. We define the reduced graph  $G_r = (\mathbf{v}, \mathbf{e}, \boldsymbol{\gamma})$  to be the graph where each edge  $e$  of  $G$  with  $\gamma_e$  occurrences is fused into one representative in  $G_r$  raised to power  $\gamma_e$ . From here on, any graph quantity will refer to the reduced graph rather than the original graph. Any threshold of the three-dimensional representation of the supergraph can be associated to a connected subgraph identified by the set of vertices  $\mathbf{s} \subset \mathbf{v}$  (the subgraph is identified from the graph by the set  $\mathbf{s}$  and the collection of the edges of the original graph whose vertices are in  $\mathbf{s}$ ). Let  $\mathcal{E}$  be the collection of all such connected subgraphs. The implicit equation defining the location of each of such thresholds is the support of the function  $\eta_{(\mathbf{s}, \alpha)}$ , defined by

$$\eta_{(\mathbf{s}, \alpha)} = \sum_{e \in \delta(\mathbf{s}) \cap \mathbf{a}_{\text{in}}} E_e - \sum_{e \in \delta(\mathbf{s}) \cap \mathbf{a}_{\text{out}}} E_e - \alpha \sum_{e \in \delta(\mathbf{s}) \setminus \mathbf{e}_{\text{ext}}} E_e = 0, \quad (2.1)$$

where  $E_e = \sqrt{|\vec{p}_e|^2 + m_e^2}$  is the on-shell energy associated to the particular edge  $e$  carrying the spatial momentum  $\vec{p}_e$ ,  $\alpha \in \{\pm 1\}$ , and  $\delta(\mathbf{s}) = \{e = \{v, v'\} \in \mathbf{e} \mid v \in \mathbf{s}, v' \in \mathbf{v} \setminus \mathbf{s}\}$  denotes the collection of all edges that are at the boundary of the subgraph identified by the set  $\mathbf{s} \subset \mathbf{v}$ . When momentum conservation conditions are assumed to hold on external particles, we have that  $\eta_{(\mathbf{s}, \alpha)} = -\eta_{(\mathbf{v} \setminus \mathbf{s}, -\alpha)}$ . Instead,  $\eta_{(\mathbf{s}, \alpha)}$  and  $\eta_{(\mathbf{s}, -\alpha)}$  correspond in general to different thresholds. In light of this definition, the thresholds can be classified into four categories based on specific properties of  $\mathbf{s}$ . We list below the precise definition of these categories and give diagrammatic representatives of each category in figure 1:

- s-channel: if  $\delta(\mathbf{s}) \cap \mathbf{e}_{\text{ext}} = \mathbf{a}_{\text{in}}$  or  $\delta(\mathbf{s}) \cap \mathbf{e}_{\text{ext}} = \mathbf{a}_{\text{out}}$ . We then write that  $(\mathbf{s}, 1) \in \mathcal{E}_{\text{s-ch}}^{+, \text{in}}$ ,  $(\mathbf{s}, -1) \in \mathcal{E}_{\text{s-ch}}^{-, \text{in}}$ , in the first case and  $(\mathbf{s}, 1) \in \mathcal{E}_{\text{s-ch}}^{+, \text{out}}$ ,  $(\mathbf{s}, -1) \in \mathcal{E}_{\text{s-ch}}^{-, \text{out}}$  in the second. Because of the equivalence  $\eta_{(\mathbf{s}, \alpha)} = -\eta_{(\mathbf{v} \setminus \mathbf{s}, -\alpha)}$ , we set  $\mathcal{E}_{\text{s-ch}}^+ = \mathcal{E}_{\text{s-ch}}^{+, \text{in}} = \mathcal{E}_{\text{s-ch}}^{-, \text{out}}$  and  $\mathcal{E}_{\text{s-ch}}^- = \mathcal{E}_{\text{s-ch}}^{-, \text{in}} = \mathcal{E}_{\text{s-ch}}^{+, \text{out}}$ . Observe that, if the initial-state particles have energies larger than zero, any surface in  $\mathcal{E}_{\text{s-ch}}^-$  is empty, i.e. eq. (2.1) has no solution.
- t-channel: if  $\delta(\mathbf{s}) \cap \mathbf{a}_{\text{in}} \neq \emptyset$ ,  $\mathbf{a}_{\text{in}}$  and  $\delta(\mathbf{s}) \cap \mathbf{a}_{\text{out}} \neq \emptyset$ ,  $\mathbf{a}_{\text{out}}$ . Such thresholds are generally non empty for both  $\alpha = 1$  and  $\alpha = -1$ .

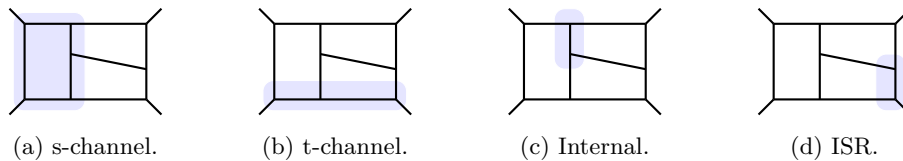


**Figure 1.** Pictorial representation of thresholds for a  $2 \rightarrow 2$  diagram. Highlighted in blue are the vertex sets  $\mathbf{s}$ , corresponding to subgraphs of the original graph. The complement of each subgraph corresponds to a threshold of the same type.

- internal-like: if  $\delta(\mathbf{s}) \cap \mathbf{e}_{\text{ext}} \in \{\emptyset, \mathbf{e}_{\text{ext}}\}$ . The locus of such singularities can only be a soft location, when all the particles in  $\delta(\mathbf{s})$  are massless. For these thresholds, it also holds that  $\eta_{(\mathbf{s}, \alpha)} = -\eta_{(\mathbf{s}, -\alpha)}$ .
- ISR-like: if it is not s-channel, t-channel or internal-like.

For what concerns this paper and ref. [46] (which focuses on FSR singularities), a Cutkosky cut is a connected subgraph of the supergraph  $\mathbf{s}$  such that either  $\delta(\mathbf{s}) \cap \mathbf{e}_{\text{ext}} = \mathbf{a}_{\text{in}}$  or  $\delta(\mathbf{s}) \cap \mathbf{e}_{\text{ext}} = \mathbf{a}_{\text{out}}$ . That is, each Cutkosky cut is in one-to-one correspondence with s-channel thresholds in  $\mathcal{E}_{\text{s-ch}}^+$ . Alternatively, the Cutkosky cut can be denoted by the set  $\mathbf{c}_{\mathbf{s}} = \delta(\mathbf{s}) \setminus \mathbf{e}_{\text{ext}}$ . Generalisations of the notion of Cutkosky cuts can be used to also include t-channel or ISR cuts [67].

In the following, we will assume that  $\mathcal{E} = \mathcal{E}_{\text{s-ch}}^+ \cup \mathcal{E}_{\text{s-ch}}^- \cup \mathcal{E}_{\text{int}}$ . For the purposes of IR finiteness, this is equivalent to assuming that there is no t-channel or ISR-like singularity, which is the assumption that we will consider in this paper, for simplicity. This assumption is manifestly true for two-point functions, due to  $\mathbf{a}_{\text{in}}$  and  $\mathbf{a}_{\text{out}}$  each having one element only.

Alternatively, one can prove local IR-finiteness of the LU representation in the complete phase-space minus small volumes around the location of t-channel and ISR-like singularities: this is the strategy that was used in ref. [46]. ISR-like and t-channel singularities would traditionally be handled within the parton model paradigm and using a factorisation approach.

The three-dimensional representation of the supergraph can be written as

$$f_{3\text{d}}(G_{\text{r}}) = \frac{g(\vec{k})}{\prod_{e \in \mathbf{e}} E_e^{\beta_e} \prod_{\mathbf{s} \in \mathcal{E}_{\text{s-ch}}^+} \eta_{\mathbf{s}}^{\beta_{\mathbf{s}}} \prod_{\mathbf{s} \in \mathcal{E}_{\text{s-ch}}^-} \eta_{\mathbf{s}}^{\beta_{\mathbf{s}}} \prod_{\mathbf{s} \in \mathcal{E}_{\text{int}}} \eta_{\mathbf{s}}^{\beta_{\mathbf{s}}}}, \quad (2.2)$$

where  $g$  is a polynomial in the on-shell energies and spatial momenta. We stress that  $f_{3\text{d}}$  also depends on the original graph  $G$  for what concerns the expression of the numerator. We denote with  $\vec{k} = (\vec{k}_1, \dots, \vec{k}_L)$  the collection of all spatial loop momenta of the graph. In this way, we have extracted all the singularities of  $f_{3\text{d}}(G_{\text{r}})$  with their respective powers  $\beta_e$  (for the inverse energies) and  $\beta_{\mathbf{s}}$  (for the thresholds), which can be determined in terms of the raising powers  $\gamma$  of the propagators of  $G_{\text{r}} = (\mathbf{v}, \mathbf{e}, \gamma)$ . The specific structure of  $g$  is irrelevant for what concerns the proof of cancellation of thresholds, that is the cancellation of the enhancements associated with any of the  $\eta_{\mathbf{s}}$ , for  $\mathbf{s} \in \mathcal{E}_{\text{s-ch}}^+$ . On the other hand, the structure of  $g$  is important for a rigorous proof of the integrability of soft singularities. For



this section, we will write the function  $g$  in the following manner, which is valid for any arbitrary supergraph:

$$g(\vec{k}) = \sum_{F \in \mathcal{F}} c_F(\vec{k}) \prod_{s \in \mathcal{E} \setminus F} \eta_s^{\beta_s}, \quad (2.3)$$

where  $\mathcal{F}$  is the collection of all cross-free families of connected cuts of the supergraph, with the added constraint that any subgraph in any of the families cannot be written as the union of its children (see figure 10 of ref. [46]).  $c(\vec{k})$  is a polynomial in the on-shell energies and the spatial components of the external momenta and loop momenta. This is a weak constraint on the structure of  $g$ , and stronger constraints may be formulated. Such constraint is relevant for what concerns the soft scaling of  $f_{3d}(G_r)$ , and in particular it can be used (as in ref. [46]) to show that in gauge theories the LU representation is locally IR finite unless there are spurious soft singularities (see section 4.2).

Given this, we would like to construct interference diagrams from  $f_{3d}(G_r)$ . Cutkosky's original work [68] clearly showed that interference diagrams correspond to thresholds of supergraphs, and we would like to replicate such result here, but at the local level. In order to do this, we introduce an auxiliary variable that allows us to clearly parametrise the distance of a point to any threshold. Such auxiliary variable corresponds to the group parameter of the causal flow introduced in section 3.2 of ref. [46]. In particular, since any Cutkosky cut corresponds to an s-channel threshold, let us consider a vector field  $\kappa$  such that

$$\kappa \cdot \nabla \eta_s < 0, \quad \forall \vec{k} \in \partial \eta_s, \quad \forall s \in \mathcal{E}_{s\text{-ch}}^+, \quad (2.4)$$

i.e., it has positive projection onto the outward-pointing normal to any s-channel threshold when evaluated on that threshold. Such constraint arises from the causal  $i\epsilon$  prescription, which forces  $\text{Im}[\eta_s] < 0$  (see ref. [32] for more details). Furthermore, we shall require that

$$\lim_{|q_e| \rightarrow 0} \frac{|\vec{Q}_e(\kappa)|}{E_e} < c, \quad \forall e \in \mathbf{e}, \quad (2.5)$$

where  $c$  is finite and if  $\vec{q}_e = \sum_{i=1}^L s_{ei} \vec{k}_i + \vec{p}$  for the chosen loop momentum basis, then  $\vec{Q}_e(\vec{k}) = \vec{q}_e - \vec{p}$ . Such constraint is required in order to obtain an integrable behaviour close to soft singularities. We have shown in ref. [32] that such a vector field  $\kappa$  always exists for *any* given graph and we described a deterministic procedure that allows one to generically construct it. In the same reference, we have also shown that for any two-point graph with a massive external four-momentum set in its rest-frame, a simple and valid choice of vector field  $\kappa$  is given by

$$\kappa_{2p} = -\lambda \vec{k}, \quad \lambda \in (0, 1]. \quad (2.6)$$

In particular,  $\kappa_{2p}$  satisfies both eq. (2.4) and eq. (2.5) when the two-point graph is evaluated in the rest frame of its massive external momentum. We note that  $\kappa_{2p}$  also has the clear interpretation of being the deformation vector field needed to contour-deform the thresholds in  $\mathcal{E}_{s\text{-ch}}^+$ .

Given the vector field  $\kappa$ , we consider the following Cauchy problem

$$\begin{cases} \partial_t \phi_t = \kappa \circ \phi_t \\ \phi_0 = \vec{k} \end{cases} . \quad (2.7)$$



This Cauchy problem defines a flow  $\phi_t$ , which we call causal flow in connection with the fact that the vector field generating the flow,  $\kappa$ , satisfies the causal prescription given in eq. (2.4). For any two-point supergraph with a massive external momentum, the causal flow can be obtained in an analytic form. Indeed, in this case we can choose  $\kappa = \kappa_{2p}$  for which the ODE system has the following solution:

$$\phi_t^{2p} = e^{-\lambda t \vec{k}}. \tag{2.8}$$

The causal flow inherits a series of crucial properties from the field  $\kappa$  when interpreted as a contour deformation. First, for any given  $\vec{k}$ , the curve  $\phi_t$  satisfying eq. (2.7) intersects any of the thresholds  $\mathbf{s} \in \mathcal{E}_{\text{s-ch}}^+$  at most once, for otherwise the vector field  $\kappa$  could not flow consistently inwards of the surface defined by  $\eta_{\mathbf{s}} = 0$ , as established by eq. (2.4). Second, given the curve  $\phi_t$  for  $t \in (-\infty, \infty)$  and the unique value  $t_{\mathbf{s}}^*$  for which  $\eta_{\mathbf{s}} \circ \phi_{t_{\mathbf{s}}^*} = 0$ , we must have  $\eta_{\mathbf{s}} \circ \phi_t \approx (t - t_{\mathbf{s}}^*)$  for  $t$  approaching  $t_{\mathbf{s}}^*$ . These two key properties can be summarised as follows. Let  $\vec{k}$  be fixed and let

$$\mathcal{E}_{\text{s-ch}, \vec{k}} = \{\mathbf{s} \in \mathcal{E}_{\text{s-ch}}^+ \mid \exists t_{\mathbf{s}}^* \in (-\infty, \infty) \text{ with } \eta_{\mathbf{s}} \circ \phi_{t_{\mathbf{s}}^*} = 0\}. \tag{2.9}$$

Then the expansion of  $\eta_{\mathbf{s}} \circ \phi_t$ , for any threshold  $\mathbf{s} \in \mathcal{E}_{\text{s-ch}, \vec{k}}$  around a unique zero  $t = t_{\mathbf{s}}^*$  reads

$$\eta_{\mathbf{s}} \circ \phi_t = (t - t_{\mathbf{s}}^*) \partial_t (\eta_{\mathbf{s}} \circ \phi_t) \Big|_{t=t_{\mathbf{s}}^*} + \mathcal{O}\left((t - t_{\mathbf{s}}^*)^2\right) = (t - t_{\mathbf{s}}^*) (\kappa \cdot \nabla \eta_{\mathbf{s}}) \Big|_{\vec{k}=\phi_{t_{\mathbf{s}}^*}} + \mathcal{O}\left((t - t_{\mathbf{s}}^*)^2\right), \tag{2.10}$$

where we used the chain rule and eq. (2.7) to obtain the second equality. In particular, we observe that  $(\kappa \cdot \nabla \eta_{\mathbf{s}}) \Big|_{\vec{k}=\phi_{t_{\mathbf{s}}^*}}$  is always guaranteed to be strictly positive in virtue of eq. (2.4) and thus the expansion of  $\eta_{\mathbf{s}} \circ \phi_t$  is always guaranteed to scale linearly in  $t - t_{\mathbf{s}}^*$  close to a threshold location. In other words, any threshold  $\mathbf{s}$  with  $\beta_{\mathbf{s}} = 1$  appears as a simple pole along the causal flow lines. In turn, this means that each threshold  $\eta_{\mathbf{s}}$  with power  $\beta_{\mathbf{s}}$  appears as a pole of order  $\beta_{\mathbf{s}}$  of the integrand. Another useful way to state this same idea is the following. Consider the function

$$w_t(\vec{k}) = \prod_{\mathbf{s} \in \mathcal{E}_{\text{s-ch}, \vec{k}}} \frac{(t - t_{\mathbf{s}}^*)^{\beta_{\mathbf{s}}}}{[(\eta_{\mathbf{s}} \circ \phi_t)(\vec{k})]^{\beta_{\mathbf{s}}}}. \tag{2.11}$$

Then  $w_t$  is bounded for any  $\vec{k}$  and any  $t$ . The introduction of  $w_t$  allows us to clearly isolate the scaling behaviour of  $f_{3d}(G)$  close to a threshold:

$$f_{3d}(G_{\text{r}}) \circ \phi_t = \frac{w_t(\vec{k})}{\prod_{\mathbf{s} \in \mathcal{E}_{\text{s-ch}}^+} (t - t_{\mathbf{s}}^*)^{\beta_{\mathbf{s}}}} f \circ \phi_t, \quad f = \frac{g}{\prod_{e \in \mathbf{e}} E_e^{\beta_e} \prod_{\mathbf{s} \in \mathcal{E}_{\text{s-ch}}^-} \eta_{\mathbf{s}}^{\beta_{\mathbf{s}}} \prod_{\mathbf{s} \in \mathcal{E}_{\text{int}}} \eta_{\mathbf{s}}^{\beta_{\mathbf{s}}}}, \tag{2.12}$$

where  $f$  is an integrable function (provided  $g$  vanishes fast enough in the UV region). We are now ready to construct the LU representation generalised to the case of raised propagators. From the construction above, it is clear that  $\eta_{\mathbf{s}}$  scales like  $(t - t_{\mathbf{s}}^*)$  in the limit of  $t \rightarrow t_{\mathbf{s}}^*$ . Thus, if a threshold  $\eta_{\mathbf{s}}$  itself appears raised to a power  $\beta_{\mathbf{s}}$  within  $f_{3d}(G)$ , that threshold corresponds to a pole in the variable  $t$  of order  $\beta_{\mathbf{s}}$  of the function  $f_{3d}(G) \circ \phi_t$ . Cutkosky

cuts that intersect any propagator raised to a power larger than one then correspond to higher-order residues in the variable  $t$  of the LU representation of the supergraph.

Finally, we observe that the construction of the Local Unitarity representation from a three-dimensional representation of the supergraph implies that all interference diagrams arising from the same supergraph share the same numerator (given as a function of four-momenta). This would not be the case if we had constructed interference diagrams from the S-matrix by summing over only the physical degrees of freedom of the final state gluons, i.e. using covariantly-gauge-fixed propagators and thus not considering external ghosts. Such construction would break the *local* cancellation pattern of LU. Instead, we choose to treat internal propagators in the Feynman gauge and we sum over all, physical and unphysical, polarisations of final state gluons, and thus also include external ghosts. In such a setup, interference diagrams arising from the same underlying supergraph all share the same numerator and the cancellation of IR singularities take place locally as prescribed by LU. Notice that the same setup is also what allows one to diagrammatically prove unitarity at the integrated level.

### 2.1.1 Local Unitarity representation

We are now ready to write the LU representation for  $f_{3d}(G)$ , generalised to the case of  $\beta_s \geq 1$  by a straightforward application of the residue formula:

$$\sigma_d^G(\vec{k}) = \sum_{\mathbf{s} \in \mathcal{E}_{s\text{-ch}, \vec{k}}} \frac{1}{(\beta_s - 1)!} \lim_{t \rightarrow t_s^*} \frac{d^{\beta_s - 1}}{dt^{\beta_s - 1}} \left[ (t - t_s^*)^{\beta_s} (f_{3d}(G_r) \circ \phi_t) f_s(\mathcal{O}) \mathbb{J}[\phi_t] h(t) \right], \quad (2.13)$$

for a given normalised function  $h(t)$ .  $\mathbb{J}[\phi_t]$  is the Jacobian of the causal flow  $\phi$  with respect to the variables  $\vec{k}$  (for more details on  $h(t)$  and  $\mathbb{J}[\phi_t]$ , we refer the reader to ref. [46]).  $f_s(\mathcal{O})$  is a final-state density that measures the value of an observable  $\mathcal{O}$ . From  $\sigma_d$  we obtain the LU representation for the contribution from the supergraph  $G$  to any differential cross-section

$$\frac{d\sigma^G}{d\mathcal{O}} = \int \left[ \prod_{i=1}^L \frac{d\vec{k}_i}{(2\pi)^3} \right] \sigma_d^G(\vec{k}). \quad (2.14)$$

We already mentioned that eq. (2.13) could in principle be obtained from its analogue presented in ref. [46] by first assigning fictitious momenta to the raised propagators, then computing the LU representation, and finally sending such fictitious momenta to zero. Let us perform this exact procedure.

The fictitious momenta that we plan to introduce can be added to propagators before the integration of the energy components of loop momenta or to the thresholds after the integration of the energies. The simplest path to the result is that of introducing them after the integration over the energy components. Let us start then with the integrand

$$f_{3d}(G_r) = \int \left[ \prod_{i=1}^L \frac{dk_i^0}{(2\pi)} \right] \frac{N}{\prod_{e \in \mathbf{e}} (q_e^2 - m_e^2 + i\epsilon)^{\gamma_e}} = \frac{f}{\prod_{\mathbf{s} \in \mathcal{E}_{s\text{-ch}}^+} \eta_s^{\beta_s}}, \quad (2.15)$$

On the right-hand side, we explicitly performed the integration of energy components and made explicit the dependence on non-empty s-channel thresholds only. For two-point supergraphs,  $f$  is only singular at soft points but it is integrable ( $f$  is defined in eq. (2.12)).

We now introduce fictitious shifts to the surfaces  $\eta_{\mathbf{s}}$ . In particular, consider the threshold

$$\eta_{\mathbf{s}i} = \eta_{\mathbf{s}} + p_{\mathbf{s}i}^0, \quad i = 1, \dots, \beta_{\mathbf{s}}, \quad (2.16)$$

where  $p_{\mathbf{s}i}^0$  are real constants, and  $p_{\mathbf{s}1}^0 = 0$ . The dependence of  $\eta_{\mathbf{s}i}$  on the index  $i$  is fully contained in the fictitious shift  $p_{\mathbf{s}i}^0$ . Setting  $\eta_{\mathbf{s}i}$  to zero gives the implicit equation for a level surface of  $\eta_{\mathbf{s}}$ . Then, we can write eq. (2.15) as a limit of a quantity with no raised propagator

$$\tilde{f}_{3d}(G_r) = \frac{f}{\prod_{\mathbf{s} \in \mathcal{E}_{\text{s-ch}}^+} \prod_{i=1}^{\beta_{\mathbf{s}}} \eta_{\mathbf{s}i}}, \quad f_{3d} = \lim_{\{p_{\mathbf{s}i}^0\} \rightarrow 0} \tilde{f}_{3d}. \quad (2.17)$$

The LU representation associated with the function of which we are taking the limit now only involves single poles. Furthermore, if the shifts  $p_{e_j}^0$  are small enough, then the causal flow for the thresholds eq. (2.16) can be set to be the same as the causal flow for the thresholds with shifts set to zero. Let  $\phi_t$  be such a causal flow. We will exchange the limiting procedure associated with the Local Unitarity representation with that associated with the fictitious momenta going to zero. We now consider the value of  $\tilde{f}_{3d}$  along the flow lines identified by  $\phi_t$ , and cast it into a form analogous to eq. (2.12),

$$\tilde{f}_{3d} \circ \phi_t = \frac{(f \circ \phi_t) w_t}{\prod_{\mathbf{s} \in \mathcal{E}_{\text{s-ch}}^+} \prod_{i=1}^{\beta_{\mathbf{s}}} (t - t_{\mathbf{s}i}^*)}, \quad w_t = \prod_{\mathbf{s} \in \mathcal{E}_{\text{s-ch}}^+} \prod_{i=1}^{\beta_{\mathbf{s}}} \frac{(t - t_{\mathbf{s}i}^*)}{\eta_{\mathbf{s}i}}. \quad (2.18)$$

where  $t_{\mathbf{s}i}^*$  is the solution in  $t$  of the equation  $\eta_{\mathbf{s}i} \circ \phi_t = 0$ . Because of the way we introduced the fictitious shifts, it is straightforward to determine the one-to-one relation between  $t_{\mathbf{s}i}^*$  and  $p_{\mathbf{s}i}^0$ ,

$$p_{\mathbf{s}i}^0(t_{\mathbf{s}i}^*) = -\eta_{\mathbf{s}} \circ \phi_{t_{\mathbf{s}i}^*}, \quad (2.19)$$

which is also invertible for small  $p_{\mathbf{s}i}^0$ . We are ready to construct the LU representation for  $\tilde{f}_{3d}$ .  $\tilde{f}_{3d}$  now only features simple poles in  $t$ , and we can directly use the formula from ref. [46]. Let us focus, in particular, on the sum of all residues obtained by fixing  $\mathbf{s}$  and varying  $i$ ; from this result, after summing over all thresholds  $\mathbf{s}$ , we will directly obtain the desired result of eq. (2.13). We have

$$\tilde{\sigma}_{\mathbf{s}} = \sum_{i=1}^{\beta_{\mathbf{s}}} \lim_{t \rightarrow t_{\mathbf{s}i}^*} (t - t_{\mathbf{s}i}^*) \tilde{f}_{3d} \circ \phi_t = \sum_{i=1}^{\beta_{\mathbf{s}}} \frac{y_{\mathbf{s},i}}{\prod_{\substack{j=1 \\ j \neq i}}^{\beta_{\mathbf{s}}} (t_{\mathbf{s}i}^* - t_{\mathbf{s}j}^*)}, \quad y_{\mathbf{s},i} = \lim_{t \rightarrow t_{\mathbf{s}i}^*} \prod_{\substack{j=1 \\ j \neq i}}^{\beta_{\mathbf{s}}} (t - t_{\mathbf{s}j}^*) \tilde{f}_{3d}. \quad (2.20)$$

The expression on the right-hand-side of eq. (2.20) is a divided difference in the variables  $t_{\mathbf{s}1}^*, \dots, t_{\mathbf{s}\beta_{\mathbf{s}}}^*$  (see analogous discussion in section 2.2 of ref. [31]). Finally, we take the limit of all shifts  $p_{\mathbf{s}i}^0$  going to zero. Observe that eq. (2.19) shows that the limit of  $p_{\mathbf{s}i}$  going to zero is equivalent to the limit of  $t_{\mathbf{s}i}^*$  going to  $t_{\mathbf{s}}^*$ . We then have

$$\lim_{\{p_{\mathbf{s}i}^0\}_{i \rightarrow 0}} \tilde{\sigma}_{\mathbf{s}} = \lim_{t \rightarrow t_{\mathbf{s}}^*} \frac{1}{(\beta_{\mathbf{s}} - 1)!} \frac{d^{\beta_{\mathbf{s}} - 1}}{dt^{\beta_{\mathbf{s}} - 1}} (t - t_{\mathbf{s}}^*)^{\beta_{\mathbf{s}}} f_{3d}(G_r), \quad (2.21)$$

obtained directly from the application of divided differences. Eq. (2.21) finalises our argument supporting the explicit LU expression of eq. (2.13). It shows that the correct way to

interpret Cutkosky cuts that go through raised propagators is that of higher-order residues in the variable that is used to approach the corresponding threshold.

The overarching argument that directly guides the construction of eq. (2.13) is that interference diagrams are weighted residues of a parent diagram, the supergraph. Very much related to this principle is that of IR-finiteness. The KLN cancellation pattern exhibited here and in ref. [46] is a direct consequence of the pattern of divided differences that arises from taking different residues of one single integrand.

In particular, we stress that the local FSR-finiteness of  $\sigma_d$  as defined in eq. (2.13) is guaranteed by the work of ref. [46] since we constructed eq. (2.13) as a specific limit of the LU formula of ref. [46]. This implies that there is a deep relationship between higher-order poles, the derivatives that are needed to compute their residues and local IR-finiteness.

## 2.2 Interference diagrams (distributional approach)

Although the LU expression of eq. (2.13) is compact and well-suited to prove its FSR-finiteness, it is difficult to use it in practice because it requires explicitly taking a limit in  $t$  of a function. It is much easier then, to construct the integrand *after* that limit has been taken. In particular, we will show now that it is possible to obtain eq. (2.13) starting from interference diagrams directly, and finding the correct distributional cutting rules for raised propagators. Because we started motivating eq. (2.13) with the three-dimensional representation of a Feynman diagram with raised propagators, we can already anticipate that these cutting rules involve derivatives in the energy components of the loop momenta of the supergraph. It is also manifest from eq. (2.13) that these cutting rules should ultimately also involve derivatives in the  $t$  variable.

### 2.2.1 Generalised cutting rules

We start by defining a distribution whose action on a test function gives the divided differences of the test function  $f$  at given loci  $x_1, \dots, x_n$ . It is defined by recursion as

$$\delta[x - x_1, \dots, x - x_n] = \frac{\delta[x - x_2, \dots, x - x_n] - \delta[x - x_1, \dots, x - x_{n-1}]}{x_n - x_1}, \quad \delta[x] = \delta(x). \tag{2.22}$$

We can then define a new distribution  $\delta^{(n)}[x]$  as the limit of that in eq. (2.22) when  $x_i = x_j$  for any  $i$  and  $j$ . In this limit both the denominator and numerator of eq. (2.22) vanish.

$$\delta^{(n)}[x] = \lim_{\{x_i\}_{i=1}^n \rightarrow 0} \delta[x - x_1, \dots, x - x_n]. \tag{2.23}$$

Carrying out the distributional limit, we have that the action of  $\delta^{(n+1)}[x]$  produces the  $n$ -th coefficient of the Taylor expansion of  $f$ ,

$$\int dx \delta^{(n+1)}[x] f(x) = \frac{1}{n!} \left. \frac{d^n f}{dx^n} \right|_{x=0}, \tag{2.24}$$

that is, the effect of  $\delta^{(n)}[x]$  is to compute the  $n$ -th derivative of the test function divided by the factorial of  $n$ . We observe that  $\delta^{(n)}[x]$  does not correspond to the usual definition of a

derivative of a Dirac delta function. Instead,  $\delta^{(n)}[x]$  implements divided differences of the test function  $f$ , in the limit of all the variables defining the divided difference converging to the same value. This limit is computed explicitly on the right-hand-side of eq. (2.24). The extra combinatorial factor  $1/n!$  arising from divided differences is fundamental in order to obtain the equivalence with the application of the residue theorem given in section 2.1.

Two properties of the  $\delta^{(n)}[x]$  distribution are especially important. The first one concerns the action of the derivative on  $\delta^{(n)}[x]$

$$\frac{d}{dx}\delta^{(n)}[x] = n\delta^{(n+1)}[x], \tag{2.25}$$

i.e., the derivative simply raises the degree of the  $\delta^{(n)}$  distribution by one. The second property is the composition rule

$$\delta^{(n)}[g(x)] = \delta^{(n)}[x - g^{-1}(0)]w_n[g](x), \tag{2.26}$$

with

$$w_n[g](x) = \text{sgn}[g'(g^{-1}(0))] \lim_{x' \rightarrow x} \left[ \frac{(x' - g^{-1}(0))^n}{g(x')} \right] \tag{2.27}$$

assuming  $g(x)$  has a unique zero located at  $g^{-1}(0)$ , and  $w_1[g](x)$  corresponds to the composition rule of the Dirac delta distribution. Note that while  $w_n[g](g^{-1}(0)) = 1/g'(g^{-1}(0))^n$ , it is incorrect to directly substitute  $w_n[g](x)$  with its value at  $x = g^{-1}(0)$  in eq. (2.26), as  $\delta^{(n)}$  will eventually set  $x = g^{-1}(0)$  only *after* taking  $n - 1$  derivatives of it. Even though the function  $w_n[g]$  is given by a limit, it can be explicitly written in terms of a power series in  $x$  around  $g^{-1}(0)$ , so that its derivatives become trivial to compute (see example in eq. (2.37)). The expression one obtains is not compact, so we do not report it here. Alternatively, one can use a change of variables in the integration in order to show that

$$\int dx \delta^{(n)}[g(x)]f(x) = \frac{1}{(n-1)!} \frac{d^{n-1}}{dy^{n-1}} \left[ \frac{f(g^{-1}(y))}{|g'(g^{-1}(y))|} \right]_{y=0}, \tag{2.28}$$

where we stress again that the assignment  $y = 0$  takes place *after* the  $n - 1$  derivatives have been evaluated. The result for  $g$  having many zero can be trivially obtained by recalling that divided differences are linear. Finally, we are ready to present the modified cutting rules. A propagator raised to a power  $n$  must be substituted with the distribution

$$\underbrace{\begin{array}{c} \xrightarrow{p} \bullet \bullet \bullet \xrightarrow{p} \\ \left. \vphantom{\xrightarrow{p}} \right\}^{\pm} \\ \bullet \bullet \bullet \xrightarrow{p} \end{array}}_{n \text{ times}} = -2\pi i \delta^{(n,\pm)}[p^2 - m^2] = \mp 2\pi i \frac{\delta^{(n)}[p^0 \mp E_{\vec{p}}]}{(p^0 \pm E_{\vec{p}})^n}, \tag{2.29}$$

which enforces on-shellness of  $p$  through the modified distribution  $\delta^{(n-1)}[x]$ , effectively computing the residue corresponding to the factor  $(p^0 \mp E_{\vec{p}})^{-n}$  obtained by factoring  $(p^2 - m^2)^{-n}$ . The denominator then features the remaining part of the raised propagator, that is  $(p^0 \pm E_{\vec{p}})^{-n}$ .

**2.2.2 Example of application of the generalised cutting rules**

We will now apply the modified cutting rules to an example interference diagram and show that it reproduces what is expected from the residue theorem. Let us start from the following example supergraph:

$$I = \text{diagram} \tag{2.30}$$

The mathematical expression for the interference diagram obtained from  $I$  by cutting the edges labelled  $p_1$ ,  $p_2$  and  $p_3$  using the generalised cutting rules of eq. (2.29) is:

$$= \int \left[ \prod_{i=1}^3 d^4 p_i \frac{\delta^{(i)}[p_i^0 + E_i]}{(p_i^0 - E_i)^i} \right] \delta \left( \sum_{i=1}^3 p_i - q \right) G_L G_R^\dagger f_3. \tag{2.31}$$

where  $f_3$  is a test function of the momenta  $p_1$ ,  $p_2$  and  $p_3$ , and for simplicity we normalised the integration measure of  $p_i$  by  $-(2\pi i)$ . Note that we aligned the labelling of the edges with the power of the propagators in order to obtain a more compact expression (i.e. for this example the propagator with momentum  $p_i$  is raised to power  $i$ ). In order to solve all the delta distributions explicitly, we must choose a particular order in which to solve them. We start with the delta function enforcing energy-momentum conservation, which we solve using the  $p_3$  integration. Next, we solve the Dirac delta function enforcing on-shellness of  $p_1$  using the  $p_1^0$  integration, then the delta function enforcing on-shellness of  $p_2$  using the  $p_2^0$  integration, and finally the delta function enforcing on-shellness of  $p_3$  using the causal flow, i.e. the integration over the parameter  $t$ . This particular ordering choice is arbitrary, and any other choice would be locally equivalent. We begin by solving the overall momentum-conservation delta function and the delta function enforcing on-shellness of  $p_1$ :

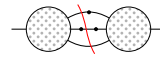
$$= \int d^3 \vec{p}_1 d^4 p_2 \frac{\delta^{(2)}[p_2^0 - E_2] \delta^{(3)}[-p_2^0 + q^0 - E_3 - E_1] f_3}{2E_1(-p_2^0 + q^0 + E_3 - E_1)^3 (p_2^0 + E_2)^2} G_L G_R^\dagger \Big|_{p_1^0 = E_1}. \tag{2.32}$$

The next delta function is then solved in the variable  $p_2^0$ . This time the generalised cutting rule yields a derivative in that variable; specifically

$$= \int d^3 \vec{p}_1 d^3 \vec{p}_2 \frac{d}{dp_2^0} \left[ \frac{\delta^{(3)}[-p_2^0 + q^0 - E_3 - E_1] [G_L G_R^\dagger f_3]_{p_1^0 = E_1}}{2E_1(-p_2^0 + q^0 + E_3 - E_1)^3 (p_2^0 + E_2)^2} \right]_{p_2^0 = E_2}. \tag{2.33}$$

When unfolding the action of this derivative explicitly, we obtain two terms, one corresponding to the derivative acting on the remaining generalised Dirac delta distribution, and the other resulting from the derivative acting on all other terms. The derivative of the

generalised delta distribution is obtained following eq. (2.25):

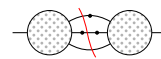


$$= \int d^3\vec{p}_1 d^3\vec{p}_2 \frac{3\delta^{(4)}\left[q^0 - \sum_{i=1}^3 E_i\right] \left[G_L G_R^\dagger f_3\right]_{p_1^0=E_1, p_2^0=E_2}}{2E_1(q^0 + E_3 - E_2 - E_1)^3 (2E_2)^2} \quad (2.34)$$

$$+ \delta^{(3)}\left[q^0 - \sum_{i=1}^3 E_i\right] \frac{d}{dp_2^0} \left[ \frac{\left[G_L G_R^\dagger f_3\right]_{p_1^0=E_1}}{2E_1(-p_2^0 + q^0 + E_3 - E_1)^3 (p_2^0 + E_2)^2} \right]_{p_2^0=E_2}. \quad (2.35)$$

Such distinction is important because the two terms have different pole orders, and thus require a different number of derivatives when acted upon by the last generalised delta distribution.

This final Dirac delta distribution must then be solved using the causal flow. Let us introduce the one-parameter group  $\phi_t$ , solution of the ODE in eq. (2.7), by first introducing a resolution of the identity by rewriting 1 as the integral of a normalised function  $h(t)$ . Next, we change variables from  $\vec{p}_1, \vec{p}_2$  to  $(\phi_t)_1, (\phi_t)_2$ . We can then solve the remaining delta function using the variable  $t$ :



$$= -\frac{1}{2} \int d^3\vec{p}_1 d^3\vec{p}_2 \frac{d^3}{dt^3} \left[ \frac{\left[h(t) w_4(t) \mathbb{J}\phi_t G_L G_R^\dagger f_3\right]_{p_1^0=E_1, p_2^0=E_2}}{2E_1(q^0 + E_3 - E_2 - E_1)^3 (2E_2)^2} \right]_{t=t^*} + \frac{d^2}{dt^2} \left[ \frac{d}{dp_2^0} \left[ \frac{\left[w_3(t) h(t) \mathbb{J}\phi_t G_L G_R^\dagger f_3\right]_{p_1^0=E_1}}{2E_1(-p_2^0 + q^0 + E_3 - E_2)^3 (p_2^0 + E_2)^2} \right]_{p_2^0=E_2} \right]_{t=t^*}. \quad (2.36)$$

where we introduced the Jacobian of the change of variables  $\mathbb{J}\phi_t$  and the derivative factor  $w_n(t)$  arising from solving the delta distribution in the variable  $t$ , which is also subject to the derivative in  $t$  (see eq. (2.26)). The explicit expression of the  $w_n$  derivative factor is:

$$w_n(t) = \left[ \frac{t - t^*}{(E_1 + E_2 + E_3 - q^0) \circ \phi_t} \right]^n, \quad (2.37)$$

and  $t^*$  is the unique value of  $t$  such that  $(E_1 + E_2 + E_3 - q^0) \circ \phi_t = 0$ . This concludes the explicit solving of all the delta distributions associated with the phase space measure of the example interference diagram introduced in eq. (2.31). At first sight, it may appear as if the analytic computation of the required derivatives could be a cumbersome obstacle for an efficient and automated implementation of LU. However, we show in appendix. C that these derivatives can instead be computed *exactly* and *numerically* using a construction known as *dual numbers*, and we demonstrate in section B with explicit timing benchmarks that the resulting implementation is efficient.

### 2.3 Generalised cutting rules and truncated Green's functions

We have seen that constructing a local representation of cross-sections that is FSR-finite requires a careful treatment of raised propagators, which results in derivatives of amplitudes on both sides of the cut. An even more noteworthy feature of eq. (2.13) is that



the derivatives in  $p_1^0, \dots, p_{n-1}^0, t$  act on the final-state density  $f(\mathcal{O})$  associated with the observable  $\mathcal{O}$ . Such derivatives are never considered within the traditional approach in which external propagators, including their self-energy corrections, are truncated, taking advantage of the OS mass renormalisation scheme. In the following we will clarify the interplay between the OS scheme, raised propagators and the request of local IR finiteness. Let us discuss the OS renormalisation of masses and fields separately:

**OS mass counterterm.** Let us start by showing that we can eliminate the derivatives of amplitudes arising from raised propagators when we renormalise the masses in the OS scheme. As an example, we will focus on self-energy corrections within a scalar theory, and consider the application of generalised cutting rules on OS renormalised quantities:

$$\frac{(\Sigma(p^2) - \delta m^{os})^n}{(p^2 - m^2)^{n+1}} f(p) \rightarrow (-2\pi i) \frac{(\Sigma(p^2) - \delta m^{os})^n}{(p^0 + E_{\vec{p}})^{n+1}} \delta^{(n+1)}[p^0 - E_{\vec{p}}] f(p). \quad (2.38)$$

where  $f$  is a test function (for example, it could be the product of two amplitudes, contracted and already integrated over all common external momenta aside from  $p$ ). The resolution of the generalised cutting rule yields

$$\int dp^0 \frac{(\Sigma(p^2) - \delta m^{os})^n}{(p^0 + E_{\vec{p}})^{n+1}} \delta^{(n+1)}[p^0 - E_{\vec{p}}] f(p) = \frac{1}{n!} \frac{\partial^n}{(\partial p^0)^n} \left[ \frac{(\Sigma(p^2) - \delta m^{os})^n}{(p^0 + E_{\vec{p}})^{n+1}} f(p) \right]_{p^0=E_{\vec{p}}}. \quad (2.39)$$

and using the integrated level identity  $\Sigma(m^2) = \delta m^{os}$  stemming from OS renormalisation conditions, we obtain:

$$\int dp^0 \frac{(\Sigma(p^2) - \delta m^{os})^n}{(p^0 + E_{\vec{p}})^{n+1}} \delta^{(n+1)}[p^0 - E_{\vec{p}}] f(p) = \frac{\Sigma'(m^2)^n}{2E_{\vec{p}}} f(p^{os}) \quad (2.40)$$

This confirms that within the OS scheme, all contributions arising from derivatives of amplitudes or observables vanish, and we are left with the OS field renormalisation counterterm  $\Sigma'(m^2)$  multiplying the truncated integrand. Importantly, we note that the last equality of eq. (2.39) was obtained by enforcing that  $\Sigma(m^2) = \delta m^{os}$ , which is a result that holds only at the integrated level, but not at the local level.

The fact that  $\Sigma(m^2) = \delta m^{os}$  holds at the integrated level and not at the local level is precisely why generalised cutting rules are required. At the local level, the effect of raised propagators and the derivatives generated by the cutting rules is relevant, so much so that not including such derivatives would break the LU IR cancellation pattern. In other words, because the cancellation of raised propagators given in eq. (2.40) does not hold locally, then the LU construction forces to first include the full effect of the generalised cutting rules and only later renormalise masses in the OS scheme.

**OS field counterterm.** We now discuss OS field counterterms within LU. The OS field counterterms contain IR poles as well as UV poles, which are needed to achieve local IR finiteness within LU. Thus, performing OS field renormalisation before the construction of the LU renormalisation would break the KLN cancellation mechanism upon which LU relies. In order to preserve the KLN cancellation pattern, one must renormalise fields in

the OS scheme (if desired) only *after* the application of LU, through couplings redefinition, which we will detail in section 5.2.3. We view the separation of handling IR and UV singularities as theoretically more appealing than the usual dimensional-regularisation approach which blurs the distinction of these two opposite regimes by using a single regulator for both.

In summary, our handling of external self-energy corrections is separated into two independent steps: a) we first construct an unrenormalised and locally IR-finite integrand and b) we locally subtract its UV divergences (see section 3.1), and add compensating terms (see section 5.2.1) to accommodate a choice of renormalisation conditions. Within this two-step procedure, it is clear that the role of the derivatives introduced within the LU formulation of section 2.1 is only that of guaranteeing *local* IR-finiteness and they bring no overall contribution to the differential cross-section when working within the OS renormalisation scheme. We also stress that the formalism of generalised cutting rules opens the possibility of constructing a LSZ formula that allows for the renormalisation of external particles in generic schemes.

Finally, we briefly discuss the effect of taking derivatives of the observable functions. We distinguish the case of continuous observables and piece-wise constant observables. Continuous observable densities often correspond to some variant of an event shape. In that case, the derivatives of the observable density induced by the generalised cutting rule must *always* be accounted for since the terms of sub-leading order in  $(t - t^*)$  that are generated in this way are essential for guaranteeing local FSR-finiteness of the LU representation (much like it is the case for derivatives of the  $h(t)$  normalising function). This is however not an obstacle since in practice the continuous observables typically considered are differentiable, such that computing their derivatives can easily be done numerically, similarly as it is done for graph numerators, using the dual numbers whose construction we detail in appendix C. Other common observables are piece-wise constant, i.e. a histogram. In that case, the observable derivatives are zero everywhere except at the bin-boundary where the observable is technically not IR-safe (which leads to the common misbinning feature). At the bin boundaries however, the observable derivatives are delta functions whose contributions are however typically excluded from the bin weights (and anyway zero at the integrated level when renormalizing external masses in the OS scheme, as we already discussed).

### 3 The $R$ -operation

We have seen that the Local Unitarity representation allows to cast the sum over all interference diagrams arising from a given supergraph as the integral of a function that is free of IR singularities. Interference diagrams, however, also feature UV singularities. Each interference diagram is split by the Cutkosky cut into two diagrams which may have loops and, consequently, UV divergences. These singularities need to be regulated locally, in order for the LU framework to be effective. Thankfully, the understanding of UV divergences of amplitudes is far more advanced than of IR divergences and a fully generic framework for their treatment is known.

In particular, for renormalisable theories, UV poles of complete amplitudes are known to be factorisable and can be removed through parameter re-definitions. Diagrammatic proofs of this fact usually follow the  $R$  formalism [70, 71], which establishes a recursive subtraction procedure, or the BPHZ [70, 72–74] formalism, the unfolding of the  $R$  procedure in terms of a forest subtraction formula. These procedures can be applied to an individual diagram and render it UV-finite. Although the generic framework was available since the end of the sixties and has been extended to subtract internal soft divergences in the eighties [75–79], there have been few automated implementations of the framework for relevant and complete physical theories. In particular, rarely is it discussed how to construct the renormalisation operator  $K$ , upon which the  $R$ -formalism critically relies. A proper definition of  $K$  requires disentangling its role as a subtraction operator and as a renormalisation operator. Furthermore, if the  $R$ -operation is to be applied within the LU framework, it also needs to satisfy local properties that are crucial to the realisation of both IR and UV cancellations.

In this section, we will start by discussing the general features of the  $R$  formalism, including the definition of the objects participating in its construction, namely the renormalisation operator  $K$  and the *wood* of a graph. We will then discuss four important properties that we wish to impose on our construction. Finally, we will briefly comment on the interplay between the KLN cancellation pattern that underlies the construction of the LU formula and the UV subtraction implemented by the  $R$ -operation.

### 3.1 The $R$ -operation master formula

The first step in constructing a UV subtraction formula is to determine all divergent 1PI subgraphs, classified according to their *dod*. The *dod* of a graph is defined as the integer corresponding to the sum of all mass dimensions of vertices and edges of the graph (i.e., a quark propagator has mass dimension -1, a triple gluon vertex +1) and its integration measure. If the degree of divergence is greater or equal to zero, the graph is ultraviolet divergent, and requires subtraction. The degree of divergence of a given subgraph has the direct interpretation of being the leading power in the Taylor expansion around the infinity limit of a parameter rescaling all loop momentum components to infinity. Note that it can be that the superficial degree of divergence of a graph is higher than its actual degree of divergence.

For gauge theories and for a given graph  $\Gamma$  with  $N_f$  external fermionic lines and  $N_A$  external bosonic lines, the *dod* is

$$\text{dod}(\Gamma) = 4 - \frac{3}{2}N_f - N_A. \tag{3.1}$$

As an example, we list all divergent subgraphs for the Feynman diagram  $\Gamma$  in figure 2. The UV divergent subgraphs  $\gamma$  are characterised by the numbers that label the edges of the subgraph. The vertices at the endpoint of the edges are understood to be part of the subgraph as well. The set of all UV divergent subgraphs is  $D(\Gamma) = \{\gamma_{67}, \gamma_{123}, \gamma_{345}, \gamma_{1245}, \gamma_{12345}, \gamma_{1\dots 12}\}$ , with the *dod* being 1, 0, 0, 0, 2 and 0 respectively.

Given the set of all divergent subgraphs  $D(\Gamma)$ , one can construct all families of subgraphs for which any two subgraphs are disjoint, i.e. they share no edge or vertex. We refer

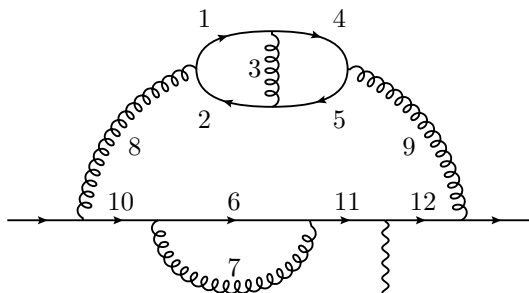


**Figure 2.** Example graph  $\Gamma$  with nested ultraviolet divergences. Its collection of UV divergent subgraphs is  $D(\Gamma) = \{\gamma_{67}, \gamma_{123}, \gamma_{345}, \gamma_{1245}, \gamma_{12345}, \gamma_{1\dots 12}\}$ , with dod's being 1, 0, 0, 0, 2 and 0 respectively.

to these families as spinneys and the collection of all spinneys as the wood  $W(D(\Gamma)) =: W(\Gamma)$ . The wood obtained from the divergent subgraphs for the example of figure 2 is:

$$W(\Gamma) = \{\{\}, \{\gamma_{67}\}, \{\gamma_{123}\}, \{\gamma_{345}\}, \{\gamma_{1245}\}, \{\gamma_{12345}\}, \{\gamma_{1\dots 12}\}, \{\gamma_{123}, \gamma_{67}\}, \{\gamma_{345}, \gamma_{67}\}, \{\gamma_{1245}, \gamma_{67}\}, \{\gamma_{12345}, \gamma_{67}\}\}. \quad (3.2)$$

Having defined the wood of a graph, we now present the  $R$ -procedure [70] that makes any diagram  $\Gamma$  UV finite:

$$R(\Gamma) = \sum_{S \in W(\Gamma)} \Gamma \setminus S * \prod_{\gamma \in S} Z(\gamma), \quad Z(\gamma) = -K \left( \sum_{S \in W(\gamma) \setminus \gamma} \gamma \setminus S * \prod_{\gamma' \in S} Z(\gamma') \right). \quad (3.3)$$

where  $Z(\gamma)$  is the local UV counterterm operator and is defined recursively through  $Z(\emptyset) = 1$ .  $Z(\gamma)$  is the object that captures the divergence of the entire UV subgraph  $\gamma$  going to infinity with the subdivergences of  $\gamma$  subtracted. It is a polynomial in the external momenta and masses of  $\gamma$ .  $\Gamma \setminus S$  is the graph where the edges of the UV divergent graphs contained in  $S$  have all been shrunk to a point serving as an effective vertex of the remaining graph. Its corresponding integrand is contracted with the counterterm  $Z(\gamma)$  obtained from  $\gamma$ . In general, both  $Z(\gamma)$  and  $\Gamma \setminus S$  are tensors stemming from the numerator structure of the edges and vertices contained with the graph. We leave these tensor indices implicit, but remind their presence by using the  $*$  symbol to indicate the combination and contraction of indices when ‘multiplying’ the tensorial representations of the two subgraphs. The minus sign in the definition of  $Z(\Gamma)$  takes care of the proper subtraction of overlapping divergences through an inclusion-exclusion principle. The operator  $K$  is a scheme-dependent renormalization operator that is not uniquely defined, but must reproduce the divergent part of the integral expressed in some regulator. We will further constrain  $K$  in section 3.2.

Finally, note that the  $R$ -operation can also be written in terms of the Zimmermann’s forest formula [72, 73], which however displays in a less manifest way the nested structure of renormalisation and introduces some subtleties regarding the operator ordering of  $K$ s which are captured more clearly in the iterated definition of  $Z$ .

In order to properly identify the numerator specific to each subgraph and compute its approximation obtained by the application of  $K$ , it is important that the numerator algebra be performed after the application of the  $R$ -operation [71, 78].

For the example graph in figure 2, the contribution to  $R(\Gamma)$  from the spinney  $\{\gamma_{12345}, \gamma_{67}\}$  yields:

$$\begin{aligned} \prod_{\gamma \in \{\gamma_{12345}, \gamma_{67}\}} Z(\gamma) * \Gamma \setminus \{\gamma_{12345}, \gamma_{67}\} &= \\ &= K(\gamma_{67}) * K\left(\gamma_{12345} - K(\gamma_{123}) * \gamma_{45} - K(\gamma_{345}) * \gamma_{12} - K(\gamma_{1245}) * \gamma_3\right) * \gamma_{8\dots 12}. \end{aligned} \tag{3.4}$$

As long as  $K$  is a well-defined renormalisation operator, the application of  $R$  on any graph is ensured to yield a quantity that is UV-finite and that reproduces a consistent renormalisation scheme.  $K$  itself can be defined at the local or integrated level and in the following we will focus on a local level construction of it that is compatible with Local Unitarity.

### 3.2 Constraints on the renormalisation operator $K$

$K$ , being a renormalisation operator, is constrained by definition to subtract the superficial UV divergence of a graph it acts on and at the same time to implement a valid renormalisation scheme. Because we want the  $R$ -operation to be compatible with Local Unitarity, we stress that  $R$  acts on the Minkowski representation of a graph's integrand. In other words, given a graph's integrand  $\gamma(k_1, \dots, k_L)$  which is a rational function in the loop momenta  $\{k_i\}_{i=1}^L$ , external momenta  $\{p_i\}_{i=1}^n$  and masses  $\mathbf{m}$ , we can generically write  $K(\gamma)$  as:

$$K(\gamma) = \frac{P\left(\{k_i\}_{i=1}^L, \{p_i\}_{i=1}^n, \mathbf{m}\right)}{Q\left(\{k_i\}_{i=1}^L, \{p_i\}_{i=1}^n, \mathbf{m}\right)}. \tag{3.5}$$

where  $P$  and  $Q$  are polynomials. We formulate four more constraints on the action of  $K$ :

1. **Local UV convergence:** the result of applying the  $R$ -operation to a graph's  $G$  integrand with  $K$  being the subtraction operator yields a *locally* UV finite quantity. We require that:

- $K$  locally subtracts the superficial UV divergence of any graph it is applied to, i.e. if  $\lambda k_1, \dots, \lambda k_L$  are the loop momenta of the graph  $\gamma$ , then

$$\lim_{\lambda \rightarrow \infty} \lambda^{4L} |\gamma - K(\gamma)| \in \mathbb{R}^+, \tag{3.6}$$

i.e. the subtracted graph is finite when all its loop momenta go to infinity.

- $K$  preserves nested cancellations, i.e. if  $\lambda k_1, \dots, \lambda k_{L_2}$  are the loop momenta of the graph  $\gamma_2$ , and  $\tilde{k}_1, \dots, \tilde{k}_{L_1}$  are the loop momenta of the graph  $\gamma_1$ , then

$$\lim_{\lambda \rightarrow \infty} \lambda^{4L_2} |K(\gamma_1) * \gamma_2 - K(K(\gamma_1) * \gamma_2)| \in \mathbb{R}^+. \tag{3.7}$$

$$\lim_{\lambda \rightarrow \infty} \lambda^{4L_2} |K(\gamma_1 * \gamma_2) - K(\gamma_1 * K(\gamma_2))| \in \mathbb{R}^+, \tag{3.8}$$

2. **Spurious soft subtraction:**  $R(\Gamma)$  should be locally free of soft singularities for non-exceptional external momenta (see section 4.2).

3. **Minimal analytic complexity:** the construction of  $K$  should only involve the analytic computation of at most single-scale vacuum diagrams, with all propagators having the same mass.
4. **Hybrid  $\overline{\text{MS}}$ +OS renormalisation:**  $R(\Gamma)$  should give the renormalised expression for  $\Gamma$ , where masses of massive particles are renormalised in the OS scheme and the fields and vertices are renormalised in  $\overline{\text{MS}}$ .

In the following, we will construct a renormalisation operator that satisfies all four constraints. In order to compartmentalise the discussion, we decompose the operator  $K$  as follows:

$$K = \mathbf{T} + \bar{K}, \tag{3.9}$$

where  $\mathbf{T}$  the *local* subtraction operator and  $\bar{K}(\Gamma)$  is a UV (and IR) finite function of the loop momenta of the graph  $\Gamma$ , and a polynomial in the external momenta of  $\Gamma$ . In section 4, we will construct the local subtraction operator  $\mathbf{T}$  that manifestly satisfies the first two constraints. In section 5, we will determine  $\bar{K}$  and show that such a choice also satisfies the last two constraints.

### 3.3 IR-finiteness of the UV forest

We briefly discuss the interplay between subtraction of UV divergences and the pattern of cancellations of IR divergences predicted by the KLN theorem, which itself underlies the local IR finiteness of the LU representation. Let us thus consider a fixed forward-scattering (connected) diagram  $\Gamma$  and the set of all Cutkosky cuts  $\mathcal{C} = \{\mathbf{c}_i\}$  that can be operated on it. Recall that a Cutkosky cut is characterised by a subset  $\mathbf{c}$  of the edges of  $\Gamma$  such that the deletion of the edges in  $\mathbf{c}$  produces two connected diagrams, and that is minimal under this property (any subset of  $\mathbf{c}$  does not satisfy such property). The KLN cancellation mechanism ensures that the sum over all interference diagrams obtained from the Cutkosky cuts  $\{\mathbf{c}_i\}$  is free of final state IR singularities (see figure 3).

The structure described above of identifying diagrammatic contributions to transition probabilities as arising from the couplets of forward-scattering diagrams and Cutkosky cuts, should be preserved by the UV subtraction procedure. Given  $\Gamma$  and a fixed Cutkosky cut  $\mathbf{c}$  on it, we denote by  $\Gamma_1$  and  $\Gamma_2$  the graphs obtained from the deletion of  $\mathbf{c}$  from  $\Gamma$ . We then consider the counterterms obtained from the application of the  $R$ -operation on each of these two graphs; specifically, to each element in the wood  $S \in W(\Gamma_i)$ , corresponds a UV counterterm. Given  $\Gamma_i$  and  $S$ , the reduced graph is obtained by contracting to a point all of the subgraphs  $\gamma \in S$  of  $\Gamma_i$ , denoted with  $\Gamma_i^S$ , and it is a diagrammatic representation of the UV counterterm constructed from  $S$ . The contracted graph does not have IR singularities, since the propagators of IR-divergent graphs, and only those, will have been assigned a UV mass.

This diagrammatic representation of the UV counterterms of  $\Gamma_1$  and  $\Gamma_2$  can be included into a similar representation for the interference diagram  $(\Gamma, \mathbf{c})$ . Indeed, given two elements  $S_1 \in W(\Gamma_1)$  and  $S_2 \in W(\Gamma_2)$ , we can consider the reduced diagram  $\Gamma^{S_1 S_2}$ , which is divided by  $\mathbf{c}$  into the two reduced diagrams  $\Gamma_1^{S_1}$  and  $\Gamma_2^{S_2}$ .  $(\Gamma^{S_1 S_2}, \mathbf{c})$  is then an interference diagram that could potentially feature IR divergences. Thus we have to show that the  $R$ -operation

$$\sum_{\mathbf{c}} C_{\mathbf{c}} \left[ \text{triangle diagram} \right] = \text{cut diagrams 1} + \text{cut diagrams 2} + \text{cut diagrams 3} + \text{cut diagrams 4} + \text{cut diagrams 5} + \text{cut diagrams 6}$$

**Figure 3.** The sum over all Cutkosky cuts of a forward-scattering diagram is IR-finite.

$$(R - \mathbb{1}) \left[ \text{triangle diagram} \right] = \text{cut diagrams 1} + \text{cut diagrams 2} + \text{cut diagrams 3}, \quad (R - \mathbb{1}) \left[ \text{triangle diagram} \right] = \text{cut diagrams 4},$$

$$(R - \mathbb{1}) \left[ \text{triangle diagram} \right] = \text{cut diagrams 5} + \text{cut diagrams 6} + \text{cut diagrams 7}, \quad (R - \mathbb{1}) \left[ \text{triangle diagram} \right] = \text{cut diagrams 8}.$$

**Figure 4.** The  $R$ -operation can be appropriately defined so as to act on interference diagrams.

applied to the full sum of interference diagrams arising from  $G$  also yields all of the other reduced interference diagrams that can be constructed by operating Cutkosky cuts on the reduced forward-scattering diagram  $\Gamma^{S_1 S_2}$ .

This is straightforward to prove: for any other Cutkosky cut  $\mathbf{c}'$  of  $\Gamma^{S_1 S_2}$ , the two graphs obtained from deletion of the edges in  $\mathbf{c}'$  of the *original* graph  $\Gamma$  have forests with unique elements  $S_1$  and  $S_2$  belonging to them. Thus, the reduced interference diagram  $(\Gamma^{S_1 S_2}, \mathbf{c}')$  is also produced by the subtraction procedure. For fixed  $S_1$  and  $S_2$ , each reduced interference diagram is in a one-to-one correspondence with Cutkosky cuts (although different elements of the forest could produce the same reduced diagram). This ensures that the KLN cancellation mechanism is preserved across UV counterterms. In general, all discussion and results pertaining to the LU representation of a forward-scattering diagram equally apply to the forward-scattering diagrams  $\Gamma$  and to any individual term stemming from the  $R$ -operation and generating forward-scattering diagrams like  $\Gamma^{S_1 S_2}$ .

We can restate this result in other words: let  $(S, \mathbf{c})$  be the couplet obtained from an element of the wood  $S \in W(\Gamma)$  of the forward-scattering diagram  $\Gamma$  and a Cutkosky cut  $\mathbf{c}$ , such that any subgraph  $\gamma \in S$  does not share an edge with  $\mathbf{c}$ . Then,  $S$  does not intersect  $\mathbf{c}$ . Let  $W_{\text{ext}}$  be the set of all such elements. If we define  $C_{\mathbf{c}}$  as cutting only *non-contracted* parts of a reduced graph or  $R$  as being the UV subtraction operator that contracts only *non-cut* parts of the graph, then

$$R_{\text{cut}}(\Gamma) = R \left( \sum_{\mathbf{c} \in \mathcal{C}} C_{\mathbf{c}}(\Gamma) \right) = \sum_{\mathbf{c} \in \mathcal{C}} C_{\mathbf{c}}(R(\Gamma)) = \sum_{(S, \mathbf{c}) \in W_{\text{ext}}} C_{\mathbf{c}}(\Gamma \setminus S) * \prod_{\gamma \in S} Z(\gamma) \quad (3.10)$$

is both IR and UV finite, where  $C_{\mathbf{c}}$  is the cut-taking operator, that substitutes the propagators corresponding to edges in  $\mathbf{c}$  with their cut versions. The diagrammatic application of both cutting rules and the  $R$ -operations are especially clear. In figure 4 we show the result of applying the  $R$ -operation to interference diagrams, for an example forward-scattering diagram. We then show in figure 5 that the result of applying  $R$  on the whole sum of interference diagrams can be cast in a way that manifestly exhibits its IR finiteness.



$$(R - \mathbb{1}) \sum_c C_c \left[ \text{triangle diagram} \right] = \left[ \text{triangle with red line} + \text{triangle with red line} \right] + \left[ \text{triangle with red line} + \text{triangle with red line} \right] +$$

$$\text{triangle with red line} + \text{triangle with red line} + \text{triangle with red line} + \text{triangle with red line}$$

**Figure 5.** Applying the  $R$ -operation on the sum of all the interference diagrams arising from a given forward-scattering diagram yields IR-finite contributions. In particular, each expression in square brackets of the first line is separately IR finite, and each diagram on the second line is also IR finite, provided that  $q^2 > 0$ .

### 4 Subtraction operators

Having expressed the local renormalisation operator  $K$  as the sum of a subtraction operator  $\mathbf{T}$  and a finite quantity  $\bar{K}$ , and having defined the relevant constraints on  $K$ , we proceed to construct the subtraction operator  $\mathbf{T}$ . In the following, we will limit ourselves to introducing  $\mathbf{T}$  and arguing that it satisfies the first two constraints of those laid out in section 3.2, associated with the *local* UV convergence of  $R(\Gamma)$  and to the absence of spurious soft enhancements due to raised massless propagators. If we wish the subtraction implemented by  $K$  to be local, so that the integral corresponding to such amplitudes can be obtained by direct Monte-Carlo integration, we need both  $\mathbf{T}$  and  $\bar{K}$  to have a local representation. The construction of  $\mathbf{T}$  follows four steps:

1. The construction of  $T$ , a local subtraction operator that satisfies the first constraint of section 3.2, but not the second one.
2. The construction of  $\tilde{T}$ , a local subtraction operator that satisfies the second constraint of section 3.2, but not the first one.
3. The construction of  $\hat{T} = \tilde{T} + T - T\tilde{T}$ , a local subtraction operator that satisfies both constraints of section 3.2.
4. The construction of  $\mathbf{T}$ , a refined version of  $\hat{T}$ , whose action on massive fermionic self-energy corrections also reproduces the OS renormalisation of the fermion’s mass.

Ultimately, a full understanding of the  $\mathbf{T}$  operator and its properties can only be obtained after it is combined with  $\bar{K}$ , and  $K$  is then shown to also satisfy the last two constraints laid out in section 3.2. This last step is performed in section 5.

#### 4.1 The UV subtraction operator

In order to construct local UV counterterms, we consider a modified expansion of the propagators so that the denominator of each approximated propagator includes an arbitrary mass term  $m_{UV}$  that regulates the soft behaviour of the UV counterterms. Let  $\gamma$  be a subgraph depending on the external momenta  $p_1, \dots, p_n$ , loop momenta  $k_1, \dots, k_L$  and masses  $\mathbf{m} = (m_1, \dots, m_l)$ . Let us then start by considering the case in which we write

$K(\gamma) = T_{\text{dod}}(\gamma)$ , where  $T$  is the Taylor expansion operator that expands in the parameter  $\lambda$  that rescales the external scales, including masses, of the graph  $\gamma$ . The ‘dod’ subscript refers to the degree of divergence of  $\gamma$  which also corresponds to the order in  $\lambda$  at which the Taylor series is truncated. By setting  $K = T$ , we can already assess the UV convergence of the  $R$ -operation (Note however that we will eventually use a different version for  $K$ ). More precisely, let  $\gamma^\lambda$  be defined as

$$\gamma^\lambda = \frac{\mathcal{N}\left(\{\lambda p_i\}_{i=1}^n, \{\lambda m_j\}_{j=1}^l, \{k_m\}_{m=1}^L\right)}{\prod_{e \in \mathbf{e}} D_{e,\lambda}}, \quad (4.1)$$

where  $\mathcal{N}$  is a polynomial numerator. We have  $\gamma^1 = \gamma$ . We stress that the numerator of  $\gamma$  is *not* equivalent to the numerator of the complete supergraph  $\Gamma$ , and that the expansion is performed only in the numerator and denominator of the subgraph  $\gamma$ .  $D_e^\lambda$  is the inverse propagator defined as

$$D_{e,\lambda} = k_e^2 - m_{\text{UV}}^2 + 2\lambda k_e \cdot p_e + \lambda^2 p_e^2 - \lambda^2 (m_e^2 - m_{\text{UV}}^2), \quad (4.2)$$

where  $p_e$  is constrained to be a linear combination of the external momenta  $p_1, \dots, p_m$ ,  $k_e$  is a linear combination of the loop momenta  $k_1, \dots, k_L$ , and  $m_e$  can be either zero or equal one of the masses  $m_1, \dots, m_l$ .  $m_{\text{UV}}$  is a UV mass that is introduced as a regulator for the IR behaviour of the UV subtraction counterterm. We define  $K(\gamma) = T_{\text{dod}}(\gamma)$ , with

$$T(\gamma) = T_{\text{dod}}(\gamma) = \sum_{j=0}^{\text{dod}} \frac{1}{j!} \frac{d^j}{d\lambda^j} \gamma^\lambda \Big|_{\lambda=0} \quad (4.3)$$

We note that with this definition, the approximation of a graph always corresponds to a polynomial in the external momenta and internal masses, with coefficients that are vacuum tensor integrands with a single scale  $m_{\text{UV}}^2$  appearing as the mass of each denominator. Importantly, the infrared rearrangement [80, 81] operated by introducing a  $m_{\text{UV}}$  does not spoil the local cancellation of the counterterm. The substitution of eq. (4.1) is *not* equivalent to an expansion in the propagator mass  $m_e^2$  around  $m_e^2 = m_{\text{UV}}^2$ , and this is especially manifest when considering a numerator with a dependence on  $m$ .

For our example spinney  $\{\gamma_{12345}, \gamma_{67}\}$ , we obtain the following contribution to  $R(\Gamma)$ :

$$\begin{aligned} Z(\gamma_{12345})Z(\gamma_{67}) * \Gamma \setminus \{\gamma_{12345}, \gamma_{67}\} &= \\ &= T_1(\gamma_{67})T_2\left(\gamma_{12345} - T_0(\gamma_{123}) * \gamma_{45} - T_0(\gamma_{345}) * \gamma_{12} - T_0(\gamma_{1245}) * \gamma_3\right) * \gamma_{8\dots 12}. \end{aligned} \quad (4.4)$$

The Taylor expansions  $T_{\text{dod}}$  yield tensor graphs in terms of the polynomial in internal masses and the external momenta of the subgraph. We remind the reader that our use of the symbol  $*$  indicates that indices that are in common between the subgraphs multiplied are contracted whereas those that are different combine as in a tensor product. Note that in the case of nested  $T_{\text{dod}}$  approximations, the outermost approximation must expand over the  $m_{\text{UV}}$  factors introduced in the numerator by the innermost Taylor expansion (see eq. (4.3)).

The separation of the dependence of  $D_e^\lambda$  and  $\mathcal{N}$  into linear combinations of *loop* momenta  $k_e$  (not rescaled with  $\lambda$ ) and linear combinations of *external* momenta  $p_e$  (rescaled

with  $\lambda$ ) is in principle ambiguous as it depends on a particular choice of a loop momentum basis for performing the expansion. It is important that such a change of loop momentum basis to an expansion basis is performed consistently to preserve the cancellation pattern of nested divergences. Given the contributions  $Z(\gamma_a * \gamma_b + Z(\gamma_a) * \gamma_b) + Z(\gamma_a) * \gamma_b$ , the first cancellation to consider is the one between  $Z(\gamma_a) * \gamma_b$  and  $Z(Z(\gamma_a) * \gamma_b)$  in the limit where the cycles of  $\gamma_b$  go to infinity (see eq. (3.7)). This first type of nested cancellations is guaranteed by fixing the expansion basis for the  $n$ -loop UV subgraph  $\gamma_a$ , wherever it appears in the  $R$ -operation, to consist of the same fixed  $n$  loop basis momenta. The second type of nested cancellations (see eq. (3.8)) concerns the UV expanded version of the remaining graph and is between  $Z(\gamma_a * \gamma_b)$  and  $Z(Z(\gamma_a) * \gamma_b)$  in the limit where the cycles in  $\gamma_a$  go to infinity (and therefore the cycles in the remaining graph are a constant). This second requirement is achieved by choosing the expansion basis of  $\gamma_b$  to involve only linear combinations of the basis momenta chosen for  $\gamma_a * \gamma_b$ . Similar prescriptions appear in refs. [72, 80, 82].

As an example, we perform such a change of basis for the term  $T_0(\gamma_{123}) * \gamma_{45}$ :

$$T \left( \begin{array}{c} \text{Diagram 1} \end{array} \right) * \begin{array}{c} \text{Diagram 2} \end{array} \rightarrow T \left( \begin{array}{c} \text{Diagram 3} \end{array} \right) * \begin{array}{c} \text{Diagram 4} \end{array} \quad (4.5)$$

where on the right we changed the loop momentum basis that is used as a reference for the Taylor expansion into the expansion basis  $c_1 = k, c_2 = k + l$ . In order to illustrate the first type of nested cancellations, we give here an example of an *inconsistent* choice of expansion basis, for example when electing the basis  $c_1 = k, c_2 = k + l$  for the implementation of  $T_0(\gamma_{123}) * \gamma_{45}$  and  $c'_1 = k - p, c'_2 = k + l$  for implementing  $-T_2(T_0(\gamma_{123}) * \gamma_{45})$ . Then, there would be local UV miscancellation when  $l \rightarrow \infty$ :

$$T_0(\gamma_{123}) * \gamma_{45} - T_2(T_0(\gamma_{123}) * \gamma_{45}) \xrightarrow{l \rightarrow \infty} \frac{\mathcal{N}'_1(k, l, p)}{(k^2)^2(l^2)^2} - \frac{\mathcal{N}'_2(k, l, p)}{((k - p)^2)^2(l^2)^2} + \dots \quad (4.6)$$

A miscancellation of the second type of nested cancellations would occur when selecting the bad basis  $c_1 = k, c_2 = k + l - p$  for  $-T_2(T_0(\gamma_{123}) * \gamma_{45})$  and the basis  $c'_1 = k, c'_2 = l$  for  $T_2(\gamma_{12345})$ . In the limit of  $k \rightarrow \infty$  these two terms should locally cancel, but they do not since the UV propagator in  $\gamma_{45}$  has a different shift.

Section 3.3 proves that the UV-subtracted LU expression is IR-finite, but for the arguments laid out in that section to hold, it is important that the *same* expansion basis momenta be chosen across all identical UV subgraphs appearing in the woods of amplitudes arising from different the Cutkosky cuts. This is because the UV counterterms of the amplitudes defined by these Cutkosky cuts must locally match on collinear limits so as to preserve the local cancellations of IR singularities featured by the LU representation. This can be achieved by electing the momenta for the expansion basis of each UV-subgraph  $Z(\gamma)$  at the supergraph level.

## 4.2 Spurious soft divergences

In section 2.1, we have argued that in order to faithfully reproduce the KLN cancellation pattern at the local level, Cutkosky cuts crossing raised propagators must be interpreted in

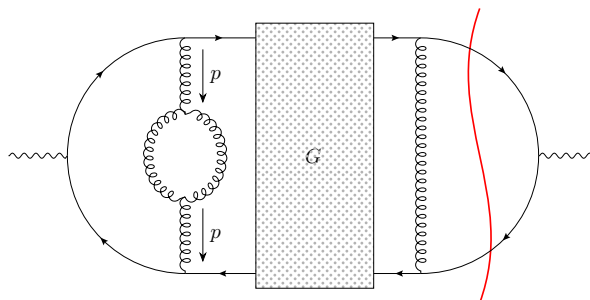


**Figure 6.** Example of an amplitude diagram featuring a spurious local soft singularity in the limit  $p^\mu \rightarrow 0$  (i.e. spurious because it leads to no pole at the integrated level) due to the insertion of a self-energy subgraph on an internal loop line. The cancellation of such a spurious soft singularity is completely unrelated to the KLN cancellation pattern, and its regularisation within the LU integrand therefore necessitates a subtraction procedure.

terms of residues of higher-order poles. The KLN cancellation pattern then eliminates all collinear enhancements. In turn, this should make the scaling around the soft region tame enough so that also soft singularities become integrable, and can be completely eliminated (i.e. bounded) using a multi-channeling procedure.

This last statement, however, is not manifestly true when self-energies are inserted on propagators of massless particles. For example, we consider the diagram shown in figure 6, where  $G$  is any graph featuring four external (anti-)quarks. In the soft limit  $p^\mu \rightarrow 0$ , the integrand corresponding to the amplitude of figure 6 scales at best as  $(p^2)^{-2}$  (excluding the scaling of the integral measure), independent of the value of the cut momenta. In general, the lower bound on the soft dod of a massless vector propagator subject to  $n$  self-energy corrections is  $4 - 2(n + 1)$  and it is  $4 - (n + 1)$  for a massless quark. Notice that in this soft limit  $p^\mu \rightarrow 0$ , no particle other than the gluon itself, and in particular not any of the propagators internal to the self-energy inserted, is forced to lie on its mass-shell. These two observations establish that such soft singularities are not related to the KLN cancellation mechanism, and are therefore expected to remain present in the LU representation of cross-sections.

However, these soft singularities are spurious in gauge theories. In other words, gauge symmetry guarantees that *at the integrated level*, the gluonic self-energy itself scales quadratically in the soft region. This is clear given that the general tensor structure of the integrated self-energy of a massless vector reads  $A(p^2)(p^2 g^{\mu\nu} + p^\mu p^\nu)$ , where  $A$  behaves like a constant in the soft limit. Similarly, the massless fermionic integrated self-energy scales linearly given its tensor structure of  $B(p^2)\not{p}$ , where  $B$  is again a constant in the soft limit. This ensures that the IR pole structure of integrated loop-amplitudes remains unaffected by such spurious soft singularities. However, at the local level the generic configuration of figure 6 has a soft divergence. Such configurations can happen only at NNLO and beyond, where the momentum of a propagator that is corrected by one or more self-energies can itself become soft.

In this work, we will seek to remedy these spurious soft divergences by the introduction of local soft counterterms. As we shall see, the soft counterterms we will construct satisfy the following two key requirements: they are inherently local and, in gauge theories and

when regularising spurious soft singularities stemming from the insertion of self-energy subgraphs, they directly integrate to zero.

### 4.2.1 Subtraction of spurious soft singularities

Local counterterms for the spurious soft divergence discussed in this section can be obtained by Taylor-expanding around  $p \rightarrow 0$  all  $n$  self-energy subgraphs correcting the raised propagator. The depth of this expansion, henceforth referred to as soft expansion depth, is chosen to be the minimal order required in order to eliminate the additional soft scaling introduced by the insertion of the self-energy subgraphs. The expansion is only performed in the external momentum  $p$  of the self-energy subgraphs, and all other scales, which for a two-point-function can only be masses, are kept unexpanded. Once combined with such a soft counterterm, the soft scaling of the subtracted graph together with its two neighbouring repeated propagators is restored to that of a single propagator without self-energy insertion, thus ensuring the IR-finiteness property of the LU representation is recovered. Quite remarkably, for renormalisable theories the soft expansion depth in the momentum external to a self-energy is always equal to the UV dod of the self-energy graph minus one. For example, in QCD, we consider the following soft expansions:

$$\tilde{T}_{\text{dod}-1} \left( \text{diagram with wavy line and self-energy} \right) = \text{diagram with wavy line} \Big|_{p=0} + p^\mu \partial_\mu \text{diagram with wavy line and self-energy} \Big|_{p=0} \quad (4.7)$$

$$\tilde{T}_{\text{dod}-1} \left( \text{diagram with fermion line and self-energy} \right) = \text{diagram with fermion line} \Big|_{p=0}, \quad (4.8)$$

where dod in the subscript of the soft-expansion operator  $\tilde{T}$  refers to the UV dod of the graph in argument. As shown in eqs. (4.7) and (4.8), the soft expansion depth  $\text{dod} - 1$  is always equal to 1 for any self-energy graph correcting a vector propagator and always 0 when correcting a fermionic propagator. The application of the operator  $(1 - \tilde{T}_{\text{dod}-1})$  to any self-energy subgraph guarantees that, together with its two adjacent propagators, its soft scaling becomes identical to that of a single soft propagator. Finally, we report the generic action of  $\tilde{T}_{\text{dod}}$  on an arbitrary graph  $\Gamma$  depending on external momenta  $\{p_i\}_{i=1}^n$ , loop momenta  $\{k_j\}_{j=1}^L$ , and internal masses  $\mathbf{m}$ , as it will be useful for future discussion. It is the multi-variate Taylor expansion of  $\Gamma$  in the rescaled external momenta only

$$\tilde{T}_{\text{dod}} \left( \Gamma(\{p_i\}_{i=0}^n, \{k_j\}_{j=1}^L, \mathbf{m}) \right) = \sum_{i=0}^{\text{dod}} \frac{1}{i!} \frac{d^i}{d\lambda^i} \Gamma \left( \{\lambda p_i\}_{i=1}^n, \{k_j\}_{j=1}^L, \mathbf{m} \right) \Big|_{\lambda=0} \quad (4.9)$$

In order to study the soft scaling of the *subtracted* object (whose actual soft scaling cannot be easily related to the UV dod anymore), we explicitly define the soft dod of an integrand  $f(k_1, \dots, k_m)$  of a graph  $\Gamma$  in a particular soft limit  $k_1, \dots, k_m \rightarrow 0$  ( $k_1, \dots, k_m$  are independent momenta), to be the leading power of its Taylor expansion in the parameter  $\lambda$  rescaling the momenta,  $k_i \rightarrow 1/\lambda k_i$ , both in the arguments of the integrand and in the integration measure for the momenta involved in the limit. In other words, for a soft limit

$$\text{dod}_{k_1, \dots, k_m}^{\text{soft}}(\Gamma) = -4m + n, \quad \text{where } \lim_{\lambda \rightarrow 0} \lambda^n f(\lambda k_1, \dots, \lambda k_m) \in \mathbb{R} \setminus \{0\}. \quad (4.10)$$



**Figure 7.** Soft subtraction for two consecutive gluonic self-energy corrections. The two 1PI subgraphs result in an  $R$ -style subtraction once the product above is expanded. In this form shown however, the correct scaling of the subtracted quantity is manifest: the subtracted consecutive self-energy scales like a single propagator would in the soft limit.

Specifically  $n$  is the integer corresponding to the leading term in the expansion of the integrand in the limit  $\lambda \rightarrow 0$ . Defined this way, a soft dod of 0 indicates a logarithmic divergence whereas a negative dod indicates convergence. We will now explore this type of subtraction when multiple self-energy corrections are present for two specific cases, before presenting the general construction.

Our first example, shown in figure 7, features the complete soft subtraction of two consecutive self-energy corrections. The overall leading soft scaling of the original graph when the momentum  $p$  of the external gluon becomes soft is  $(p^2)^{-3}$  at the local level. Once subtracted, this overall leading soft scaling becomes  $(p^2)^{-1}$ . In other words, after soft-subtraction the propagator dressed with two successive self-energy corrections still scales in the soft limit exactly as a single propagator would.

Our second example is the more complicated case involving the nesting of spurious soft divergences, as shown in figure 8 that features the nesting of a 1PI gluonic self-energy correction within another 1PI gluonic self-energy correction. The spurious soft subtraction structure in that cases bears a striking resemblance with the structure generated by the  $R$ -operation for UV divergences. The main difference being that subtraction terms  $\tilde{T}_{\text{dod}-1}(\gamma)$  are now constructed for self-energy subgraphs only, and Taylor-expanded around the spurious soft limit  $p^\mu = 0$  only (e.g. no expansion of masses) and up to a depth given by the UV dod of the graph in argument *minus one*.

In more details, we denote the local tensorial expression of the subgraphs  $G_1$ , resp.  $G_2$  in figure 8 with  $\Gamma_1$ , resp.  $\Gamma_2$ , and write  $\Gamma_{12}$  as the complete graph, including its two adjacent propagators  $\frac{1}{(p^2)^2}$  that can become soft. We can then write the soft-subtraction of  $\Gamma_{12}$  in the Feynman gauge as follows:

$$\mathcal{F}(\Gamma_{12}) = \frac{(\Gamma_1 - \Gamma_1|_{p=0} - p^\mu \partial_\mu \Gamma_1|_{p=0})^{\mu_1 \mu_2 \mu_3 \mu_4} (\Gamma_2 - \Gamma_2|_{q=0} - q^\nu \partial_\nu \Gamma_2|_{q=0})_{\mu_2 \mu_3}}{(q^2)^2 (p^2)^2}. \quad (4.11)$$

This expression of eq. (4.11) is factorised since  $q$  and  $p$  are treated as independent momenta (this cannot be done in general, but it can in this case and it simplifies the discussion), however  $\Gamma_1$  is a function of both  $q$  and  $p$ . We now investigate the two spurious soft limits  $q \rightarrow 0$  and  $p \rightarrow 0$ . We start by rescaling  $p$  with  $\lambda$ , and investigate the limit  $p \rightarrow 0$ . In the limit of  $p \rightarrow 0$  with  $q$  finite, the leading behaviour of  $\mathcal{F}(\Gamma_{12})$  is

$$\text{dod}_p^{\text{soft}}(\Gamma_{12}) = -2. \quad (4.12)$$

We now consider the spurious soft limit  $q \rightarrow 0$  for non-zero  $p$ . In that limit,  $\Gamma_1|_{p=0}$  and  $p^\mu \partial_\mu \Gamma_1|_{p=0}$  may scale like a negative power of  $q^2$ , which is potentially problematic. We

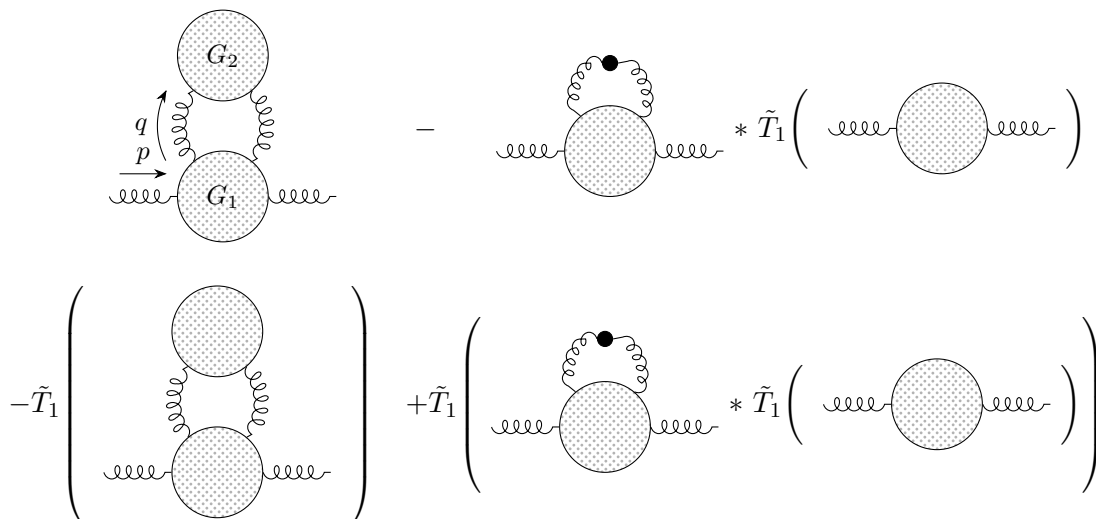


**Figure 8.** Soft subtraction for a gluonic self-energy nested within another gluonic self-energy. The collection of all 1PI two-point subgraphs of  $\Gamma$  is  $\mathcal{B}(\Gamma) = \{G_2, G_{12}\}$ . The wood of this graph, that is the collection of all its spinneys, is  $W(\mathcal{B}) = \{\{\}, \{G_2\}, \{G_{12}\}\}$ .

want to derive a bound on this power within massless gauge theories (adding masses can only improve the soft behaviour). A diagrammatic analysis shows that

$$\text{dod}_q^{\text{soft}}(\Gamma_{12}) = -1. \tag{4.13}$$

We finally look at the double limit in which  $p, q \rightarrow 0$ . The scaling in this case equals

$$\text{dod}_{p,q}^{\text{soft}}(\Gamma_{12}) = -2. \tag{4.14}$$

which leads to the conclusion that in the nested case the worst possible soft scaling (in this case the limit  $q \rightarrow 0$ ) has a dod equal to -1, which is still convergent.

As already mentioned, the generic form of the forest matches that obtained by unfolding the subtracted quantity obtained through the  $R$ -operation. Let us consider a graph  $G$  and the collection  $\mathcal{B}$  of 1PI two-point subgraphs of  $\Gamma$ . Assume, for the purpose of the correct soft power-counting, that the particles external to  $\Gamma$  are all off-shell (the enhancements created by putting external particles on-shell are exactly those cancelled by the Local Unitarity procedure). Then consider the set of all spinneys created from  $\mathcal{B}$ , denoted as  $W(\mathcal{B})$ . Finally, we set up the  $R$ -subtraction procedure of eq. (3.3), using  $K = \tilde{T}_{\text{dod}}$  as an approximant. The resulting subtracted integrand does not have any non-integrable soft singularities.

In principle, one may perform the subtraction of spurious soft divergences before applying the UV  $R$ -operation completely independently, since the introduction of the UV mass  $m_{\text{UV}}$  prevents the UV counterterms from reintroducing any IR singularity. However, in the next section, we will study a more efficient alternative whereby both spurious soft and UV subtractions are performed simultaneously within a single modified  $R$ -operation.

### 4.2.2 Embedding spurious soft subtraction within the UV $R$ -operation

A more refined way to perform the subtraction of spurious soft and UV divergences is to combine the two subtractions into one unique  $R$ -type of operation. The merging of the



two different forest structures stemming from the spurious soft and UV subtractions is a delicate process, and achieving this relies on the scaling properties of renormalisable theories, and the ensuing relationship between UV and spurious soft power-counting. A systematic approach for constructing such combined  $R$  operator is to seek for a subtraction operator that regulates *both* the spurious soft and UV behaviour of certain subgraphs. This was the original inspiration to refs. [72, 83]. In this section, we will consider a specific subtraction operator for which the all-order proof of ref. [83] holds and which also coincides with the subtraction of ref. [72] when applied to  $\phi^4$  theory. In particular, let us consider

$$\hat{T}_{\text{dod}} = T_{\text{dod}} + \tilde{T}_{\text{dod}-1} - T_{\text{dod}}\tilde{T}_{\text{dod}-1}, \tag{4.15}$$

where the subscript *dod* in that case refers to UV *dod* of the graph that the operator  $\hat{T}_{\text{dod}}$  acts on, and it will also dictate the depth of the Taylor expansion it contains. In short,  $\hat{T}$  is a subtraction operator that includes the full UV subtraction of the graph and the soft subtraction of the graph minus the UV behaviour of the soft subtraction, so that it is manifestly a good UV approximant of the graph it acts on. As an example, let us consider a gluonic 1PI graph and the action of  $\hat{T}$  on it. We consider specifically a graph that features an incoming gluon momentum  $p$  and an internal quark of mass  $m$  (for example, the top quark). In this case

$$\hat{T}_2 \left( \text{Diagram} \right) = \text{Diagram} \Big|_{p=0} + p^\mu \partial_\mu \text{Diagram} \Big|_{p=0} + \frac{p^\mu p^\nu}{2} \partial_\mu \partial_\nu \text{Diagram} \Big|_{\substack{p=0 \\ m=0 \\ m_{\text{UV}}}} \tag{4.16}$$

where thicker lines indicate the introduction of a UV mass in the denominators of the Feynman rules (according to the introduction of UV masses established by eq. (4.1) and eq. (4.2)) and the light line indicates that the propagator retains its original mass, i.e.

$$\text{Diagram} \rightarrow \text{Diagram} = i \frac{\not{p} + m}{p^2 - m^2 + i\epsilon} \rightarrow \text{Diagram} = i \frac{\not{p}}{p^2 - m_{\text{UV}}^2 + i\epsilon} \tag{4.17}$$

$$\text{Diagram} = -i \frac{g^{\mu\nu}}{p^2 + i\epsilon} \rightarrow \text{Diagram} = -i \frac{g^{\mu\nu}}{p^2 - m_{\text{UV}}^2 + i\epsilon} \tag{4.18}$$

in the Feynman gauge. Eq. (4.16) makes it clear that the effect of  $\hat{T}$  is to consider the soft approximation for the first *dod* – 1 terms of expansion in the UV limit and the UV approximation for the term of order *dod*. Observe specifically that the first two orders in the expansion of the gluonic self-energy are evaluated at internal mass  $m$  that is unchanged with respect to that of the original graph, whereas the logarithmic order is evaluated at  $m = 0$  and to every propagator a mass  $m_{\text{UV}}$  is assigned. Had we not assigned a mass to every propagator, the last term would feature a new IR singularity in the loop momentum of the quark. On the other hand the first two terms do not require a UV mass.

We also note that for any graph that is UV divergent at most logarithmically, we have  $\hat{T}_0 = T$ . Thus, in QCD, for the four-gluon vertex and the quark-gluon interaction vertices, we have  $\hat{T} = T$ . On the other hand, for the three-gluonic vertex the situation is different since it is linearly divergent in the UV, and thus the action of  $\hat{T}$  on it does include a soft

counterterm:

$$\hat{T}_1 \left( \text{triangle diagram} \right) = \text{triangle diagram} \Big|_{\substack{p_1=0 \\ p_2=0 \\ p_3=0}} + p_i^\mu \frac{\partial}{\partial p_i^\mu} \text{triangle diagram} \Big|_{\substack{p_1=0 \\ p_2=0 \\ p_3=0 \\ m_{UV}}} \quad (4.19)$$

where in the last term on the right-hand side a UV mass has been assigned to the gluons (again, only in denominators, as established by eq. (4.1) and eq. (4.2)), and summation over all indices is assumed. We observe again that due to the relation between soft and UV power-counting in renormalisable theories, the first diagram on the r.h.s. of the equation does not have a non-integrable singularity in the limit of the gluon in the loop becoming soft. A singularity would instead be present in the second term if no UV mass was assigned.

Because  $\hat{T}$  is a valid and consistent subtraction operator, the subtraction of UV divergences performed with the  $R$ -operation and  $K = \hat{T}$  is guaranteed. At the same time, the subtraction of IR divergences is guaranteed by the fact that the wood constructed using  $T$  contains the soft wood constructed in the previous section.

As an example of the nested application of  $\hat{T}$ , we work out the  $R$ -operation for a gluonic self-energy nested in a fermionic self-energy, as shown in figure 9. The spinneys and the wood are by definition the same as that of the UV  $R$ -operation: in this case, the two spinneys correspond with the nested gluonic self-energy and the full fermionic self-energy. The UV subtraction operator and the soft subtraction operator only differ by the way masses are expanded (and re-arranged, for the UV operator), and this particular way of treating masses in the merged wood is key in order to obtain the right cancellations. Specifically, observe that in the last two lines of figure 9, corresponding to the nesting of the  $\hat{T}$  operation, the second term has all masses set to zero and to every propagator a mass  $m_{UV}$  is assigned.

Finally, we discuss the case in which we want to compute QCD corrections to processes that involve the Higgs or electro-weak bosons. In this case, studying the superficial degree of divergence of all three-point graphs connecting QCD particles to electro-weak bosons, we realise that we only need to discuss the action of  $\hat{T}$  in the following cases

- a graph coupling two gluons or ghosts with a Higgs boson: we observe that such vertex must contain a fermionic loop from which the Higgs boson is spawned. So, even if the superficial degree of divergence yields that such vertex diverges linearly in the ultraviolet region, in practice the linearly divergent term vanishes identically once gamma traces are performed for the fermionic loop spawning the Higgs boson. That is, if  $\Gamma$  is a vertex coupling two gluons or ghosts and a Higgs, then

$$\tilde{T}(\Gamma) = 0. \quad (4.20)$$

Thus, for all purposes,  $\hat{T} = T$  on such fermionic loop corrections.

$$\begin{aligned}
 R_{\hat{T}} \left[ \text{Diagram} \right] &= \text{Diagram} \\
 - \text{Diagram} &\left( \text{Diagram} \Big|_{p=0} + p^\mu \partial_\mu \text{Diagram} \Big|_{p=0} + \frac{1}{2} p^\mu p^\nu \partial_\mu \partial_\nu \text{Diagram} \Big|_{\substack{p=0 \\ \mathbf{m}=0 \\ m_{UV}}} \right) \\
 - \text{Diagram} \Big|_{q=0} &- q^\mu \partial_\mu \text{Diagram} \Big|_{\substack{q=0 \\ \mathbf{m}=0 \\ m_{UV}}} \\
 + \left[ \text{Diagram} \Big|_{q=0} \right. &\left( \text{Diagram} \Big|_{p=0} + p^\mu \partial_\mu \text{Diagram} \Big|_{p=0} + \frac{1}{2} p^\mu p^\nu \partial_\mu \partial_\nu \text{Diagram} \Big|_{\substack{p=0 \\ \mathbf{m}=0 \\ m_{UV}}} \right) \Big|_{q=0} \\
 + q^\mu \partial_\mu \left[ \text{Diagram} \right. &\left. \left( \text{Diagram} \Big|_{\substack{p=0 \\ m_{UV}}} + p^\mu \partial_\mu \text{Diagram} \Big|_{\substack{p=0 \\ m_{UV}}} + \frac{1}{2} p^\mu p^\nu \partial_\mu \partial_\nu \text{Diagram} \Big|_{\substack{p=0 \\ \mathbf{m}=0 \\ m_{UV}}} \right) \right]_{\substack{q=0 \\ \mathbf{m}=0 \\ m_{UV}}}
 \end{aligned}$$

**Figure 9.** Merging of the soft and UV forest for a gluonic self-energy correction nested in a fermionic self-energy correction. The action of  $\hat{T}$  is unfolded explicitly. The four-momentum  $p$  (resp.  $q$ ) corresponds to the external momentum of the inner (resp. outer) self-energy diagram.

- a graph  $\Gamma$  coupling one or two electroweak bosons with two or one gluons. In this case, the application of  $\hat{T}$  works exactly the same as the gluonic three-vertex, i.e.

$$\hat{T}(\Gamma) = \tilde{T}_0(\Gamma) + T_1(\Gamma) - T_1(\tilde{T}_0(\Gamma)). \quad (4.21)$$

- for all graphs coupling a quark, an anti-quark and a gauge boson or a Higgs boson, then the superficial degree of divergence yields a logarithmic ultraviolet behaviour, so that  $\hat{T} = T$ .

This concludes the discussion of  $\hat{T}$  on all relevant graphs.  $\hat{T}$  manifestly satisfies both constraints laid out in section 3.2.

### 4.3 On-shell counterterms for massive fermions

The arguments we presented for the soft subtraction hold for any particle content, including massive particles. Specifically, one can also use  $\hat{T}$  to subtract the divergent UV behaviour of a massive fermionic self-energy correction. However, the soft limit of a massive self-energy does not have a particular physical meaning, and specifically it does not correspond to the massive particle becoming on-shell. This implies that the integrated soft counterterms of a massive self-energy (or a vertex in which a massive particle interacts) is non-zero and the analytic integration of the corresponding integrated UV counterterm would involve multiple scales. To avoid these complications, we propose yet another modification for the subtraction operator:

$$T^{\text{os}} = \frac{1}{2}(T^{\text{os}+} - TT^{\text{os}+}) + \frac{1}{2}(T^{\text{os}-} - TT^{\text{os}-}) + T, \quad (4.22)$$

where  $T^{\text{os}\pm}$  is the on-shell subtraction operator. We will show in section 5.1.3 that computing its integrated counterterm is not needed, as it reproduces the OS mass counterterm.

The action of  $T^{\text{os}\pm}$  is only defined for a given fermionic 1PI self-energy correction  $\Sigma$

$$T^{\text{os}\pm}(\Sigma(p, \{k_j\}_{j=1}^L, \mathbf{m})) = (1 \pm \gamma^0)\Sigma(\pm p^{\text{os}}, \{k_j\}_{j=1}^L, \mathbf{m}), \quad (4.23)$$

where  $p^{\text{os}} = (m, 0, 0, 0)$  is the at-rest on-shell momentum for massive particles, and  $p^{\text{os}} = (0, 0, 0, 0)$  for massless particles,  $m$  is the mass of the fermion and  $\mathbf{m}$  is any collection of masses the self-energy might depend on. As for  $T$  and  $\hat{T}$ , also  $T^{\text{os}\pm}$  is an operator acting on the local expression of the graph, hence the dependence of  $\Sigma$  on a set of loop momenta  $\{k_j\}_{j=1}^L$ . In general, one can substitute  $p^{\text{os}}$  with any fixed on-shell momentum and  $\gamma^0$  with  $\not{p}^{\text{os}}/m$ .

First, we simplify the action of  $T^{\text{os}}$  on a self-energy correction to a massive particle by filling in all operators participating in the definition of eq. (4.22):

$$T^{\text{os}}(\Sigma(p, \{k_j\}_{j=1}^L, \mathbf{m})) = \sum_{\sigma \in \{\pm 1\}} \frac{1 + \sigma \gamma^0}{2} \Sigma(\sigma p^{\text{os}}, \{k_j\}_{j=1}^L, \mathbf{m}) + (p^\mu - \gamma^0 (p^{\text{os}})^\mu) \frac{\partial}{\partial p^\mu} \Sigma(p, \{k_j\}_{j=1}^L, \mathbf{m}) \Bigg|_{\substack{p=0, \\ \mathbf{m}=0, \\ m_{\text{uv}}}}, \quad (4.24)$$

where  $m_{\text{uv}}$  again indicates that every propagator of the self-energy has been given the UV mass  $m_{\text{uv}}$ . Eq. (4.22) is manifestly a valid UV subtraction operator. However, in order to show that it can be used in general, one has to discuss the nesting of  $T^{\text{os}}$ .

Let us study the action of  $T^{\text{os}}$  on two relevant examples. To keep the notation compact, let us define the operator

$$P_\pm = \frac{1}{2}(1 \pm \gamma^0), \quad (4.25)$$

which is a projector on the first (last) two spinor components. We start with a massive fermionic self-energy correction nested in a gluonic self-energy correction (figure 10). In this case the  $R$ -operation with subtraction operator  $T^{\text{os}}$ , which we will write as  $R_{T^{\text{os}}}$ , achieves three objectives simultaneously. First, it regulates the UV divergent behaviour of the entire graph. Second, it subtracts the fictitious soft divergence associated with the outer gluonic correction, i.e.  $R_{T^{\text{os}}}(\Gamma) \approx q^2$  as  $q \rightarrow 0$ . Third, as we will see in the next section, it implements on-shell mass renormalisation of the fermionic two-point function.

The second example is that of a massive fermionic self-energy nested in a massive fermionic self-energy (figure 11).  $T^{\text{os}}$  is a valid subtraction operator, and thus  $R_{T^{\text{os}}}(\Gamma)$  is UV finite. As we will see in section 5.1.3,  $R_{T^{\text{os}}}(\Gamma)$  also contains the necessary pieces needed to perform OS renormalisation of both self-energies, in virtue of the nested structure of  $R_{T^{\text{os}}}$ .

#### 4.4 Summary: the $\mathbf{T}$ subtraction operator

The discussion of on-shell counterterms concludes the study of subtraction operators required for our purposes. We will now define the  $\mathbf{T}$  operator, which includes the requirements of UV convergence and absence of spurious soft propagators, including the correct extension of the soft subtraction operator to self-energy corrections of massive particles. The reasons behind the construction of the  $\mathbf{T}$  operator can only be fully explained after its relationship with the renormalisation operator  $K$  is clarified in the next section.

In this work we limit ourselves to summarising the action of  $\mathbf{T}$  on all vertices and self-energies that are relevant for QCD corrections to any process. We will explicitly separate

$$\begin{aligned}
 & R_{T^{\text{os}}} \left[ \text{diagram} \right] = \text{diagram} \\
 & - \text{diagram} \left( P_+ \rightarrow \text{diagram} \Big|_{p=p^{\text{os}}} + P_- \rightarrow \text{diagram} \Big|_{p=-p^{\text{os}}} + (p - b\gamma^0 p^{\text{os}})^\mu \partial_\mu \rightarrow \text{diagram} \Big|_{\substack{p=0 \\ \mathbf{m}=0 \\ m_{\text{UV}}}} \right) \\
 & - \text{diagram} \Big|_{q=0} - q^\mu \partial_\mu \text{diagram} \Big|_{q=0} - \frac{1}{2} q^\mu q^\nu \partial_\mu \partial_\nu \text{diagram} \Big|_{\substack{q=0 \\ \mathbf{m}=0 \\ m_{\text{UV}}}} \\
 & + \left[ \text{diagram} \left( P_+ \rightarrow \text{diagram} \Big|_{p=p^{\text{os}}} + P_- \rightarrow \text{diagram} \Big|_{p=-p^{\text{os}}} + (p - b\gamma^0 p^{\text{os}})^\mu \partial_\mu \rightarrow \text{diagram} \Big|_{\substack{p=0 \\ \mathbf{m}=0 \\ m_{\text{UV}}}} \right) \right]_{q=0} \\
 & + q^\mu \partial_\mu \left[ \text{diagram} \left( P_+ \rightarrow \text{diagram} \Big|_{p=p^{\text{os}}} + P_- \rightarrow \text{diagram} \Big|_{p=-p^{\text{os}}} + (p - b\gamma^0 p^{\text{os}})^\mu \partial_\mu \rightarrow \text{diagram} \Big|_{\substack{p=0 \\ \mathbf{m}=0 \\ m_{\text{UV}}}} \right) \right]_{q=0} \\
 & + \frac{1}{2} q^\mu q^\nu \partial_\mu \partial_\nu \left[ \text{diagram} \left( \text{diagram} \Big|_{p=0} + p^\mu \partial_\mu \text{diagram} \Big|_{\substack{p=0 \\ \mathbf{m}=0 \\ m_{\text{UV}}}} \right) \right]_{\substack{q=0 \\ \mathbf{m}=0 \\ m_{\text{UV}}}}
 \end{aligned}$$

**Figure 10.** On-shell/soft subtraction for a massive quark self-energy nested within a gluon self-energy connection, performed using the approximation operator  $T^{\text{os}}$ . The four-momentum  $p$  (resp.  $q$ ) corresponds to the external momentum of the inner (resp. outer) self-energy diagram.

$$\begin{aligned}
 & R_{T^{\text{os}}} \left[ \text{diagram} \right] = \text{diagram} \\
 & - \text{diagram} \left( P_+ \rightarrow \text{diagram} \Big|_{p=p^{\text{os}}} + P_- \rightarrow \text{diagram} \Big|_{p=-p^{\text{os}}} + (p - b\gamma^0 p^{\text{os}})^\mu \partial_\mu \rightarrow \text{diagram} \Big|_{\substack{p=0 \\ \mathbf{m}=0 \\ m_{\text{UV}}}} \right) \\
 & - P_+ \text{diagram} \Big|_{q=q^{\text{os}}} - P_- \text{diagram} \Big|_{q=-q^{\text{os}}} - (q - b\gamma^0 q^{\text{os}})^\mu \partial_\mu \text{diagram} \Big|_{\substack{q=0 \\ \mathbf{m}=0 \\ m_{\text{UV}}}} \\
 & + P_+ \left[ \text{diagram} \left( P_+ \rightarrow \text{diagram} \Big|_{p=p^{\text{os}}} + P_- \rightarrow \text{diagram} \Big|_{p=-p^{\text{os}}} + (p - b\gamma^0 p^{\text{os}})^\mu \partial_\mu \rightarrow \text{diagram} \Big|_{\substack{p=0 \\ \mathbf{m}=0 \\ m_{\text{UV}}}} \right) \right]_{q=q^{\text{os}}} \\
 & + P_- \left[ \text{diagram} \left( P_+ \rightarrow \text{diagram} \Big|_{p=p^{\text{os}}} + P_- \rightarrow \text{diagram} \Big|_{p=-p^{\text{os}}} + (p - b\gamma^0 p^{\text{os}})^\mu \partial_\mu \rightarrow \text{diagram} \Big|_{\substack{p=0 \\ \mathbf{m}=0 \\ m_{\text{UV}}}} \right) \right]_{q=-q^{\text{os}}} \\
 & + (q - b\gamma^0 q^{\text{os}})^\nu \partial_\nu \left[ \text{diagram} \left( \text{diagram} \Big|_{p=0} + p^\mu \partial_\mu \text{diagram} \Big|_{\substack{p=0 \\ \mathbf{m}=0 \\ m_{\text{UV}}}} \right) \right]_{\substack{q=0 \\ \mathbf{m}=0 \\ m_{\text{UV}}}}
 \end{aligned}$$

**Figure 11.** On-shell subtraction of a massive quark self-energy correction nested within a massive quark self-energy correction, performed using the approximation operator  $T^{\text{os}}$ . The four-momentum  $p$  (resp.  $q$ ) corresponds to the external momentum of the inner (resp. outer) self-energy diagram.

cases that could be more compactly grouped together for the sake of clarity.

$$\mathbf{T}(\Gamma) = \begin{cases} \hat{T}(\Gamma) = T_0(\Gamma) & \text{for } \Gamma \in V_0 \\ \hat{T}(\Gamma) = \tilde{T}_0(\Gamma) + T_1(\Gamma) - T_1(\tilde{T}_0(\Gamma)) & \text{for } \Gamma \in V_1 \\ \hat{T}(\Gamma) = \tilde{T}_1(\Gamma) + T_2(\Gamma) - T_2(\tilde{T}_1(\Gamma)) & \text{for } \Gamma \in \left\{ \begin{array}{c} \text{---} \circ \text{---} \\ \text{---} \circ \text{---} \end{array} \right\} \\ T^{\text{os}}(\Gamma) = \sum_{\sigma \in \{\pm 1\}} (T^{\text{os},\sigma} - T_1 T^{\text{os},\sigma})(\Gamma) + T_1(\Gamma) & \text{for } \Gamma \in \left\{ \begin{array}{c} \text{---} \circ \text{---} \\ \text{---} \circ \text{---} \end{array} \right\} \end{cases} \quad (4.26)$$

where  $V_0$  and  $V_1$  are the vertices with *true*, *local* dod being equal to 0 and 1 respectively, that is

$$V_0 = \left\{ \begin{array}{c} \begin{array}{ccccccc} \text{---} \circ \text{---} & \text{---} \circ \text{---} & \text{---} \circ \text{---} & \text{---} \circ \text{---} & \text{---} \circ \text{---} & \text{---} \circ \text{---} & \text{---} \circ \text{---} \\ \text{---} \circ \text{---} & \text{---} \circ \text{---} & \text{---} \circ \text{---} & \text{---} \circ \text{---} & \text{---} \circ \text{---} & \text{---} \circ \text{---} & \text{---} \circ \text{---} \end{array} \\ \text{---} \circ \text{---} & \text{---} \circ \text{---} & \text{---} \circ \text{---} & \text{---} \circ \text{---} & \text{---} \circ \text{---} & \text{---} \circ \text{---} & \text{---} \circ \text{---} \end{array} \right\}$$

where the last two vertices could be seen as an outlier as it has an *apparent* dod of 1, while an exact investigation of its UV behaviour reveals it is logarithmic. All other vertices (e.g. the vertex connecting one (three) gluon with three (one) electro-weak bosons) are identically zero due to their colour structure. The linearly-divergent vertices all involve the interaction of bosons and ghosts, i.e.

$$V_1 = \left\{ \begin{array}{cccc} \text{---} \circ \text{---} & \text{---} \circ \text{---} & \text{---} \circ \text{---} & \text{---} \circ \text{---} \end{array} \right\}. \quad (4.27)$$

We see that the subtraction of every divergent 1PI is performed using  $\hat{T}$  while for fermionic self-energy corrections (both massive and massless),  $T^{\text{os}}$  should be used. For a massless self-energy correction  $\Sigma$ , one can easily see that  $T^{\text{os}}(\Sigma) = \hat{T}(\Sigma)$ . Finally, the construction of OS counterterms for massive gauge bosons is left to future work, although a similar construction will apply in that case as well.

## 5 Localised renormalisation

The  $\mathbf{T}$  approximation operator satisfies the first two constraints laid out in section 3.2. Specifically,  $R(\Gamma)$ , for non-exceptional external momenta, is integrable. After the  $R$ -operation is applied to each interference diagram (as specified in section 3.3), the Local Unitarity representation that is constructed from such subtracted interference diagrams is also integrable. In summary,  $\mathbf{T}$  satisfies all *local* requirements.

On the other hand, *integrated-level* constraints should also be satisfied by  $\mathbf{T}$ , and specifically, as laid out in section 3.2, we want the renormalisation operator  $K = \mathbf{T} + \bar{K}$  to reproduce the hybrid  $\overline{\text{MS}}$ +OS scheme, and  $\bar{K}$  to be obtainable with minimal analytic work, that is through the computation of single-scale vacuum diagrams. We will achieve these goals in this section.

## 5.1 Integrated counterterms

We start by discussing the integrated version of  $\mathbf{T}(\Gamma)$ , which we denote with  $\langle \mathbf{T}(\Gamma) \rangle$ , where we consider the analytic integration of  $\Gamma$  in  $d = 4 - 2\epsilon$  dimensions, which can be formally written as a Laurent series in the dimensional regulator  $\epsilon$ :

$$\langle \Gamma \rangle = \left( \frac{\mu_r^2}{4\pi e^{-\gamma_E}} \right)^{L\epsilon} \int \left[ \prod_{i=1}^L d^{4-2\epsilon} k_i \right] \Gamma(k_1, \dots, k_L) = \sum_{k=-\infty}^{+\infty} \alpha_k \epsilon^k, \quad (5.1)$$

where  $\mu_r$  is the renormalisation scale,  $L$  is the loop count of the graph  $\Gamma$  and the expansion coefficients  $\alpha_k$  are tensors function of internal masses and external momenta, and the normalisation is chosen so as to facilitate enforcing  $\overline{\text{MS}}$  conventions on  $\langle \Gamma \rangle$ .

Because three operators,  $T, \tilde{T}, T^{\text{os}}$  participate in the definition of  $\mathbf{T}(\Gamma)$ , we will devote one section for each operator's integrated counterpart,  $\langle T(\Gamma) \rangle, \langle \tilde{T}(\Gamma) \rangle$ , and  $\langle T^{\text{os}}(\Gamma) \rangle$ .

### 5.1.1 Integrated UV counterterms

We start by discussing  $T(\Gamma)$ . One particular advantage of the local operator  $T$  is that its analytic computation  $\langle T(\Gamma) \rangle$  only involves single-scale massive tensor vacuum graphs and it can be performed in  $d = 4 - 2\epsilon$  dimensional Minkowski space using traditional techniques. Specifically, each local counterterm originating from  $T(\Gamma)$  is of the form

$$T(\Gamma) = \frac{N(\{p_j\}, \{k_i\}, \mathbf{m})}{\prod_{e \in \mathbf{e}} (q_e(\{k_i\})^2 - m_{\text{uv}}^2)^{\alpha_e}}, \quad (5.2)$$

where  $q(\{k_i\})$  is a linear combination of the loop momenta which does not depend on the external momenta  $\{p_j\}$  or the masses  $\mathbf{m}$ , and  $N$  is a polynomial, tensorial numerator in its input. Their integrated counterparts simply read

$$\langle T(\Gamma) \rangle = \left( \frac{\mu_r^2}{4\pi e^{-\gamma_E}} \right)^{L\epsilon} \int \left[ \prod_{i=1}^L d^{4-2\epsilon} k_i \right] \frac{N(\{p_j\}, \{k_i\}, \mathbf{m})}{\prod_{e \in \mathbf{e}} (q_e(\{k_i\})^2 - m_{\text{uv}}^2)^{\alpha_e}}, \quad (5.3)$$

Our current implementation offers full support for these computations up to and including three-loop amplitudes. Note that in principle, this can be extended to four loops [84] and beyond. Below we sketch the construction of our automated setup.

The first step is to tensor reduce the analytic integrand in order to obtain scalar integrands. Since the integral is a vacuum bubble, all tensor structures reduce to combinations of the metric. For example, for a rank two integral:

$$\Gamma^{\mu\nu} = Ag^{\mu\nu} = \frac{\Gamma_{\alpha}^{\alpha}}{d} g^{\mu\nu} \quad (5.4)$$

and for a rank four integral (odd ranks are 0 as there is no possible tensor basis):

$$\begin{aligned} \Gamma^{\mu\nu\rho\sigma} = Ag^{\mu\nu}g^{\rho\sigma} + Bg^{\mu\rho}g^{\nu\sigma} + Cg^{\mu\sigma}g^{\nu\rho} &= \frac{1}{(-1+d)d(2+d)} \\ &\times \left( \left( (1+d)\Gamma_{\alpha\beta}^{\alpha\beta} - \Gamma_{\alpha\beta}^{\alpha\beta} - \Gamma_{\beta\alpha}^{\alpha\beta} \right) g^{\mu\nu}g^{\rho\sigma} \right. \\ &+ \left( (1+d)\Gamma_{\alpha\beta}^{\alpha\beta} - \Gamma_{\alpha\beta}^{\alpha\beta} - \Gamma_{\beta\alpha}^{\alpha\beta} \right) g^{\mu\rho}g^{\nu\sigma} \\ &\left. + \left( (1+d)\Gamma_{\beta\alpha}^{\alpha\beta} - \Gamma_{\alpha\beta}^{\alpha\beta} - \Gamma_{\alpha\beta}^{\alpha\beta} \right) g^{\mu\sigma}g^{\nu\rho} \right). \end{aligned} \quad (5.5)$$



With increasing tensor rank, the number of possible metric structures  $n$  grows exponentially (rank 6 gives  $n = 15$ , rank 8 gives  $n = 105$ ). A naive tensor reduction algorithm would have to solve an  $n \times n$  linear system, which is slow for high rank (although this only needs to be performed once when generating the LU integrand for a particular process). An improved algorithm that exploits the underlying symmetry group and symmetries of the momenta that the indices belong to was derived in ref. [85] and is used in our implementation.

All up to three-loop vacuum graphs are linear combinations (with tensorial coefficients) of the following three topologies:


(5.6)

since all other topologies can be reproduced from the above three by setting certain edge powers to zero. For the three topologies, the denominator momenta form a complete basis for scalar products. As a result, all scalar products in the numerator can be rewritten as a polynomial in the propagator denominators.

The resulting integrals with numerator 1 and various powers of the denominator can be reduced to a set of master integrals using integration-by-parts (IBP) identities [86]. We use LiteRed [87, 88] to generate a parametric reduction for each of the three topologies. The resulting 7 master integrals have been taken from the literature [89, 90] with sufficiently deep expansions in  $\epsilon$  for three-loop computations. The IBP reduction and master integral computation has been verified by comparing various numerator and denominator configurations with numerical results from pySecDec [91].

### 5.1.2 Integrated spurious soft subtraction counterterms

In massless gauge theories, all soft counterterms integrate to zero. This means that at the integrated level,

$$\langle \hat{T}_{\text{dod}}(\Gamma) \rangle = \langle T_{\text{dod}}(\Gamma) \rangle - \langle T_{\text{dod}}(\tilde{T}_{\text{dod}-1}(\Gamma)) \rangle. \tag{5.7}$$

which only requires the analytic integration of one-scale vacuum bubbles.

The reason why  $\langle \tilde{T}_{\text{dod}-1}(\Gamma) \rangle = 0$  can be traced back to gauge invariance. According to section 4.4, we only need to study the cases in which  $\Gamma$  is a gluonic, fermionic or ghost self-energy and that in which  $\Gamma$  is a three vertex connecting bosons and ghosts. If

- $\Gamma$  is a self-energy, then  $\langle \tilde{T}_{\text{dod}-1}(\Gamma) \rangle = 0$  for otherwise radiative correction would generate a mass for the gluon, massless quark or ghost, which is protected against by gauge invariance.
- $\Gamma$  is a gluonic three-vertex, then  $\langle \tilde{T}_{\text{dod}-1}(\Gamma) \rangle = 0$  is a tensor with three indices and does not depend on any four-momentum. Thus it allows no Lorentz decomposition and it must be a vanishing tensor. For the same reason, if  $\Gamma$  is a vertex at which a ghost, an anti-ghost and a gluon meet, then  $\langle \tilde{T}_{\text{dod}-1}(\Gamma) \rangle = 0$ .
- $\Gamma$  is a vertex coupling three gauge bosons (of any type), we can iterate the argument that we introduced for the three gluons:  $\langle \tilde{T}_{\text{dod}-1}(\Gamma) \rangle = 0$  is a tensor with three

indices and that does not depend on any four momentum, and thus it is zero at the integrated level.

### 5.1.3 Integrated OS counterterms

Consider now a two point function subgraph  $\Sigma$ . For the OS subtraction operator we will show that while  $\langle T^{\text{os}}(\Sigma) \rangle$  cannot be fully written in terms of one-scale vacuum diagrams,  $\langle T^{\text{os}}(\Sigma) \rangle - \delta m^{\text{os}}$  can, where  $\delta m^{\text{os}}$  is the OS renormalised mass correction. Writing the expression of  $T^{\text{os}}$  in terms of  $T$  and  $T^{\text{os}\pm}$ , we get

$$\langle T^{\text{os}}(\Sigma) \rangle = \frac{1}{2} \langle T^{\text{os}+}(\Sigma) \rangle + \frac{1}{2} \langle T^{\text{os}-}(\Sigma) \rangle - \frac{1}{2} \langle T(T^{\text{os}+}(\Sigma)) \rangle - \frac{1}{2} \langle T(T^{\text{os}-}(\Sigma)) \rangle + \langle T(\Sigma) \rangle, \quad (5.8)$$

which shows we only need to discuss  $\langle T^{\text{os}\pm}(\Sigma) \rangle$ , as all other integrated counterterms are of the form discussed in section 5.1.1. It is also clear that  $\langle T^{\text{os}\pm}(\Sigma) \rangle$  cannot be expressed as a one-scale vacuum diagram and that it is not identically zero, unlike soft counterterms. Instead,  $T^{\text{os}\pm}$  corresponds to the self-energy being evaluated at an on-shell momentum, and being projected on the subspaces identified by  $P_{\pm}$ . Thus, it is intimately related with the on-shell behaviour of the resummed fermionic propagator. We now consider the Lorentz decomposition of the integrated self-energy  $\langle \Sigma \rangle$ :

$$\langle \Sigma \rangle(p, \mathbf{m}) = \not{p} \Sigma_{\psi}(p^2, \mathbf{m}) + m \mathbb{1} \Sigma_m(p^2, \mathbf{m}). \quad (5.9)$$

$\Sigma_{\psi}$  and  $\Sigma_m$  are scalar functions of  $p^2$  and of the mass vector  $\mathbf{m}$ . Evaluating this expression for  $p = p^{\text{os}} = (m, 0, 0, 0)$ , we obtain

$$\langle \Sigma \rangle(p^{\text{os}}, \mathbf{m}) = \not{p}^{\text{os}} \Sigma_{\psi}(m^2, \mathbf{m}) + m \mathbb{1} \Sigma_m(m^2, \mathbf{m}). \quad (5.10)$$

We have that  $\not{p}^{\text{os}} = m \gamma^0$ . The value of  $\Sigma_{\psi}(m^2, \mathbf{m})$  and  $\Sigma_m(m^2, \mathbf{m})$  defines the renormalisation constants of the field and mass in the OS scheme. Inserting the decomposition of  $\langle \Sigma \rangle(p, \mathbf{m})$  into  $\langle T^{\text{os}\pm}(\Sigma) \rangle$ , we obtain

$$\frac{1}{2} (\langle T^{\text{os}+}(\Sigma) \rangle + \langle T^{\text{os}-}(\Sigma) \rangle) = m \left( \Sigma_{\psi}(m^2, \mathbf{m}) + \Sigma_m(m^2, \mathbf{m}) \right) = \delta m^{\text{os}, \Sigma}. \quad (5.11)$$

which agrees with the renormalisation expressions given in e.g. ref. [92]. In other words, the integrals in  $\langle T^{\text{os}}(\Sigma) \rangle$ , whose integration involves the computation of multi-scale integrals, actually reproduce the OS mass correction to the fermionic propagator. Unfolding the action of  $T$ , we can finally write a compact and more explicit formula for the full integrated  $\langle T^{\text{os}}(\Sigma) \rangle$ :

$$\langle T^{\text{os}}(\Sigma) \rangle = \delta m^{\text{os}, \Sigma} + (p - \gamma^0 p^{\text{os}})^{\mu} \left\langle \frac{\partial}{\partial p^{\mu}} \Sigma \Big|_{\substack{p=0, \\ \mathbf{m}=0, \\ m_{uv}}} \right\rangle. \quad (5.12)$$

The last term on the right-hand side of eq. (5.12) is a one-scale vacuum diagram, and the discussion of section 5.1.1 applies. This concludes our discussion of the integrated version of  $T^{\text{os}}$ . We have shown that, up to single-scale vacuum integrals,  $\langle T^{\text{os}}(\Sigma) \rangle$  is the correction to the fermion mass in the OS scheme. As discussed in the next section 5.2, we will use this fact to automatically reproduce the hybrid  $\overline{\text{MS}} + \text{OS}$  scheme.

## 5.2 Localised renormalisation in the hybrid $\overline{\text{MS}}$ + OS scheme

Having determined what the integrated version of any counterterm  $\langle \mathbf{T}(\Gamma) \rangle$  is, we are ready to discuss the value  $\bar{K}(\Gamma)$  should take in order to reproduce the  $\overline{\text{MS}}$  + OS scheme at the integrated level.  $\bar{K}(\Gamma)$  is thus determined by constraining  $K(\Gamma) = \mathbf{T}(\Gamma) + \bar{K}(\Gamma)$  to reproduce the desired scheme. We will show that

- $\bar{K}(\Gamma)$  can be entirely written in terms of integrated one-scale vacuum bubbles with the  $\overline{\text{MS}}$  integration measure, showing that the constraint of minimal analytic work is satisfied.
- Given the above  $\bar{K}(\Gamma)$ , the mass is renormalised in the OS scheme directly through the  $\delta m^{\text{os}}$  piece participating in the definition of  $T^{\text{os}}$ , whereas fields and couplings are renormalised in  $\overline{\text{MS}}$ .
- Couplings can be redefined in order to reproduce OS renormalisation of fields and  $\overline{\text{MS}}$  renormalisation of vertices.

Furthermore, because  $K(\Gamma)$  is required to have a local representation, much like  $\mathbf{T}(\Gamma)$ ,  $\bar{K}(\Gamma)$  also needs to have a local representation. Therefore, we will talk of localised renormalisation, for three reasons: a) renormalisation counterterms are localised *within the graph* by the  $R$ -operation, b)  $\overline{\text{MS}}$  counterterms will be localised by multiplying them with convergent, normalised tadpoles, c) OS mass counterterms will be localised by the definition of  $T^{\text{os}}$  itself, which provides a local representation of  $\delta m^{\text{os}}$ .

In summary, the full, carefully-constructed  $K$  will satisfy all four constraints laid out in section 3.2.

### 5.2.1 Field and coupling renormalization in the $\overline{\text{MS}}$ scheme

In this section we will determine  $\bar{K}$  by imposing the constraint that fields and couplings are renormalised in the  $\overline{\text{MS}}$  scheme. In the next section, we will argue that this also reproduces OS renormalisation of masses. We will start by determining the  $K^{\overline{\text{MS}}}$  operation, which renormalises a graph  $\Gamma$  in the  $\overline{\text{MS}}$ . Then, we will use  $K^{\overline{\text{MS}}}$  to construct  $\bar{K}$ .

We denote by  $K^{\overline{\text{MS}}}(\langle \Gamma \rangle)$  the  $\overline{\text{MS}}$  implementation of the  $K$  operator acting on the  $d$ -dimensional integral of the graph which is defined so as to remove all the poles in the Laurent series of  $\langle \Gamma \rangle$ :

$$K^{\overline{\text{MS}}}(\langle \Gamma \rangle) := \sum_{k=-\infty}^{-1} \alpha_k \epsilon^k. \tag{5.13}$$

Our objective is to build the local equivalent  $\bar{K}^{\overline{\text{MS}}}(\Gamma)$  of the integrated-level definition  $K^{\overline{\text{MS}}}(\langle \Gamma \rangle)$  above so that our subtraction terms both locally remove UV singularities and also immediately yield results where fields and couplings are renormalised in  $\overline{\text{MS}}$ . We let the local version of the  $\overline{\text{MS}}$  operator be the sum of a subtraction operator  $T$ , that captures the UV divergent part of a graph, plus a finite part  $\bar{K}^{\overline{\text{MS}}}$ , so that

$$K^{\overline{\text{MS}}}(\Gamma) = T(\Gamma) + \bar{K}^{\overline{\text{MS}}}(\Gamma). \tag{5.14}$$

In the following, we will fix  $T$ , the subtraction operator (which can be chosen arbitrarily, for the purposes of this section), and study the finite part  $\bar{K}^{\overline{\text{MS}}}$  that is required for  $K^{\overline{\text{MS}}}$  to be a faithful local representation of the  $\overline{\text{MS}}$  renormalisation operator. In particular, the relation between  $K^{\overline{\text{MS}}}(\Gamma)$  with  $K^{\overline{\text{MS}}}(\langle\Gamma\rangle)$  is simply stated: analytically integrating  $K^{\overline{\text{MS}}}(\Gamma)$  should yield  $K^{\overline{\text{MS}}}(\langle\Gamma\rangle)$ , i.e.

$$K^{\overline{\text{MS}}}(\langle\Gamma\rangle) = \langle K^{\overline{\text{MS}}}(\Gamma) \rangle = \langle T(\Gamma) \rangle + \langle \bar{K}^{\overline{\text{MS}}}(\Gamma) \rangle. \tag{5.15}$$

Now observe that the local counterterm  $Z(\gamma)$  in the  $R$ -operation as defined in eq. (3.2) captures the divergence of all loop momenta of  $\gamma$  going to infinity, minus its UV subdivergences. The poles in  $\epsilon$  from the  $d = 4 - 2\epsilon$  dimensional integral of  $Z(\gamma)$ , that is  $\langle Z(\gamma) \rangle$ , have coefficients that are polynomial in the external momenta and internal masses [70]. The same must hold for  $K(\Gamma)$ . Thus, we obtain the following key relation:

$$K^{\overline{\text{MS}}}(\langle\Gamma\rangle) = K^{\overline{\text{MS}}}(\langle T(\Gamma) \rangle). \tag{5.16}$$

We are finally ready to clarify the effect of the constraint from eq. (5.15) on  $\bar{K}^{\overline{\text{MS}}}$ . We can simply solve for  $\langle \bar{K}^{\overline{\text{MS}}}(\Gamma) \rangle$  and use eq. (5.16) to express the argument of  $K^{\overline{\text{MS}}}$  in terms of the approximation  $T(\Gamma)$

$$\langle \bar{K}^{\overline{\text{MS}}}(\Gamma) \rangle = K^{\overline{\text{MS}}}(\langle\Gamma\rangle) - \langle T(\Gamma) \rangle = (K^{\overline{\text{MS}}} - \mathbb{1})\langle T(\Gamma) \rangle. \tag{5.17}$$

Any local operator  $K^{\overline{\text{MS}}}(\Gamma)$  as in eq. (5.14) for fixed arbitrary subtraction operator  $T(\Gamma)$  must have its local renormalisation piece  $\bar{K}^{\overline{\text{MS}}}(\Gamma)$  satisfying the integrated level constraint of eq. (5.17). The action of the operator  $(\mathbb{1} - K^{\overline{\text{MS}}})$  can be understood as removing the pole parts in  $\epsilon$  of the analytic  $d$ -dimensional integral  $\langle T(\Gamma) \rangle$ , as it is the complement of eq. (5.13):

$$(\mathbb{1} - K^{\overline{\text{MS}}})(\langle\Gamma\rangle) := \alpha_0 + \alpha_1\epsilon + \dots \tag{5.18}$$

Given the integrated-level constraint of eq. (5.17), we now detail the construction of a local operator  $\bar{K}^{\overline{\text{MS}}}(\Gamma)$  that satisfies it. In practice, this means finding a function of the loop momenta  $k_1, \dots, k_L$  of the graph  $\Gamma$  whose integral yields the right-hand side of eq. (5.17), which is assumed as input. The simplest way to achieve this is to take the integrated level result and multiply it by any function of the loop momenta that is normalised to one. For example, we choose to define the *local* version  $\bar{K}(\Gamma)$  of the integrated quantity  $\langle \bar{K}(\Gamma) \rangle$  using a scalar vacuum graph as normalisation factor:

$$\bar{K}^{\overline{\text{MS}}}(\Gamma)(k_1, \dots, k_L) = \langle \bar{K}^{\overline{\text{MS}}}(\Gamma) \rangle \left( \prod_{i=1}^L N(k_i) \right), \quad \int d^4k N(k) = \int d^4k \frac{2i(4\pi)^2 m_{\text{UV}}^2}{(k^2 - m_{\text{UV}}^2)^3} = 1. \tag{5.19}$$

With this final result, we have constructed the subtraction operator  $K^{\overline{\text{MS}}}(\Gamma)$ , which is the local equivalent to the traditional integrated-level  $\overline{\text{MS}}$  subtraction operator  $K^{\overline{\text{MS}}}(\langle\Gamma\rangle)$ , but with the additional merit of locally removing UV divergences. Its final expression reads:

$$K^{\overline{\text{MS}}}(\Gamma) = T_{\text{dod}}(\Gamma) - (\mathbb{1} - K^{\overline{\text{MS}}})(\langle T_{\text{dod}}(\Gamma) \rangle) \left( \prod_{i=1}^{n_l} N(k_i) \right). \tag{5.20}$$

We stress that the integrated counterterm  $\langle \bar{K}^{\overline{\text{MS}}}(\Gamma) \rangle$  captures more than just scheme-dependent contributions; it also reproduces the rational terms [93, 94] (both  $R_1$  and  $R_2$ , in

the one-loop terminology of ref. [95]) of purely  $(d-4)$ -dimensional origin which cannot possibly be captured by the numerical four-dimensional integration of  $\Gamma - T_{\text{dod}}(\Gamma)$ , and are thus traditionally cumbersome to account for in purely numerical approaches. In other words, the choice of  $K(\Gamma) = T_{\text{dod}}(\Gamma)$  would by itself *not* correspond to a consistent renormalisation scheme because the local subtraction operator violates the gauge symmetry of the SM [96] and would effectively introduce new terms to the Lagrangian. This fact is made clear when considering for example the leading-order contribution to the loop-induced process  $gg \rightarrow HH$  which receives no contribution from any renormalisation counterterm. Yet, this process contains logarithmically UV divergent graphs, which in turn induce rational and  $m_{\text{UV}}$ -independent finite contributions from  $\langle \bar{K}(\Gamma) \rangle$ . As argued in e.g. ref. [97], such contributions could never be captured by a computation without the introduction of any UV regulator.

In our construction of the  $R$ -operator, we use the ‘t Hooft Veltman (HV) conventions for dimensional regularisation (see details of this convention in ref. [98]), meaning that indices and momenta external to  $\Gamma$  are treated strictly in 4 dimensions (as they are numerically integrated), whereas internal ones are in  $d = 4 - 2\epsilon$  dimensions. This implies that the  $d$ -dimensional conventions are effectively different for each term generated by the  $R$ -operation, since the distinction between internal and external is governed by which part of the graph is in argument of the  $K$ -operator and the remaining graph. However, since the  $(\mathbb{1} - K^{\overline{\text{MS}}})$  removes the poles, a pole can never hit the remaining graph computed in 4 dimensions. Thus, because the cross-section is finite for  $d = 4$ , using HV dimensional regularisation yields the same result as if it were computed by keeping *all* momenta and indices in  $d = 4 - 2\epsilon$  dimension (i.e. Conventional Dimensional Regularisation (CDR)) throughout the implementation of the  $R$ -operation.

### 5.2.2 Summary: the $\bar{K}$ operator

This completes our construction of  $R^{\overline{\text{MS}}}$ , a local UV subtraction procedure that automatically yields results renormalised in  $\overline{\text{MS}}$ . We can now apply it to our specific case to achieve  $\overline{\text{MS}}$  renormalisation of fields and couplings; given a graph  $\Gamma$ , we define

$$\bar{K}(\Gamma) = -(\prod_{i=1}^{n_l} N(k_i)) (\mathbb{1} - K^{\overline{\text{MS}}}) \langle T(\Gamma) - T(\hat{T}(\Gamma)) \rangle \quad (5.21)$$

if  $\Gamma \in V_0, V_1$  (as defined in section 4.4) or if  $\Gamma$  is a ghost or gluonic self-energy. For a massive fermionic self-energy  $\Sigma$ , the  $\hat{T}$  operator inside  $\bar{K}$  is substituted with  $T^{\text{os}}$ :

$$\bar{K}(\Sigma) = -(\prod_{i=1}^{n_l} N(k_i)) (\mathbb{1} - K^{\overline{\text{MS}}}) \langle T(\Sigma) - T(T^{\text{os}}(\Sigma)) \rangle. \quad (5.22)$$

This concludes the explanation of our choice for  $\bar{K}$ .

### 5.2.3 Mass and gauge field renormalisation in the OS scheme

Having now constructed  $\bar{K}$  so as to reproduce  $\overline{\text{MS}}$ -renormalised cross-sections, we set ourselves to reproducing the common OS renormalisation conditions for particle masses. The key observation is that in eq. (5.22), we omitted the  $\overline{\text{MS}}$  renormalisation of  $T^{\text{os}}(\Sigma)$ , which does contribute to the definition of  $K$ . The reason behind this omission is that the integrated version of  $T^{\text{os}}(\Sigma)$  automatically reproduces the renormalised mass correction in the

OS scheme, as we will now demonstrate. We observe that for a fermionic self-energy  $\Sigma$ , the renormalisation operator yields

$$\langle K(\Sigma) \rangle = \delta m^{\text{os}} + \not{p} \delta Z^{\overline{\text{MS}}}, \tag{5.23}$$

having used the definition of  $\bar{K}$  from the previous section and the integrated level result of section (5.1.3). In short, our definition of  $\bar{K}$  and  $\mathbf{T}$  automatically reproduces OS renormalisation conditions for particle masses, and  $\overline{\text{MS}}$  renormalisation for all fields and vertices [92].

We now briefly explain how to achieve OS renormalisation of not only masses but also gauge fields, with  $\overline{\text{MS}}$  renormalisation of vertices. The conversion to such a scheme is especially straightforward because we have already renormalised the masses in the OS scheme, and we would now only have to change the renormalisation of gauge fields from  $\overline{\text{MS}}$  to the OS scheme. To this end, observe that the renormalisation constants of the coupling, gauge fields and vertices are related through the Slavnov-Taylor identities. This implies that when dressing all vertices with the renormalisation counterterm of their respective coupling, the dependence on the gauge field renormalisation constants completely disappears. This is not immediately manifest in traditional computations that consider truncated amplitudes, because in that case the gauge field renormalisation constants must be added for each external gauge boson of the amplitude considered, in accordance with the LSZ reduction formula (see discussion around eq. 2.83 of ref. [99]). In contrast, the LU representation explicitly retains the self-energy corrections of external particles since their local expression is necessary for IR cancellations. This implies that within LU, changes in both coupling and gauge field renormalisation conditions can be captured at once by only adjusting the expression of the renormalised couplings. More precisely, transitioning from pure  $\overline{\text{MS}}$  to the hybrid  $\overline{\text{MS}}$ +OS scheme for the strong coupling  $g_s$  and gluon field renormalisation  $Z_g$  can be achieved using the following substitution:

$$g_s^{\overline{\text{MS}}} \rightarrow g_s^{\overline{\text{MS}}+\text{OS}} = g_s^{\overline{\text{MS}}} \left( \frac{Z_g^{\text{OS}}}{Z_g^{\overline{\text{MS}}}} \right)^{-\frac{3}{2}}, \tag{5.24}$$

where the quantity in parenthesis is finite, process independent and thus only needs to be computed once. In practice, such hybrid scheme for coupling renormalisation is often referred to as a *decoupling scheme* because it removes the *explicit* dependence from massive particles in the running of the coupling, see refs. [100–102]. Since each supergraph necessarily factorises a specific combination of couplings that our LU construction readily renormalises in  $\overline{\text{MS}}$  by default, then the substitution of eq. (5.24), if desired, is trivial to perform in a final post-processing step, completely independently of the  $R$ -operation.

## 6 Results

The generalisation of the LU representation in the presence of raised propagators and its renormalisation procedure presented in this work is necessary for tackling the computation of any complete physical cross-section beyond the NLO accuracy. The cross-sections presented in this section are already known and not directly relevant for phenomenology,

Parameter	value	Parameter	value	Parameter	value
$m_t^{(\overline{\text{MS}})}(\mu_r^2) = m_t^{(\text{OS})}$	173.0	$\Gamma_t$	0.0	$y_t^{(\overline{\text{MS}})}$	$m_t^{(\overline{\text{MS}})} \frac{\sqrt{2}}{v_{\text{ev}}}$
$m_H$	125.0	$m_Z$	91.188	$G_F$	$1.16639 \cdot 10^{-5}$
$\alpha_s^{(\overline{\text{MS}})}(\mu_r^2) = \alpha_s(m_Z^2)$	0.118	$\alpha_{\text{QED}}^{-1}$	132.507	$n_f$	1 ( $Q_q = 1/3$ )

**Table 1.** Common SM parameters used for obtaining all numerical results presented in section 6. Dimensionful parameters are given in GeV. Notice that for simplicity,  $\alpha_s^{(\overline{\text{MS}})}$ ,  $m_t^{(\overline{\text{MS}})}$  and  $y_t^{(\overline{\text{MS}})}$  running are disabled for the demonstrative results of this section.

however they stand as the first NNLO cross-sections ever computed fully numerically in momentum space. The aim of this section is therefore to demonstrate the viability and correctness of this generalisation. We also illustrate LU applications at NLO for  $1 \rightarrow 3$  processes with final-state observable density functions that act both on the kinematics and on the selection of Cutkosky cuts considered. Such non-trivial examples were lacking in our original publication of ref. [46], which introduced LU. Finally we conclude this section with a study of UV and IR limits of individual supergraphs contributing up to N3LO. This highlights our automated testing procedures and provides an overview of the current performance of our implementation.

All results within this section are obtained in the SM with the following choice of parameters:

Throughout this section, we will detail results for individual supergraphs which are not individually gauge-invariant, and are computed in the Feynman gauge. Whenever  $n_f = 1$  contributions are reported, it refers only to the contribution from one massless fermion to the gluon self-energy, i.e. there is always a single quark connected to the photon, and with an electric charge of  $Q_q = 1/3$ . Finally, note that depending on what is most convenient to compare against we report result from either  $e^+e^- \rightarrow \gamma \rightarrow X$  or  $\gamma^* \rightarrow X$ , with  $p_{e^+} = (E/2, 0, 0, E/2)$ ,  $p_{e^-} = (E/2, 0, 0, -E/2)$  and  $p_{\gamma^*} = (E, 0, 0, 0)$ . Given that we are only considering QCD corrections, the *inclusive* cross-sections of both processes can be related at any perturbative order through the following simple relation reproducing the effect of the closed lepton trace:

$$\sigma_{e^+e^- \rightarrow \gamma \rightarrow X} = \frac{2}{3} \frac{g_e^2 Q_e^2}{E^3} \sigma_{\gamma^* \rightarrow X}, \tag{6.1}$$

with  $g_e^2 Q_e^2 = 4\pi\alpha_{\text{QED}}$  for the coupling strength of the electron to the photon. The conventional conversion factor of  $1[\text{pb}] = 0.389379304 \cdot 10^9 [\text{GeV}^{-2}]$  is also applied in the report of our results for  $\sigma_{e^+e^- \rightarrow \gamma \rightarrow X}$ .

In all cases, we checked that the result for each individual supergraph is independent of the arbitrary choice of  $m_{\text{UV}}$  introduced in the local UV subtraction counterterms, and which we set equal to  $\mu_r$  by default.

### 6.1 Inclusive NNLO cross-section of $\gamma^* \rightarrow jj$ and $\gamma^* \rightarrow t\bar{t}$

We start by presenting NNLO inclusive cross-sections for the production of a pair of jets and a pair of massive quarks from an off-shell vector current, i.e photon. The observable



function is in this case simply the identity function and the contribution from all Cutkosky cuts of the supergraphs will be retained. In such a case, the introduction of a contour deformation is not necessary since all non-pinched threshold singularities are guaranteed to also cancel in virtue of the general LU pair-wise threshold algebraic cancellation mechanism.

In order to facilitate comparison with the analytic computation of the R-ratio given in ref. [106], we choose here to produce results for the inclusive cross-section of  $\gamma^*(p) \rightarrow jj$  up to order  $\mathcal{O}(\alpha_s^2)$  and renormalised completely in  $\overline{\text{MS}}$  at  $p^2 = \mu_r^2 = (400 \text{ GeV})^2$ . We consider a single massless quark flavour and the running of  $\alpha_s$  is disabled and kept fixed at the value given in table 1. For convenience, we report here the analytical result given in eqs. (5.1) and (5.2) of ref. [106]:

$$\begin{aligned} \sigma_{\gamma^* \rightarrow jj}^{\overline{\text{MS}}}(p^2, \mu_r^2 = p^2) &= \sigma_{\gamma^* \rightarrow d\bar{d}}^{(\text{LO})}(p^2) \\ &\times \left[ 1 + (3C_F) \frac{\alpha_s}{4\pi} + \left( -\frac{3}{2}C_F^2 + C_A C_F \left[ \frac{123}{2} - 44\zeta_3 \right] - C_F n_f [11 - 8\zeta_3] \right) \left( \frac{\alpha_s}{4\pi} \right)^2 + \mathcal{O}(\alpha_s^3) \right] \end{aligned} \quad (6.2)$$

The NNLO cross-section for  $\gamma^*(p) \rightarrow t\bar{t}$  has been computed completely analytically using the optical theorem in refs. [107, 108] (and at  $\mathcal{O}(\alpha_s^3)$  in ref. [109]). The computation of the  $n_f$  part is exact, whereas the rest of the contributions are computed using a Padé approximant interpolating between the threshold and high-energy regimes. The benchmark results reported in table 3 are computed from the analytical formulae presented in refs. [107, 108] that are too long to be reported here. Differential and numerical NNLO results obtained using traditional phase-space subtraction methods have been presented more recently in e.g. refs. [110–113].

We show in table 2 the contribution from each of the seventeen supergraphs listed in figure 12, which make up the cross-section up to order  $\mathcal{O}(\alpha_s^2)$  for this class of processes and renormalised completely in  $\overline{\text{MS}}$ . In the second column of table 2, we also present similar results but for the process  $\gamma^* \rightarrow t\bar{t}$  at  $p^2 = \mu_r^2 = (600 \text{ GeV})^2$ . Cross-sections for external particles whose mass is renormalised in  $\overline{\text{MS}}$  are typically not readily available in the literature since the usual reduction formula of the cross-section in terms of truncated Green’s functions is not directly applicable and amplitude derivatives arise.<sup>1</sup> This is the reason why no comparison benchmark is given in this scheme.

However, as discussed in section 5.2, our final implementation of the  $R$ -operation automatically produces cross-sections in the hybrid  $\overline{\text{MS}}$ +OS scheme, which we denote  $\sigma_{\gamma^* \rightarrow t\bar{t}}^{\left[ \alpha_s^{(\overline{\text{MS}})}, m_t^{(\text{OS})} \right]}$  and where fermion masses (but not fields) are renormalised in the OS scheme. We thus also report in table 3 results in this more common hybrid scheme for both  $p^2 = (400 \text{ GeV})^2$  and  $p^2 = (3000 \text{ GeV})^2$  (with  $\mu_r^2 = m_t^2$ ), and compare them to the analytical benchmark from refs. [107, 108].

At NLO, we also verified that we could obtain the same hybrid scheme result from adding to our pure  $\overline{\text{MS}}$  result the well-known contribution from the one-loop mass renor-

---

<sup>1</sup>Though of little phenomenological relevance, the difficulty in computing the NNLO cross-section  $\sigma_{\gamma^* \rightarrow t\bar{t}}^{(\overline{\text{MS}})}$  renormalised entirely in  $\overline{\text{MS}}$  makes it of theoretical interest and this is why we decided to report it as well in this section.

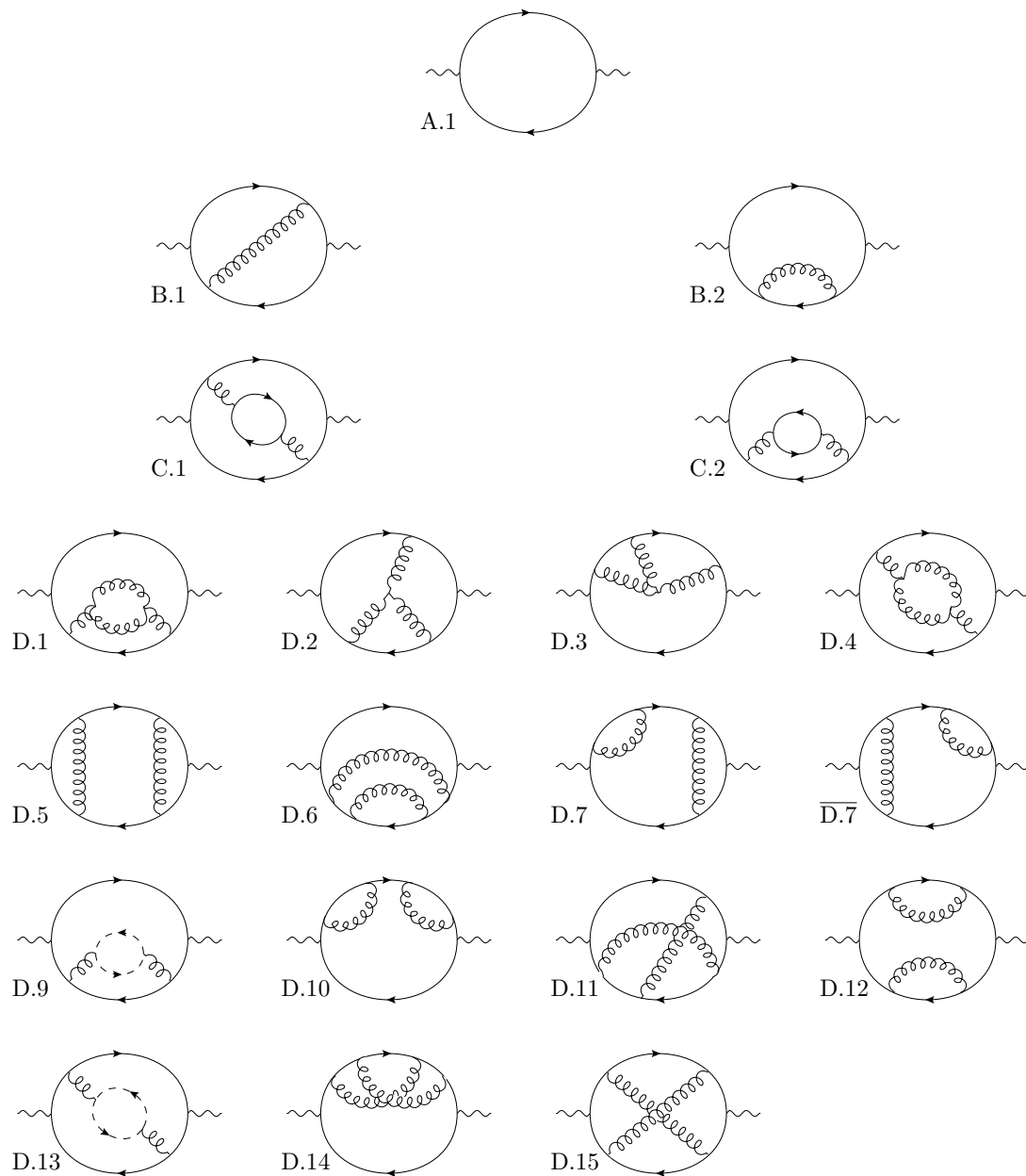


**Figure 12.** All contributing supergraphs to the class of processes  $\gamma^* \rightarrow jj + X$  and  $\gamma^* \rightarrow t\bar{t} + X$  at LO (A.1), NLO (B.i) and NNLO (C.i and D.i). The outer fermion loop is set massless for  $\gamma^* \rightarrow jj + X$  and massive with mass  $m_t$  for  $\gamma^* \rightarrow t\bar{t} + X$ . The NNLO contribution proportional to  $n_f$  only comes from the two supergraphs C.1 and C.2, when the inner fermion loop is always considered massless. We note that supergraphs D.7 and  $\bar{D}.7$  are isomorphic, but we chose to report them separately here because the symmetry from exchanging the two identical external off-shell photons was not considered at generation time.

malisation counterterm  $\delta m_t^{\alpha_s}$ :

$$\delta m_t^{\alpha_s, (OS)} - \delta m_t^{\alpha_s, (\overline{\text{MS}})} = C_F \frac{\alpha_s}{(4\pi)^2} \left( 4 + 3 \log \left( \mu_r^2 / m_t^2 \right) \right). \quad (6.3)$$

This serves as further confirmation that the integrated counterpart of our OS subtraction operator presented in section 5.1.3 does indeed reproduce the traditional NLO QCD top quark mass renormalisation counterterm in the OS scheme.

In all cases, we find agreement at, or better than, the per-mil level, similar to the Monte-Carlo accuracy of the integration of most individual supergraphs, with the exception of those with a central value accidentally close to zero. We note however that there is a small tension in NNLO cross-section of  $\sigma_{\gamma^* \rightarrow t\bar{t}}^{\left[ \alpha_s^{(\overline{\text{MS}})}, m_t^{(OS)} \right]}$  for  $p^2 = \mu_r^2 = (400 \text{ GeV})^2$ . We attribute this to the fact that the result from ref. [107] is not exact, but instead an interpolation between two asymptotic regimes of the top quark velocity  $v$  (threshold production at  $v = 0$  and high-energy limit at  $v = 1$ ). Indeed,  $p^2 = (400 \text{ GeV})^2$  corresponds to a top quark velocity of  $v = 0.5$ , which is therefore not expected to be perfectly captured by expansions around any of the two regimes. This hypothesis is supported by the observation that we find better agreement for the pure  $n_f$  contribution (for which the result given in refs. [107, 108] is exact) and also in the high-energy limit for  $p^2 = (3000 \text{ GeV})^2$ .

SG id	$\Xi$	$\sigma_{\gamma^* \rightarrow jj}^{(\overline{\text{MS}})}$ [GeV <sup>-2</sup> ] $p_{\gamma^*}^2 = \mu_r^2 = (400 \text{ GeV})^2$	$\Delta$ [%]	$\sigma_{\gamma^* \rightarrow t\bar{t}}^{(\overline{\text{MS}})}$ [GeV <sup>-2</sup> ] $p_{\gamma^*}^2 = \mu_r^2 = (600 \text{ GeV})^2$	$\Delta$ [%]
<b>LO</b> $\mathcal{O}(\alpha_s^0)$					
A.1	1	$5.031049 \cdot 10^{-01}$	0.0018	$2.876302 \cdot 10^{+00}$	0.00049
Total		$5.031049 \cdot 10^{-01}$	0.0018	$2.876302 \cdot 10^{+00}$	0.00049
<b>NLO</b> $\mathcal{O}(\alpha_s)$					
B.1	1	$5.03926 \cdot 10^{-02}$	0.0075	$3.48276 \cdot 10^{-01}$	0.023
B.2	2	$-3.14956 \cdot 10^{-02}$	0.018	$-1.46756 \cdot 10^{-01}$	0.059
Total		$1.88970 \cdot 10^{-02}$	0.036	$2.0152 \cdot 10^{-01}$	0.059
Benchmark		$1.889690 \cdot 10^{-02}$	0.00053	N/A	
<b>NNLO</b> $\mathcal{O}(\alpha_s^2)$ ( $n_f = 1$ contribution)					
C.1	1	$-4.66342 \cdot 10^{-04}$	0.019	$-3.2806 \cdot 10^{-03}$	0.066
C.2	2	$3.8448 \cdot 10^{-04}$	0.036	$1.2309 \cdot 10^{-03}$	0.23
Total		$-8.186 \cdot 10^{-05}$	0.20	$-2.0497 \cdot 10^{-03}$	0.17
Benchmark		$-8.1834 \cdot 10^{-05}$	0.036	N/A	
<b>NNLO</b> $\mathcal{O}(\alpha_s^2)$ (all other contributions)					
D.1	2	$-2.30886 \cdot 10^{-03}$	0.017	$-5.4290 \cdot 10^{-03}$	0.15
D.2	2	$6.42018 \cdot 10^{-03}$	0.0055	$4.87662 \cdot 10^{-02}$	0.018
D.3	2	$-6.91254 \cdot 10^{-03}$	0.0046	$-3.09477 \cdot 10^{-02}$	0.024
D.4	1	$3.20278 \cdot 10^{-03}$	0.0084	$2.30085 \cdot 10^{-02}$	0.028
D.5	1	$1.68148 \cdot 10^{-03}$	0.013	$1.33171 \cdot 10^{-02}$	0.045
D.6	2	$6.6698 \cdot 10^{-04}$	0.027	$8.7680 \cdot 10^{-03}$	0.074
D.7	2	$-1.30381 \cdot 10^{-03}$	0.013	$-3.2639 \cdot 10^{-03}$	0.16
$\overline{\text{D.7}}$	2	$-1.30395 \cdot 10^{-03}$	0.013	$-3.2606 \cdot 10^{-03}$	0.16
D.9	2	$-1.6661 \cdot 10^{-04}$	0.064	$-5.135 \cdot 10^{-04}$	0.40
D.10	2	$6.64155 \cdot 10^{-04}$	0.012	$-3.9986 \cdot 10^{-03}$	0.078
D.11	2	$2.34300 \cdot 10^{-04}$	0.031	$1.0696 \cdot 10^{-03}$	0.12
D.12	1	$4.11063 \cdot 10^{-04}$	0.017	$7.6693 \cdot 10^{-03}$	0.035
D.13	1	$2.41514 \cdot 10^{-04}$	0.026	$1.7054 \cdot 10^{-03}$	0.080
D.14	2	$5.8386 \cdot 10^{-05}$	0.088	$4.257 \cdot 10^{-04}$	0.34
D.15	1	$-1.75957 \cdot 10^{-04}$	0.022	$-7.9301 \cdot 10^{-04}$	0.071
Total		$1.40910 \cdot 10^{-03}$	0.056	$5.6524 \cdot 10^{-02}$	0.036
Benchmark		$1.40941 \cdot 10^{-03}$	-0.022	N/A	

**Table 2.** Contributions from individual supergraphs listed in table 12 to the cross-section up to order  $\mathcal{O}(\alpha_s^2)$  (LO+NLO+NNLO) for the processes  $\gamma^* \rightarrow jj$  and  $\gamma^* \rightarrow t\bar{t}$  with  $n_f = 1$  and  $Q_q = 1/3$  and SM parameters as given in table 1.  $\Xi$  denotes the symmetry factor of the supergraph (included in the result reported).  $\Delta$  reports the relative Monte-Carlo error, except for the “Benchmark” entry [106] where it refers to the relative difference w.r.t. the LU result instead.

SG id	$\Xi$	$\sigma_{\gamma^* \rightarrow t\bar{t}}^{[\alpha_s^{(\overline{\text{MS}})}, m_t^{(\text{OS})}]} [\text{GeV}^{-2}]$ $\mu_r^2 = m_t^2, p_{\gamma^*}^2 = (400 \text{ GeV})^2$	$\Delta$ [%]	$\sigma_{\gamma^* \rightarrow t\bar{t}}^{[\alpha_s^{(\overline{\text{MS}})}, m_t^{(\text{OS})}]} [\text{GeV}^{-2}]$ $\mu_r^2 = m_t^2, p_{\gamma^*}^2 = (3000 \text{ GeV})^2$	$\Delta$ [%]
<b>LO</b>		$\mathcal{O}(\alpha_s^0)$			
A.1	1	$1.387586 \cdot 10^{+00}$	0.0011	$1.509262 \cdot 10^{+01}$	0.000064
Total		$1.387586 \cdot 10^{+00}$	0.0011	$1.509262 \cdot 10^{+01}$	0.000064
<b>NLO</b>		$\mathcal{O}(\alpha_s^1)$			
B.1	1	$2.52705 \cdot 10^{-01}$	0.034	$-6.3725 \cdot 10^{-01}$	0.071
B.2	2	$1.80050 \cdot 10^{-01}$	0.049	$1.22702 \cdot 10^{+00}$	0.039
Total		$4.3276 \cdot 10^{-01}$	0.028	$5.8977 \cdot 10^{-01}$	0.11
Benchmark		$4.32831 \cdot 10^{-01}$	-0.018	$5.9047 \cdot 10^{-01}$	-0.12
<b>NNLO</b>		$\mathcal{O}(\alpha_s^2)$ ( $n_f = 1$ contribution)			
C.1	1	$-1.0022 \cdot 10^{-03}$	0.17	$2.6658 \cdot 10^{-02}$	0.059
C.2	2	$-4.6982 \cdot 10^{-03}$	0.081	$-8.388 \cdot 10^{-03}$	0.30
Total		$-5.7004 \cdot 10^{-03}$	0.073	$1.8270 \cdot 10^{-02}$	0.16
Benchmark		$-5.6982 \cdot 10^{-03}$	0.038	$1.8296 \cdot 10^{-02}$	-0.15
<b>NNLO</b>		$\mathcal{O}(\alpha_s^2)$ (all other contributions)			
D.1	2	$3.8886 \cdot 10^{-02}$	0.031	$6.3163 \cdot 10^{-02}$	0.11
D.2	2	$5.6351 \cdot 10^{-03}$	0.14	$-3.52337 \cdot 10^{-01}$	0.027
D.3	2	$1.76075 \cdot 10^{-02}$	0.055	$5.6646 \cdot 10^{-02}$	0.14
D.4	1	$8.8163 \cdot 10^{-03}$	0.078	$-1.83770 \cdot 10^{-01}$	0.023
D.5	1	$9.200 \cdot 10^{-04}$	0.79	$-7.9531 \cdot 10^{-02}$	0.054
D.6	2	$5.1058 \cdot 10^{-03}$	0.15	$1.1244 \cdot 10^{-02}$	0.51
D.7	2	$6.7284 \cdot 10^{-03}$	0.10	$5.2105 \cdot 10^{-02}$	0.094
$\overline{\text{D.7}}$	2	$6.7300 \cdot 10^{-03}$	0.10	$5.2171 \cdot 10^{-02}$	0.094
D.9	2	$2.3361 \cdot 10^{-03}$	0.12	$2.520 \cdot 10^{-03}$	0.73
D.10	2	$3.7418 \cdot 10^{-03}$	0.14	$3.4996 \cdot 10^{-02}$	0.11
D.11	2	$2.0845 \cdot 10^{-03}$	0.083	$2.5486 \cdot 10^{-02}$	0.060
D.12	1	$3.5114 \cdot 10^{-03}$	0.12	$2.8263 \cdot 10^{-02}$	0.10
D.13	1	$8.222 \cdot 10^{-04}$	0.19	$-7.994 \cdot 10^{-03}$	0.13
D.14	2	$1.76075 \cdot 10^{-02}$	0.055	$9.106 \cdot 10^{-03}$	0.19
D.15	1	$-7.242 \cdot 10^{-04}$	0.14	$-1.96633 \cdot 10^{-02}$	0.044
Total		$1.04214 \cdot 10^{-01}$	0.024	$-3.0760 \cdot 10^{-01}$	0.061
Benchmark		$1.0386 \cdot 10^{-01}$	0.34	$-3.0818 \cdot 10^{-01}$	-0.19

**Table 3.** Contributions from individual supergraphs listed in table 12 to the cross-section up to order  $\mathcal{O}(\alpha_s^2)$  for the process  $\gamma^* \rightarrow t\bar{t}$  and two different energies  $p_{\gamma^*}^2 = (400 \text{ GeV})^2$  and  $p_{\gamma^*}^2 = (360 \text{ GeV})^2$ . The strong coupling is renormalised in  $\overline{\text{MS}}$  with  $\mu_r^2 = m_t^2$  and the top mass in the OS scheme.  $\Xi$  denotes the symmetry factor of the supergraph (included in the result reported).  $\Delta$  reports the relative Monte-Carlo error, except for the “Benchmark” entry [107, 108] where it refers to the relative difference w.r.t. the LU result instead.

We find no sign of large gauge cancellation given that the maximal supergraph contribution (in absolute value) remains of the same order of magnitude as the total cross-section. However, we find a mild hierarchy between individual supergraph contributions, spanning two orders of magnitude at NNLO. These hierarchies typically become stronger when more supergraphs contribute (e.g. figure 12 of ref. [46] which shows the relative LO contribution from all 104 supergraphs from the process  $e^+e^- \rightarrow t\bar{t}g/g_h g/\bar{g}_h g$ ). We take advantage of such hierarchies by integrating all supergraphs together with the integrator HAVANA (see section 5.4.2 of ref. [46]) that performs a discrete importance sampling over them. This implies that the sampling statistics for obtaining each of the supergraph cross-sections shown in table 2 covers a wide range of values. For instance, at NNLO supergraph D.1 required the largest statistics ( $2.1 \cdot 10^9$  points), whereas supergraph D.15 received the smallest amount of sample points ( $0.2 \cdot 10^9$ ). Thus, discrete importance sampling over supergraphs optimises the allocation of computation time amongst supergraphs, accounting for *both* their contribution relative to the total cross-section but also the differences in the variance of the corresponding LU integrands. We anticipate that the use of this integration strategy will become increasingly more important as the number of contributing supergraphs grows larger for more complicated applications.

We also report in table 4 on the contribution analogous to that of the  $n_f$  contribution at NNLO, but instead for  $\gamma^* \rightarrow t\bar{t}$  and stemming from a nested closed *massive* fermion loop with mass  $m_t$ . Again, we do not provide a benchmark comparison for this contribution and we include it solely to demonstrate that, also beyond NLO, the LU representation and its Monte-Carlo integration can easily accommodate additional masses.

We checked that the complete NLO cross-section of  $\gamma^* \rightarrow jj$  and  $\gamma^* \rightarrow t\bar{t}$  is independent of  $\mu_r$  (as expected since this process receives no contribution from renormalisation counterterms). This test only holds for the sum of all supergraph contributions and it therefore verifies that the expected gauge cancellations across them take place. For instance, it confirms that the  $\delta Z_t^{\overline{\text{MS}}}$  contributions generated through our automated renormalisation procedure described in section 5 properly cancel out between the double-triangle (B.1) and self-energy (B.2) supergraphs. We also verified that we reproduce the correct  $\mu_r$  dependence at NNLO, as predicted by the analytical expression given in ref. [107]. In general, a similar test can always be performed by comparing the  $\mu_r$ -dependence of the LU cross-section with the logarithmic dependence reconstructed from the renormalisation group flow.

SG id	$\Xi$	$\sigma_{\gamma^* \rightarrow t\bar{t}}^{\left[\alpha_s^{(\overline{\text{MS}})}, m_t^{(\text{OS})}\right]}$ [GeV <sup>-2</sup> ]	$\Delta$ [%]
<b>NNLO</b>		$\mathcal{O}(\alpha_s^2)$ (heavy nested fermion loops)	
C.1*	1	2.8484 · 10 <sup>-02</sup>	0.061
C.2*	2	-2.3718 · 10 <sup>-02</sup>	0.11
Total		4.766 · 10 <sup>-03</sup>	0.66
Benchmark		N/A	

**Table 4.** NNLO contribution to  $\gamma^* \rightarrow t\bar{t}$  from a massive nested fermion loop with mass  $m_t$ . Same conventions as for table 3. The two supergraphs shown are denoted with a star so as to stress that the internal closed quark loop line is massive.

### 6.2 Semi-inclusive NLO cross-section of $e^+e^- \rightarrow \gamma \rightarrow jjj$

We turn to the differential NLO cross-section of  $e^+e^- \rightarrow \gamma \rightarrow jjj$ , which was already computed with a similar numerical method in refs. [114, 115] and that served as an inspiration for our original work on LU. The supergraphs contributing to this process up to NLO are identical to those contributing to  $e^+e^- \rightarrow \gamma \rightarrow jj$  up to NNLO. The difference being that in this section Cutkosky cuts traversing only two edges and leaving a two-loop amplitude on either side are removed. We view this removal of Cutkosky cuts as stemming from the final-state observable density function, which encodes the process definition in this way. It also implies that each supergraph is only IR-finite when the observable density selects IR-safe kinematics. Another important consequence of removing the Cutkosky cuts not satisfying our process definition is that it also breaks the pair-wise cancellation of *non-pinched* thresholds. Therefore, contrary to the case of inclusive  $1 \rightarrow X$  cross-sections, we must consider the deformation discussed in section 5.3.4 of ref. [46] and whose generic construction is presented in ref. [32].

Contrary to the simpler moments of an event shape computed in refs. [114, 115], we choose a more modern and complex selector that requires at least three clustered jets to be resolved, using the anti-kT [116, 117] clustering algorithm with the following parameters:

$$\Delta R = 0.7, \quad p_t(j) > 50 \text{ GeV}, \quad n_{\text{jets}} = 3. \tag{6.4}$$

In table 5, we report results in the pure  $\overline{\text{MS}}$  scheme for  $s = (p_{e^+} + p_{e^-})^2 = (1000 \text{ GeV})^2$  and at  $\mu_r^2 = m_Z^2$ . Supergraph D.2, resp. D.12, required the largest, resp. smallest, number of sample points ( $9.1 \cdot 10^9$ , resp.  $0.3 \cdot 10^9$ ). After multiple adaptive iterations, the overall sample generation efficiency reached 81% (fraction of sample points for each Cutkosky cuts passing the selection criterion of eq. (6.4)).



SG id	$\Xi$	$\text{Re} \left[ \sigma_{e^+e^- \rightarrow \gamma \rightarrow jjj}^{(\overline{\text{MS}})} \right]$ [pb]	$\Delta$ [%]	$\text{Im} \left[ \sigma_{e^+e^- \rightarrow \gamma \rightarrow jjj}^{(\overline{\text{MS}})} \right]$ [pb]
$s = (p_{e^+} + p_{e^-})^2 = (1000 \text{ GeV})^2, \mu_r^2 = m_Z^2$				
<b>LO</b>		$\mathcal{O}(\alpha_s)$		
B.1	1	$1.01001 \cdot 10^{-02}$	0.048	0
B.2	2	$1.84151 \cdot 10^{-03}$	0.0077	0
Total		$1.19416 \cdot 10^{-02}$	0.040	0
Benchmark		$1.1955 \cdot 10^{-02}$	-0.11	0
<b>NLO</b>		$\mathcal{O}(\alpha_s^2)$ ( $n_f = 1$ contribution)		
C.1	1	$2.77 \cdot 10^{-05}$	14	$3 \cdot 10^{-26}$
C.2	2	$-1.912 \cdot 10^{-04}$	3.3	$6 \cdot 10^{-18}$
Total		$-1.635 \cdot 10^{-04}$	5.5	$6 \cdot 10^{-18}$
Benchmark		$-1.51 \cdot 10^{-04}$	3.3	0
<b>NLO</b>		$\mathcal{O}(\alpha_s^2)$ (all other contributions)		
D.1	2	$1.579 \cdot 10^{-03}$	2.2	$7 \cdot 10^{-22}$
D.2	2	$1.272 \cdot 10^{-03}$	6.6	$2 \cdot 10^{-05}$
D.3	2	$1.04 \cdot 10^{-05}$	11	$2 \cdot 10^{-06}$
D.4	1	$-2.79 \cdot 10^{-04}$	5.5	$-1 \cdot 10^{-12}$
D.5	1	$-3.8878 \cdot 10^{-03}$	0.037	$-2 \cdot 10^{-07}$
D.6	2	$9.19 \cdot 10^{-06}$	0.0	$9 \cdot 10^{-06}$
D.7	2	$-1.073 \cdot 10^{-04}$	3.3	$-7.2755 \cdot 10^{-04} \pm 0.18\%$
$\overline{\text{D.7}}$	2	$-1.080 \cdot 10^{-04}$	2.2	$7.2625 \cdot 10^{-04} \pm 0.18\%$
D.9	2	$5.53 \cdot 10^{-05}$	9.9	$7 \cdot 10^{-14}$
D.10	2	$5.729 \cdot 10^{-05}$	3.3	$-6 \cdot 10^{-07}$
D.11	2	$3.872 \cdot 10^{-05}$	0.68	$2 \cdot 10^{-07}$
D.12	1	$2.3495 \cdot 10^{-05}$	0.22	$5 \cdot 10^{-16}$
D.13	1	$3.88 \cdot 10^{-05}$	4.4	$-1 \cdot 10^{-38}$
D.14	2	$8.40 \cdot 10^{-06}$	9.9	$4 \cdot 10^{-08}$
D.15	1	$-2.778 \cdot 10^{-04}$	0.86	$-3 \cdot 10^{-06}$
Total		$-1.567 \cdot 10^{-03}$	3.3	$2 \cdot 10^{-05}$
Benchmark		$-1.515 \cdot 10^{-03}$	4.4	0

**Table 5.** Contributions from individual supergraphs listed in table 12 (external current  $e^+e^- \rightarrow \gamma$  is not shown there) to the semi-inclusive cross-section up to order  $\mathcal{O}(\alpha_s^2)$  (LO+NLO) for the processes  $e^+e^- \rightarrow \gamma \rightarrow jjj$  with  $n_f = 1$  and  $Q_q = 1/3$  and SM parameters as given in table. 1 and the fiducial cuts discussed in eq. (6.4).  $\Xi$  denotes the symmetry factor of the supergraph (included in the result reported).  $\Delta$  reports the relative Monte-Carlo error, except for the “Benchmark” entry where it refers to the relative difference w.r.t. the LU result instead. The benchmark results are obtained in this case with MG5aMC [99] and are themselves subject to a 1% MC uncertainty.

In general, we find a significantly poorer integration convergence than for the inclusive NNLO counterpart, and we could not reach percent-level accuracy. We attribute this mainly to two factors. First, IR singularities are now regularised through a combined effects of the LU pair-wise cancellation and the clustering observable, and the latter leaves regions of phase-space with collinear enhancements inducing  $\log(\Delta R)$  cross-section contributions that can be difficult to accurately reproduce numerically. This is expected to be improved by a smarter parameterisation of the spatial part of the supergraph loop momenta and better sampling strategy (see section 5.4 of ref. [46]). Second, and likely more important, the introduction of a contour deformation can increase the variance significantly, especially for massless processes (e.g. see visualisations of figures 13-16 in ref. [46]). A more precise understanding of the behaviour of the contour deformation close to IR limits can help mitigate this problem and this will be the focus of future work. We note that a promising alternative is to remove the need for a deformation altogether, by instead subtracting non-pinched thresholds locally [118].

The introduction of a contour deformation generates an imaginary part for the integrand, but unitarity guarantees that, at the integrated level, any observable remains real. More pragmatically, the imaginary contribution from each Cutkosky cut with the amplitude graph  $\Gamma_L$  to its right and complex-conjugated amplitude graph  $\Gamma_R^\dagger$  to its left is cancelled by its complex-conjugated partner identifying the two graphs  $\Gamma_R$  and  $\Gamma_L^\dagger$  instead. For supergraphs that are left-right symmetric, these pairs of Cutkosky cuts related by unitarity, i.e. by overall complex-conjugation, are all contained within the same graph. Figure 12 reveals that the only supergraph contributing to  $e^+e^- \rightarrow \gamma \rightarrow jjj$  that is *not* left-right symmetric is D.7, whose symmetric partner we call  $\overline{\text{D.7}}$ . In the second column of figure 5, we report the imaginary result of the LU cross-section and, as expected, we find that it is zero (within the Monte-Carlo accuracy) for all supergraphs except D.7 and  $\overline{\text{D.7}}$  that are exactly opposite of each other. Supergraphs for which the central value of the imaginary part of the integral is extremely small corresponds to cases where no deformation was necessary or where the imaginary part of the integrand cancels locally for our choice of deformation.

### 6.3 (Semi-)inclusive NLO cross-section of $e^+e^- \rightarrow \gamma \rightarrow t\bar{t}H$

In light of the relatively poor convergence of the semi-inclusive cross-section of  $e^+e^- \rightarrow \gamma \rightarrow jjj$ , it is interesting to consider a different type of NLO-accurate cross-section for a process whose definition still requires the removal of Cutkosky cuts (so that a contour deformation is still required) but which is free of phase-space IR singularities at LO, so that it can be computed inclusively as well. To this end, we choose the process  $e^+e^- \rightarrow \gamma \rightarrow t\bar{t}H$  for which we list the contributing supergraphs up to NLO in figure 13. This process has the additional benefit of involving supergraphs with a self-energy correcting an *internal* top quark propagator (supergraphs F.1 and F.9), that typically require a contribution from the top quark mass OS renormalisation counterterm  $\delta m_t$  and that our careful definition of local UV counterterms must be able to automatically reproduce (see section 5.1.3). For this reason, we will show results with the top quark mass renormalised in the OS scheme. All other quantities (top quark field, top quark Yukawa coupling and  $\alpha_s$ ) are renormalised in  $\overline{\text{MS}}$  and their related running is ignored. We choose  $\sqrt{s} = p_{e^+}^0 + p_{e^-}^0 = 1000 \text{ GeV}$  and  $\mu_r = m_Z$ . In order to explore potential degradation of the Monte-Carlo convergence in the presence of a complicated observable selector function, we also show results for the semi-inclusive cross-section defined over a fiducial volume characterised by the following acceptance cuts:

$$\begin{aligned} 200\text{GeV} < E_t < 600\text{GeV}, & & -0.8 < \cos(\theta_t) < 0.8 \\ 250\text{GeV} < E_H < 500\text{GeV}, & & -0.6 < \cos(\theta_H) < 0.6, \end{aligned} \quad (6.5)$$

where  $E_X$  denotes the energy component of the momentum carried by *any* particle  $X$ , and the polar angle  $\theta_X$  is defined as  $\cos(\theta_X) = \vec{p}_X \cdot \hat{e}_z / |\vec{p}_X|$ ,  $\hat{e}_z = (0, 0, 1)$ .

We find a numerical convergence significantly better for this process than for  $e^+e^- \rightarrow \gamma \rightarrow jjj$ . The largest number of sample points for the inclusive, resp. semi-inclusive, cross-section is  $1.5 \cdot 10^9$ , resp.  $4 \cdot 10^9$ , for supergraph F.3 and the lowest number is  $0.16 \cdot 10^9$ , resp.  $0.95 \cdot 10^9$ , for supergraph F.5. The overall sample generation efficiency in the semi-inclusive case is 38%. We attribute the improved convergence to a better behaviour of our choice of deformation for the simpler structure of IR singularities featured in this process. This hypothesis is reinforced by the observation that imposing complicated fiducial cuts has only a minor impact on the convergence. We find agreement well below the percent level, thus offering sufficient resolution for establishing the validity of our procedure for reproducing the OS mass renormalisation counterterm. Moreover, we verified again that we could obtain the same result starting from the pure  $\overline{\text{MS}}$  implementation of  $e^+e^- \rightarrow \gamma \rightarrow t\bar{t}H$  but complemented with the insertion of explicit integrated-level expression of  $\delta m_t^{\alpha_s}$  given in eq. (6.3).

In table 6, we only show the result for the real part of the cross-section. This is because we grouped together the result from all supergraphs that are not themselves left-right symmetric, so that the imaginary part is always zero, and we verified that this is the case, within the Monte-Carlo uncertainty (similarly as what is explicitly shown in the second column of table 5).

SG id	$\Xi$	$\text{Re} \left[ \sigma_{e^+e^- \rightarrow \gamma \rightarrow t\bar{t}H}^{[y_t^{(\overline{\text{MS}})}, m_t^{(\text{OS})}]} \right]$			
		$s = (p_{e^+} + p_{e^-})^2 = (1000 \text{ GeV})^2, \mu_r^2 = m_Z^2$			
		Inclusive xs [pb]	$\Delta$ [%]	Semi-inclusive xs [pb]	$\Delta$ [%]
<b>LO</b>		$\mathcal{O}(\alpha_s)$			
E.1	1	$6.17234 \cdot 10^{-04}$	0.0097	$1.39990 \cdot 10^{-04}$	0.014
E.2	2	$9.4622 \cdot 10^{-04}$	0.044	$2.20996 \cdot 10^{-04}$	0.024
Total		$1.56345 \cdot 10^{-03}$	0.027	$3.60986 \cdot 10^{-04}$	0.015
Benchmark		$1.56331 \cdot 10^{-03}$	0.0092	$3.6070 \cdot 10^{-04}$	0.079
<b>NLO</b>		$\mathcal{O}(\alpha_s^2)$			
F.1+ $\overline{\text{F.1}}$	2	$-2.504 \cdot 10^{-06}$	5.5	$3.57 \cdot 10^{-07}$	6.6
F.2	2	$3.1908 \cdot 10^{-05}$	0.11	$9.125 \cdot 10^{-06}$	0.16
F.3	2	$1.3472 \cdot 10^{-04}$	0.72	$2.598 \cdot 10^{-05}$	0.65
F.4+ $\overline{\text{F.4}}$	1	$-1.47653 \cdot 10^{-04}$	0.061	$-3.2604 \cdot 10^{-05}$	0.042
F.5	2	$-3.2336 \cdot 10^{-06}$	0.16	$-3.4399 \cdot 10^{-07}$	0.25
F.6	2	$5.5828 \cdot 10^{-05}$	0.049	$1.5349 \cdot 10^{-05}$	0.071
F.7+ $\overline{\text{F.7}}$	2	$-1.18480 \cdot 10^{-04}$	0.042	$-2.5882 \cdot 10^{-05}$	0.052
F.8+ $\overline{\text{F.8}}$	2	$-2.4706 \cdot 10^{-04}$	0.058	$-6.2182 \cdot 10^{-05}$	0.066
F.9+ $\overline{\text{F.9}}$	2	$4.7475 \cdot 10^{-05}$	0.097	$1.4429 \cdot 10^{-05}$	0.091
F.10	2	$2.0875 \cdot 10^{-04}$	0.064	$4.4976 \cdot 10^{-05}$	0.084
F.11	2	$-9.1283 \cdot 10^{-05}$	0.041	$-1.9691 \cdot 10^{-05}$	0.052
Total		$-1.315 \cdot 10^{-04}$	0.76	$-3.048 \cdot 10^{-05}$	0.59
Benchmark		$-1.3205 \cdot 10^{-04}$	-0.38	$-3.0570 \cdot 10^{-05}$	-0.28

**Table 6.** Contributions from individual supergraphs listed in table 13 to the cross-section up to order  $\mathcal{O}(\alpha_s^2)$  (LO+NLO) for the processes  $e^+e^- \rightarrow \gamma \rightarrow t\bar{t}H$  with the SM parameters as given in table. 1 except that the top-quark mass is renormalised in the OS scheme here, and not in  $\overline{\text{MS}}$ . We show results for both the fully inclusive cross-section and for a semi-inclusive one with fiducial cuts given in eqs. 6.5. The entries labelled “F.i+ $\overline{\text{F.i}}$ ” report the result for the *sum* of the contribution from both isomorphic supergraphs F.i and  $\overline{\text{F.i}}$ .  $\Xi$  denotes the symmetry factor of the supergraph (included in the result reported).  $\Delta$  reports the relative Monte-Carlo error, except for the “Benchmark” entry where it refers to the relative difference w.r.t. the LU result instead. The benchmark results are obtained in this case from MG5aMC [99] and are themselves subject to a 0.1% MC uncertainty.

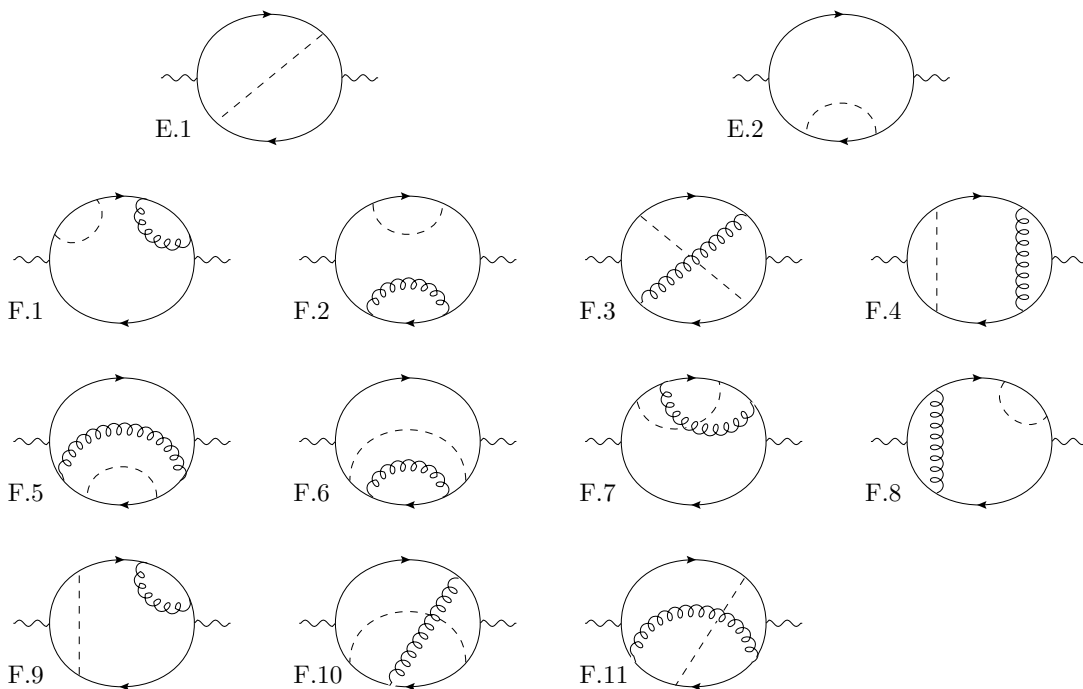
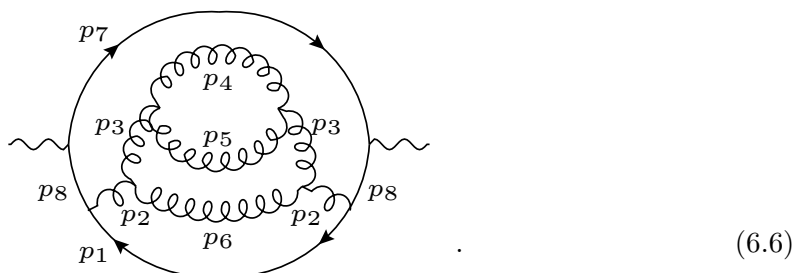


**Figure 13.** All contributing supergraphs to the class of processes  $e^+e^- \rightarrow \gamma \rightarrow t\bar{t}H + X$  at LO (E.1) and NLO (F.i). The external current  $e^+e^- \rightarrow \gamma$  is not shown. We note that we do not show the isomorphic partners  $\overline{F.1}$ ,  $\overline{F.4}$ ,  $\overline{F.7}$ ,  $\overline{F.8}$  and  $\overline{F.9}$  obtained by a mirror symmetry around the vertical central axis of the corresponding graph F.i (see explicit example with graphs D.7 and  $\overline{D.7}$  in table 12).

### 6.4 Numerical tests of the local UV subtraction of a three-loop nested self-energy

We turn to investigating explicitly the local cancellation of a curated list of UV singularities obtained by applying the R-operation to the following supergraph labelled H.3 and featuring a three-loop nested self-energy. We also specify the explicit choice of loop momentum routing considered for performing our numerical tests:



The exhaustive enumeration of UV limits can be achieved by considering all possible loop momentum bases of a given supergraph. For each basis, we test the behaviour of the LU integrand when sending to infinity all possible subset of momenta in that basis, while keeping the other ones fixed. Each three-momentum  $\vec{p}_i$  in the loop momentum basis is

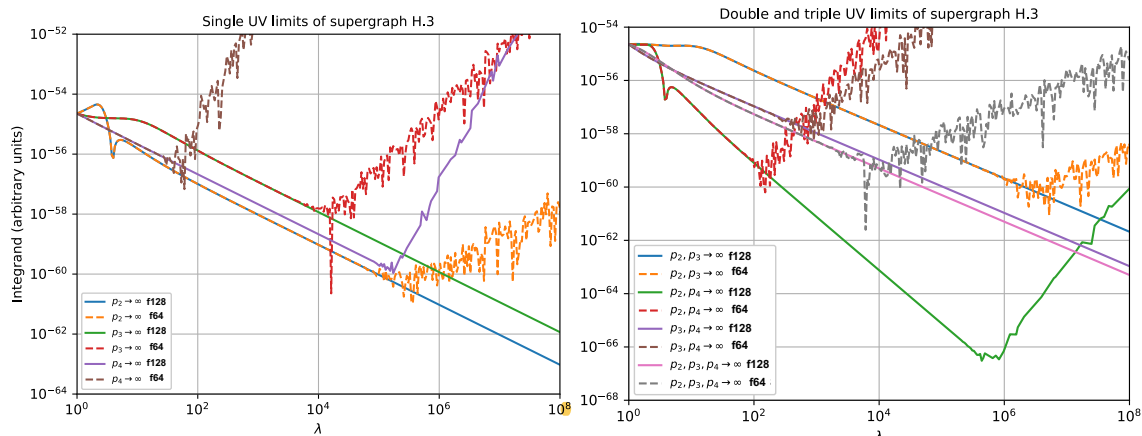


**Figure 14.** Behaviour of the LU integrand of supergraph H.3 of eq. (6.6) for each possible subset of momenta from the loop momentum basis  $\{p_1, p_2, p_3, p_4\}$  being linearly rescaled by  $\lambda$  in order to approach infinity. The UV scaling of the Minkowski integration measure (i.e.  $dp_i \rightarrow \lambda^4 dp_i$ ) is included in the results shown. Solid lines correspond to evaluations in quadruple precision (f128) whereas dashed ones are evaluations in double precision (f64).

assigned a random direction  $\vec{d}_i$  normalised to the scattering energy  $Q$  (i.e.  $|\vec{d}_i| = Q$ ), and those sent to infinity are rescaled by  $\lambda$ , i.e.  $\vec{d}_i \rightarrow \lambda \vec{d}_i$ . The Cutkosky cuts traversing edges rescaled to infinity are exponentially damped by the normalising  $h(t)$  function, whereas all others must still converge in virtue of the local UV subtraction procedure. We show in figure 14 an example of the application of this exhaustive testing strategy when considering the supergraph H.3 of eq. (6.6) and the loop momentum basis  $\{p_1, p_2, p_3, p_4\}$ .

The automation of this exhaustive testing procedure proved to be an invaluable tool for verifying the correct implementation of the  $R$ -operation on all amplitude graphs, and it can be viewed as a local analogue to the UV pole cancellation cross-check typically performed at the integrated level in traditional analytical amplitude computations in dimensional regularisation.

Our automated testing suite can generate plots like shown in figure 14, however they are typically not rendered and instead only analysed in order to automatically extract the power  $\xi$  of the leading behaviour in  $\lambda^\xi$ . When including the scaling of the measure,  $\xi$  can be associated to the  $\text{dod}$  of the subtracted amplitudes, and a successful UV subtraction will yield  $\xi \leq -1$ , indicating that the subtracted LU expression is bounded and integrable. We see that UV limits involving the innermost momentum  $p_4$  are numerically less stable because they involve the cancellation of more (nested) terms of the unfolded  $R$ -operation. In general, we find that the point of breakdown of numerical stability in double, resp. quadruple, precision which we denote  $\lambda_{f64}^*$ , resp.  $\lambda_{f128}^*$ , heuristically obeys the expected hierarchy  $\lambda_{f128}^* \gtrsim \lambda_{f64}^{*2}$ . It is also apparent that being able to leverage quadruple precision as a stability rescue mechanism is often crucial, given that we find cases of  $\lambda_{f64}^*$  as low as 100. We stress that these results are obtained using the cLTD representation of loop integrals, whose numerical stability in the UV is far superior to that of its LTD counterpart (see ref. [31]). The  $R$ -operation is designed to subtract all UV limits down to  $\xi = -1$ ,

however accidental cancellation can yield more converging behaviours, like for the double UV limit  $p_2, p_4 \rightarrow \infty$  for instance. We stress that we show in figure 14 the UV behaviour of the complete LU integrand only, however UV subtraction can also be investigated for the contribution of each Cutkosky cut individually.

## 7 Conclusion

The LU representation of differential cross-sections locally realises the cancellations of infrared singularities predicted by the KLN theorem. In this work we solved the two remaining conceptual challenges for computing physical cross sections beyond NLO with LU.

The first challenge is that self-energy corrections naturally introduce propagators with denominators raised to a higher power. We re-framed the discussion of building the LU representation of such configurations in the broader context of the analysis of higher-order residue contributions stemming from thresholds of forward-scattering diagrams. We generalised the LU construction accordingly, and from the resulting expression we identified a modification of the Cutkosky cutting rule that renders it also applicable for higher-order residues. This generalisation involves taking derivatives of amplitudes, and we showed how this can be implemented efficiently in a numerical code using dual number representations. We demonstrated that in the OS renormalisation scheme, these amplitude derivatives cancel at the integrated level, which explains why they do not appear in traditional computations.

The second challenge is that of subtracting and renormalising UV divergences from the loop amplitudes of the interference graphs. We use the  $R$ -operation to locally subtract UV singularity. We further refined the subtraction operator so as to also remove spurious soft singularities stemming from self-energy insertions, whose contribution at the integrated level leads to no pole. Finally, we redefine the local subtraction operator for massive propagators, such that its integrated version yields the On-Shell mass renormalisation counterterm. We thus construct the appropriate integrated-level counterterms such that the cross-sections obtained are automatically renormalised in the commonly used hybrid  $\overline{\text{MS}}$  and OS scheme. The analytic work necessary for achieving this only involves the computation of single-scale massive vacuum bubbles.

The refinements of the LU formulation introduced in this work address all remaining conceptual bottlenecks for applying it at any perturbative order and to any scattering process featuring only FSR singularities. This sets the stage for its first non-trivial practical applications, of which we show a curated selection. At NLO, we provide (semi-)inclusive results for  $e^+e^- \rightarrow \gamma \rightarrow jjj$  and  $e^+e^- \rightarrow \gamma \rightarrow t\bar{t}H$ . We also showed the first *purely numerical* computation in momentum-space of an inclusive NNLO cross-section, for the processes  $e^+e^- \rightarrow jj$  and  $e^+e^- \rightarrow t\bar{t}$ . Although these cross-sections were already known and are not relevant for phenomenology, the agreement with the analytic result validates our implementation. Additionally, investigation of specific supergraphs contributing up to N3LO offer a first glance at the performance of our approach, especially in terms of its scaling in both the perturbative order and process multiplicity. This first general implementation serves as a benchmark, from which incremental progress can be achieved.



Local Unitarity will soon be mature enough to tackle the computation of challenging cross-sections not yet available through other methods.

## Acknowledgments

This project has received funding from the European Research Council (ERC) under grant agreement No 694712 (PertQCD) and SNF grant No 179016. Numerical results presented in this work used computational resources from the LXPLUS computing cluster of CERN. We thank D. Kermanschah for enlightening exchanges on the contour deformation within LU, A. Schweitzer for his insight into details of the integration of integrated UV counterterms, A. Pelloni for his help with QGRAF generation and implementation of the cLTD expression and finally C. Anastasiou for his continuous support.

## A Example application of the $R$ -operation

We consider the following diagram

(A.1)

where the fermion line is considered massive with mass  $m$ . Since the  $R$ -operation requires to isolate subgraphs, we represent the graph  $\Gamma$  in terms of propagator and vertex functions in our code as follows:

```
vx(-1,21,1,-p,q,p-q,7,2,4)*vx(-1,21,1,-p+q,-q,p,5,1,8)*
vx(-1,21,1,-k,k-p,p,13,10,6)*vx(-1,21,1,-p,-k+p,k,9,11,12)*
prop(21,in,q,2)*prop(22,out,q,1)*prop(1,virtual,p-q,5,4)*
prop(1,virtual,p,7,6)*prop(1,virtual,p,9,8)*
prop(21,virtual,k-p,11,10)*prop(1,virtual,k,13,12)
```

where the Particle Group Data index of each particle is specified and a set of indices is provided. Then, to isolate the subgraph with loop momentum  $k$ , one collects all structures that contain  $k$ :

```
vx(-1,21,1,-k,k-p,p,13,10,6)*vx(-1,21,1,-p,-k+p,k,9,11,12)*
prop(21,virtual,k-p,11,10)*prop(1,virtual,k,13,12)
```

In the following we will represent the isolation of the subgraphs mathematically. After the substitution of the Feynman rules (and working in the Feynman gauge),  $\Gamma$  reads

$$\Gamma^{\mu\nu}(q) = \frac{[(\not{p} + m)\gamma^\mu(\not{p} - \not{q} + m)\gamma^\nu(\not{p} + m)]_{ij}}{(p^2 - m^2)^2(p - q)^2 - m^2} \gamma_{ji}(p), \quad \gamma_{ji}(p) = \frac{[\gamma^\nu(\not{k} + m)\gamma_\nu]_{ji}}{(k^2 - m^2)(k - p)^2}. \quad (\text{A.2})$$

The UV divergent subgraphs of  $\Gamma$  are  $\gamma_1 = \{e_4, e_5\}, \gamma_2 = \{e_1, e_2, e_4, e_5\}, \Gamma = \{e_1, e_2, e_3, e_4, e_5\}$ . The wood in this case is very simple

$$W[\Gamma] = \{\{\}, \{\gamma_1\}, \{\gamma_2\}, \{\Gamma\}\}. \quad (\text{A.3})$$

Thus, unfolding the  $R$  formula and using the linearity of  $K$ , we find

$$R[\Gamma] = \Gamma - K(\gamma_1) * (\Gamma \setminus \gamma_1) - K(\gamma_2) * (\Gamma \setminus \gamma_2) - K(\Gamma) + K(K(\gamma_1) * (\Gamma \setminus \gamma_1)) + K(K(\gamma_2) * (\Gamma \setminus \gamma_2)). \quad (\text{A.4})$$

Before continuing, we realise a special simplification:  $\Gamma \setminus \gamma_2$  is a tadpole that has the shape  $\mathcal{N}(k)_{ij}/(k^2 - m^2)$ . The  $K$  operator acting on this object leaves it identical, because in this case it consists in Taylor expanding around the external shift which is absent. As a result:

$$-K(\gamma_2) * (\Gamma \setminus \gamma_2) + K(K(\gamma_2) * (\Gamma \setminus \gamma_2)) = 0. \quad (\text{A.5})$$

and thus  $\gamma_2$  drops out of the wood.

Since  $K = \mathbf{T} + \bar{K}$ , we can always subdivide the problem of computing  $K(\gamma)$  into that of computing  $\mathbf{T}(\gamma)$  and  $\bar{K}(\gamma)$ .

**Term  $\mathbf{K}(\Gamma)$ .** We saw that for a generic gluonic self-energy  $\Pi_g(q, \mathbf{m})$

$$\mathbf{T}(\Pi_g) = \Pi_g(0, \mathbf{m}) + q^\mu \frac{\partial}{\partial q^\mu} \Pi_g(q, \mathbf{m}) \Big|_{q=0} + q^\mu q^\nu \frac{\partial}{\partial q^\mu} \frac{\partial}{\partial q^\nu} \Pi_g(q, \mathbf{0}) \Big|_{m_{uv}}. \quad (\text{A.6})$$

In this specific case we have  $\mathbf{m} = \{m\}$ . Applying this formula, we find

$$\begin{aligned} \mathbf{T}_2(\Gamma)^{\mu\nu} &= \frac{\text{Tr}[(\not{k} + m)\gamma^\rho(\not{p} + m)\gamma^\mu(\not{p} - \not{q} + m)\gamma^\nu(\not{p} + m)\gamma_\rho]}{(p^2 - m^2)^3(k^2 - m^2)(k - p)^2} \\ &+ \frac{2(p \cdot q)\text{Tr}[(\not{k} + m)\gamma^\rho(\not{p} + m)\gamma^\mu(\not{p} + m)\gamma^\nu(\not{p} + m)\gamma_\rho]}{(p^2 - m^2)^4(k^2 - m^2)(k - p)^2} \\ &+ \frac{-2(p \cdot q)\text{Tr}[\not{k}\gamma^\rho\not{p}\gamma^\mu\not{q}\gamma^\nu\not{p}\gamma_\rho] - q^2\text{Tr}[\not{k}\gamma^\rho\not{p}\gamma^\mu\not{p}\gamma^\nu\not{p}\gamma_\rho]}{(p^2 - m_{uv}^2)^4(k^2 - m_{uv}^2)((k - p)^2 - m_{uv}^2)} \\ &+ \frac{4(p \cdot q)^2\text{Tr}[\not{k}\gamma^\rho\not{p}\gamma^\mu\not{p}\gamma^\nu\not{p}\gamma_\rho]}{(p^2 - m_{uv}^2)^5(k^2 - m_{uv}^2)((k - p)^2 - m_{uv}^2)} \end{aligned} \quad (\text{A.7})$$

We now consider  $\bar{K}(\Gamma)$ . Recall that

$$\bar{K}(\Gamma) = - \prod_{i=1}^n N(k_i) \left( \mathbf{1} - K^{\overline{\text{MS}}} \right) [T(\Gamma) - T(\hat{T}(\Gamma))], \quad (\text{A.8})$$

which, for this case, evaluates to

$$\begin{aligned}
 \bar{K}(\Gamma)^{\mu\nu} &= -\frac{(2i(4\pi)^2 m_{\text{UV}}^2)^2}{(p^2 - m_{\text{UV}}^2)^3 (k^2 - m_{\text{UV}}^2)^3} (\mathbb{1} - K^{\overline{\text{MS}}}) \left( \frac{\mu^2}{4\pi e^{-\gamma_E}} \right)^{2\epsilon} \int d^{4-2\epsilon} p' d^{4-2\epsilon} k' \\
 &\times \left[ + \frac{-2(p' \cdot q) \text{Tr}[k' \gamma^\rho \not{p}' \gamma^\mu \not{q} \gamma^\nu \not{p}' \gamma_\rho] - q^2 \text{Tr}[k' \gamma^\rho \not{p}' \gamma^\mu \not{p}' \gamma^\nu \not{p}' \gamma_\rho]}{(p'^2 - m_{\text{UV}}^2)^4 (k^2 - m_{\text{UV}}^2) ((k - p')^2 - m_{\text{UV}}^2)} \right. \\
 &\quad \left. + \frac{4(p' \cdot q)^2 \text{Tr}[k' \gamma^\rho \not{p}' \gamma^\mu \not{p}' \gamma^\nu \not{p}' \gamma_\rho]}{(p'^2 - m_{\text{UV}}^2)^5 (k'^2 - m_{\text{UV}}^2) ((k' - p')^2 - m_{\text{UV}}^2)} \right] \\
 &= -\frac{(2i(4\pi)^2 m_{\text{UV}}^2)^2}{(p^2 - m_{\text{UV}}^2)^3 (k^2 - m_{\text{UV}}^2)^3} (i16\pi^2)^2 \\
 &\times \left( q^\mu q^\nu \left( \frac{31}{162} + \frac{1}{9}\pi^2 - \frac{136}{81\sqrt{3}} \text{Cl}_2\left(\frac{\pi}{3}\right) + \frac{10}{9} \ln\left(\frac{\mu^2}{m_{\text{UV}}^2}\right) + \frac{4}{3} \ln\left(\frac{\mu^2}{m_{\text{UV}}^2}\right)^2 \right) \right. \\
 &\quad \left. - g^{\mu\nu} q^2 \left( \frac{38}{81} + \frac{1}{9}\pi^2 - \frac{136}{81\sqrt{3}} \text{Cl}_2\left(\frac{\pi}{3}\right) + \frac{16}{9} \ln\left(\frac{\mu^2}{m_{\text{UV}}^2}\right) + \frac{4}{3} \ln\left(\frac{\mu^2}{m_{\text{UV}}^2}\right)^2 \right) \right), \quad (\text{A.9})
 \end{aligned}$$

where  $\text{Cl}_2$  is the Clausen function of order 2.

**Term  $\mathbf{K}(\gamma_1)$ .** Recall that, for a fermionic self-energy  $\Sigma(p, \mathbf{m})$ , one has

$$\mathbf{T}\Sigma(p, \mathbf{m}) = \frac{(1 + \gamma^0)}{2} \Sigma(p^{os}, \mathbf{m}) + \frac{(1 - \gamma^0)}{2} \Sigma(-p^{os}, \mathbf{m}) + (p - \gamma^0 p^{os})^\mu \frac{\partial}{\partial p^\mu} \Sigma(p, \mathbf{0}) \Big|_{m_{\text{UV}}}. \quad (\text{A.10})$$

In this case, the only internal mass is  $m$ , so  $\mathbf{m} = \{m\}$ . The subscript  $m_{\text{UV}}$  denotes the introduction of UV masses in all quadratic *denominators*. Applying this formula we find

$$\mathbf{T}_1(\gamma_1)_{ij} = \frac{[(1 + \gamma^0) \gamma^\nu (\not{k} + m) \gamma_\nu]_{ij}}{2(k^2 - m^2)(k - p^{os})^2} + \frac{[(1 - \gamma^0) \gamma^\nu (\not{k} + m) \gamma_\nu]_{ij}}{2(k^2 - m^2)(k + p^{os})^2} \quad (\text{A.11})$$

$$+ 2k \cdot p \frac{[\gamma^\nu \not{k} \gamma_\nu]_{ij}}{(k^2 - m_{\text{UV}}^2)^3} - 2k \cdot p^{os} \frac{[\gamma^0 \gamma^\nu \not{k} \gamma_\nu]_{ij}}{(k^2 - m_{\text{UV}}^2)^3}. \quad (\text{A.12})$$

with  $p^{os} = (m, 0, 0, 0)$ . We have, for  $\bar{K}(\gamma_1)$ :

$$\bar{K}(\gamma_1) = -\prod_{i=1}^n N(k_i) (\mathbb{1} - K^{\overline{\text{MS}}}) [T(\gamma) - T(T^{os}(\gamma))], \quad (\text{A.13})$$

which yields

$$\begin{aligned}
 \bar{K}(\gamma_1)_{ij} &= -\frac{2i(4\pi)^2 m_{\text{UV}}^2}{(k^2 - m_{\text{UV}}^2)^3} (\mathbb{1} - K^{\overline{\text{MS}}}) \left( \frac{\mu^2}{4\pi e^{-\gamma_E}} \right)^\epsilon \int d^{4-2\epsilon} k' \\
 &\times \left[ 2k' \cdot p \frac{[\gamma^\nu \not{k}' \gamma_\nu]_{ij}}{(k'^2 - m_{\text{UV}}^2)^3} - 2k' \cdot p^{os} \frac{[\gamma^0 \gamma^\nu \not{k}' \gamma_\nu]_{ij}}{(k'^2 - m_{\text{UV}}^2)^3} \right] \\
 &= \frac{2i(4\pi)^2 m_{\text{UV}}^2}{(k^2 - m_{\text{UV}}^2)^3} \frac{(\not{p} - \gamma^0 \not{p}^{os})_{ij}}{2} i\pi^2 \left( -1 - (1 - \epsilon) \ln\left(\frac{\mu^2}{m_{\text{UV}}^2}\right) + \frac{\pi^2}{12} \epsilon + \frac{1}{2} \ln\left(\frac{\mu^2}{m_{\text{UV}}^2}\right)^2 \epsilon \right). \quad (\text{A.14})
 \end{aligned}$$

**Term  $K(K(\gamma_1) * (\Gamma \setminus \gamma_1))$ .** We are now ready to discuss the nested application of  $K$ . We find

$$\begin{aligned}
 K(K(\gamma_1) * (\Gamma \setminus \gamma_1)) &= \mathbf{T}(\mathbf{T}(\gamma_1) * (\Gamma \setminus \gamma_1)) + \bar{K}(\mathbf{T}(\gamma_1) * (\Gamma \setminus \gamma_1)) \\
 &\quad + \mathbf{T}(\bar{K}(\gamma_1) * (\Gamma \setminus \gamma_1)) + \bar{K}(\bar{K}(\gamma_1) * (\Gamma \setminus \gamma_1))
 \end{aligned}
 \tag{A.15}$$

Regarding the nested application of the  $\mathbf{T}$  operator, we get the following

$$\begin{aligned}
 \mathbf{T}(\mathbf{T}(\gamma_1) * (\Gamma \setminus \gamma_1)) &= \left[ \frac{[(\not{p} + m)\gamma^\mu(\not{p} + m)\gamma^\nu(\not{p} + m)]_{ij}}{(p^2 - m^2)^3} \right. \\
 &\quad \left. - \frac{[(\not{p} + m)\gamma^\mu \not{q} \gamma^\nu(\not{p} + m)]_{ij}}{(p^2 - m^2)^3} + \frac{2(p \cdot q)[(\not{p} + m)\gamma^\mu(\not{p} + m)\gamma^\nu(\not{p} + m)]_{ij}}{(p^2 - m^2)^4} \right] \\
 &\quad * \left[ \frac{[(1 + \gamma^0)\gamma^\sigma(\not{k} + m)\gamma_\sigma]_{ji}}{2(k^2 - m^2)(k - p^{os})^2} + \frac{[(1 - \gamma^0)\gamma^\sigma(\not{k} + m)\gamma_\sigma]_{ji}}{2(k^2 - m^2)(k + p^{os})^2} + 2k \cdot p \frac{[\gamma^\sigma \not{k} \gamma_\sigma]_{ji}}{(k^2 - m_{uv}^2)^3} \right. \\
 &\quad \left. - 2k \cdot p^{os} \frac{[\gamma^0 \gamma^\sigma \not{k} \gamma_\sigma]_{ji}}{(k^2 - m_{uv}^2)^3} \right] + \left[ \frac{[\gamma^\sigma \not{k} \gamma_\sigma]_{ij}}{(k^2 - m_{uv}^2)^2} + 2(k \cdot p) \frac{[\gamma^\sigma \not{k} \gamma_\sigma]_{ij}}{(k^2 - m_{uv}^2)^3} \right] \\
 &\quad * \left[ - \frac{2(p \cdot q)[\not{p} \gamma^\mu \not{q} \gamma^\nu \not{p}]_{ji} - q^2[\not{p} \gamma^\mu \not{p} \gamma^\nu \not{p}]_{ji}}{(p^2 - m_{uv}^2)^4} + \frac{4(p \cdot q)^2[\not{p} \gamma^\mu \not{p} \gamma^\nu \not{p}]_{ji}}{(p^2 - m_{uv}^2)^5} \right].
 \end{aligned}
 \tag{A.16}$$

and similarly as before

$$\begin{aligned}
 \bar{K}(\mathbf{T}(\gamma_1) * (\Gamma \setminus \gamma_1)) &= - \frac{(2i(4\pi)^2 m_{UV}^2)^2}{(p^2 - m_{uv}^2)^3 (k^2 - m_{uv}^2)^3} (\mathbf{1} - K^{\overline{\text{MS}}}) \left( \frac{\mu^2}{4\pi e^{-\gamma_E}} \right)^{2\epsilon} \int d^{4-2\epsilon} p' d^{4-2\epsilon} k' \\
 &\quad \times \left[ \frac{[\gamma^\sigma \not{k}' \gamma_\sigma]_{ji}}{(k'^2 - m_{uv}^2)^2} + 2(k' \cdot p') \frac{[\gamma^\sigma \not{k}' \gamma_\sigma]_{ji}}{(k'^2 - m_{uv}^2)^3} \right] * \left[ - \frac{2(p' \cdot q)[\not{p}' \gamma^\mu \not{q} \gamma^\nu \not{p}']_{ij} - q^2[\not{p}' \gamma^\mu \not{p}' \gamma^\nu \not{p}']_{ij}}{(p'^2 - m_{uv}^2)^4} \right. \\
 &\quad \left. + \frac{4(p' \cdot q)^2[\not{p}' \gamma^\mu \not{p}' \gamma^\nu \not{p}']_{ij}}{(p'^2 - m_{uv}^2)^5} \right].
 \end{aligned}
 \tag{A.17}$$

We also have

$$\begin{aligned}
 \bar{K}(\bar{K}(\gamma_1) * (\Gamma \setminus \gamma_1)) &= - \frac{(2i(4\pi)^2 m_{UV}^2)^2}{(p^2 - m_{uv}^2)^3 (k^2 - m_{uv}^2)^3} (\mathbf{1} - K^{\overline{\text{MS}}}) \left( \frac{\mu^2}{4\pi e^{-\gamma_E}} \right)^\epsilon \int d^{4-2\epsilon} p' \\
 &\quad \times \left[ - \frac{2(p' \cdot q)[\not{p}' \gamma^\mu \not{q} \gamma^\nu \not{p}']_{ij} - q^2[\not{p}' \gamma^\mu \not{p}' \gamma^\nu \not{p}']_{ij}}{(p'^2 - m_{uv}^2)^4} + \frac{4(p' \cdot q)^2[\not{p}' \gamma^\mu \not{p}' \gamma^\nu \not{p}']_{ij}}{(p'^2 - m_{uv}^2)^5} \right] \\
 &\quad * (\mathbf{1} - K^{\overline{\text{MS}}}) \left( \frac{\mu^2}{4\pi e^{-\gamma_E}} \right)^\epsilon \int d^{4-2\epsilon} k' \left[ 2k' \cdot p' \frac{[\gamma^\sigma \not{k}' \gamma_\sigma]_{ji}}{(k'^2 - m_{uv}^2)^3} \right],
 \end{aligned}
 \tag{A.18}$$

where we note that the  $\epsilon$  contribution of  $\bar{K}(\gamma_1)$  will contribute to the final result, as it will hit the pole of  $[\Gamma \setminus \gamma_1]$ . Finally, we have:

$$\begin{aligned}
\mathbf{T}(\bar{K}(\gamma_1) * (\Gamma \setminus \gamma_1)) &= \frac{2i(4\pi)^2 m_{\text{UV}}^2}{(k^2 - m_{\text{uv}}^2)^3} \left[ \frac{[(\not{p} + m)\gamma^\mu(\not{p} - \not{q} + m)\gamma^\nu(\not{p} + m)]_{ij}}{(p^2 - m^2)^3} \right. \\
&\quad \left. + \frac{2(p \cdot q)[(\not{p} + m)\gamma^\mu(\not{p} + m)\gamma^\nu(\not{p} + m)]_{ij}}{(p^2 - m^2)^4} \right] \\
&\quad * \left( \mathbf{1} - K^{\overline{\text{MS}}} \right) \left( \frac{\mu^2}{4\pi e^{-\gamma_E}} \right)^\epsilon \int d^{4-2\epsilon} k' \left[ 2k' \cdot p \frac{[\gamma^\sigma \not{k}' \gamma_\sigma]_{ji}}{(k'^2 - m_{\text{uv}}^2)^3} - 2k' \cdot p^{os} \frac{[\gamma^0 \gamma^\sigma \not{k}' \gamma_\sigma]_{ji}}{(k'^2 - m_{\text{uv}}^2)^3} \right] \quad (\text{A.19}) \\
&\quad + \left[ - \frac{2(p \cdot q)[\not{p}\gamma^\mu \not{q}\gamma^\nu \not{p}]_{ij} - q^2[\not{p}\gamma^\mu \not{p}\gamma^\nu \not{p}]_{ij}}{(p^2 - m_{\text{uv}}^2)^4} + \frac{4(p \cdot q)^2[\not{p}\gamma^\mu \not{p}\gamma^\nu \not{p}]_{ij}}{(p^2 - m_{\text{uv}}^2)^5} \right] \\
&\quad * \left( \mathbf{1} - K^{\overline{\text{MS}}} \right) \left( \frac{\mu^2}{4\pi e^{-\gamma_E}} \right)^\epsilon \int d^{4-2\epsilon} k' \left[ 2k' \cdot p \frac{[\gamma^\sigma \not{k}' \gamma_\sigma]_{ji}}{(k'^2 - m_{\text{uv}}^2)^3} \right].
\end{aligned}$$

**Term  $K(\gamma_2)$ .** Finally, regarding  $\gamma_2$ , which is logarithmic, we have:

$$K(\gamma_2) * (\Gamma \setminus \gamma_2) = \frac{[\not{p}\gamma^\mu \not{p}\gamma^\nu \not{p}]_{ij} [\gamma^\sigma \not{p}\gamma_\sigma]_{ji}}{(p^2 - m_{\text{uv}}^2)^4 (k - p)^2} \quad (\text{A.20})$$

$$- \frac{g^{\alpha\sigma} 2i(4\pi)^2 m_{\text{UV}}^2}{(k - p)^2 (p^2 - m_{\text{uv}}^2)^3} \int d^{4-2\epsilon} p' \frac{[\not{p}'\gamma^\mu \not{p}'\gamma^\nu \not{p}']_{ij} [\gamma_\alpha \not{p}'\gamma_\sigma]_{ji}}{(p'^2 - m_{\text{uv}}^2)^4}. \quad (\text{A.21})$$

**Term  $K(K(\gamma_2) * (\Gamma \setminus \gamma_2))$ .** Furthermore we have:

$$\begin{aligned}
\mathbf{T}(K(\gamma_2) * (\Gamma \setminus \gamma_2)) &= \frac{[\not{p}\gamma^\mu \not{p}\gamma^\nu \not{p}]_{ij} [\gamma^\sigma \not{p}\gamma_\sigma]_{ji}}{(p^2 - m_{\text{uv}}^2)^4 (k - p)^2} \\
&\quad - \frac{g^{\alpha\sigma} 2i(4\pi)^2 m_{\text{UV}}^2}{(k - p)^2 (p^2 - m_{\text{uv}}^2)^3} \int d^{4-2\epsilon} p' \frac{[\not{p}'\gamma^\mu \not{p}'\gamma^\nu \not{p}']_{ij} [\gamma_\alpha \not{p}'\gamma_\sigma]_{ji}}{(p'^2 - m_{\text{uv}}^2)^4}, \quad (\text{A.22})
\end{aligned}$$

and

$$\bar{K}(K(\gamma_2) * (\Gamma \setminus \gamma_2)) = 0. \quad (\text{A.23})$$

This shows that

$$K(\gamma_2) * (\Gamma \setminus \gamma_2) + K(K(\gamma_2) * (\Gamma \setminus \gamma_2)) = 0. \quad (\text{A.24})$$

## B Code performance and example of specific supergraphs up to N3LO

In this appendix, we will provide more details on the current performance of our implementation of the LU representation of differential cross-sections in a private computer code named  $\alpha\text{Loop}$ . Ultimately, the objective is to minimise the total computational time for computing a given observable of a given scattering process up to a target relative accuracy and at a set perturbative order. However, such an inclusive metric aggregates the performance of many different aspects of an implementation and it is therefore not particularly insightful. We therefore find it useful to separate optimisations impacting this overall performance into two classes:

- **Integrator optimisations** aim at reducing the number of sample points that are necessary to reach a certain accuracy.
- **Integrand optimisations** aim at reducing the time necessary for evaluating a given sample point. We also include peripheral concepts such as generation timing, numerical stability and memory footprint (RAM and disk) under this umbrella term of integrand performance.

Integrator performance is mostly driven by the choice of adaptive sampling algorithms, as well as the various parameterisations considered when building the overall integrand (e.g. typically within a multi-channeling approach). The improvements foreseen in section 5.4 of ref. [46] have not yet been fully explored and as such it is too early to present details of our current integrator performance. We will limit ourselves here to stating that the results presented in section 6 were obtained in less than hundred thousand CPU hours per process.

Integrand performance is mostly driven by the many design choices entering the computer implementation of the LU representation. Only our eventual publication of the code can give a detailed account of all these choices, but they mostly relate to efficient graph manipulations and isomorphisms, FORM-optimised implementation of the cLTD [31] representation, leveraging partial factorisation in the structure of the subtraction terms generated by the  $R$ -operation and finally the use of dual numbers for the exact numerical computation of derivatives. We note that the run-time efficiency of the contour deformation also crucially depends on optimisations in its implementation. For the most part, those have already been presented in details, both qualitatively and quantitatively, in ref. [32], so that we will only consider here the profiling of LU integrands evaluated with real kinematics.

Contrary to integrator performance, our current implementation in  $\alpha$ Loop is good enough to warrant the publication of integrand performance benchmarks that are useful as an anchor point to assess future improvements (by ourselves but hopefully also independent groups seeking to replicate and improve upon our work). Together with these detailed integrand performance statistics, we also present applications of our automated testing suite to investigate the quality of cancellations in various IR and UV limits of the LU integrand.

The complexity of the LU representation of the  $N^k$ LO correction to a  $1 \rightarrow N$  process scales both in  $k$  and  $N$ . One may naively think that since LU combines phase-space and loop integrals, there should be no distinction between the complexity growth in these two scaling parameters. This is true for quantities such as the total number of contributing supergraphs and the dimensionality  $3 \times (N + k - 1)$  of the LU Monte-Carlo integral. Yet, the scaling of the overall complexity of the LU representation remains far worse in  $k$  than  $N$  for the following three reasons:

1. The numerical severity of cancellations between various terms of the LU integrand in the IR and UV limits only depends on  $k$ . In other words, the more divergent limits can be reached simultaneously, the more challenging it is to keep the LU integrand numerically stable everywhere in the integration space.
2. Most importantly, the complexity of the UV subtraction grows exponentially with  $k$  and not at all with  $N$ . This is because the number of subtraction terms generated by

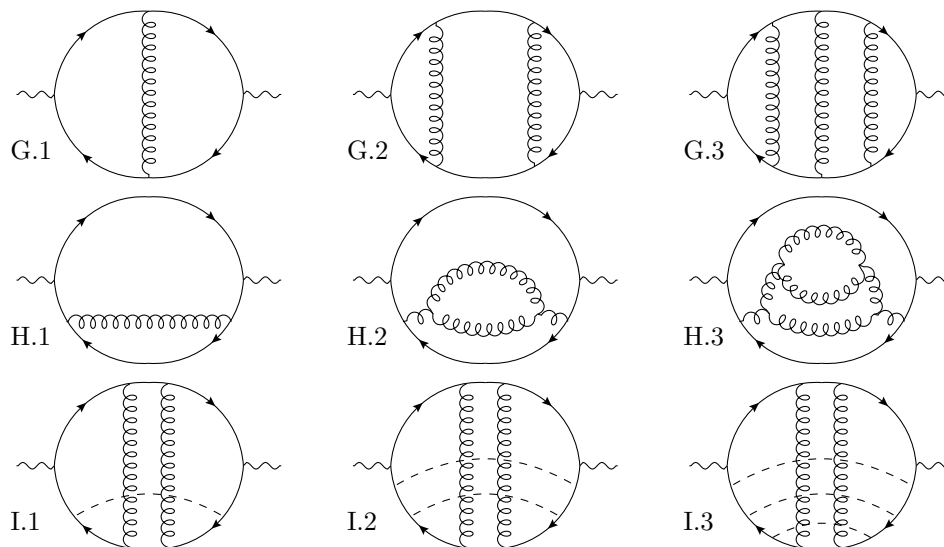


**Figure 15.** Example supergraphs for increasing  $N^k\text{LO}$  perturbative order, with  $k = 1, 2, 3$  for the “double-triangle” class  $G.x$  and the “nested self-energy” class  $H.x$ . The class of supergraphs  $I.x$  corresponds to NNLO contributions to the process  $\gamma^* \rightarrow t\bar{t} + N \times H$  where  $N = 1, 2, 3$ .

the  $R$ -operator is dictated by its maximum recursion depth, which is the maximum loop count  $k$  that can appear in any amplitude on either side of a Cutkosky cut.

3. Even without UV subtraction, the LU integrand still involves the cLTD expression of multi-loop amplitudes, whose complexity scales with both  $N$  and  $k$ , but was shown to be milder in  $N$  (see ref. [31]).

In order to investigate separately the scaling of our implementation in both  $k$  and  $N$ , we choose to study the three different series of characteristic supergraphs shown in figure 15. The first two series are contributions to  $\gamma^* \rightarrow jj$  (so  $N = 2$ ) at  $N^k\text{LO}$ , with  $k = 1, 2, 3$ . The third series are contributions to  $\gamma^* \rightarrow t\bar{t} + N \times H$  at NNLO (so  $k = 2$ ) with  $N = 1, 2, 3$ .

We start by reporting in table 7 the following key metrics for each of the nine supergraphs of figure 15:

- $t_{\text{gen}}$  [s]: time spent in FORM for generating the source code of this supergraph (compilation time is typically less than  $t_{\text{gen}}$  with sufficiently many cores).
- $M_{\text{disk}}$  [MB]: size of the compiled shared library on disk.
- $N_{\text{sg}}$  [-]: total number of non-isomorphic supergraphs with a unique contribution to the process this supergraph belongs to. Distinct supergraphs related by a symmetry interchanging the two external photons are counted twice.
- $N_{\text{cuts}}$  [-]: total number of Cutkosky cuts for this supergraph.
- $t_{\text{eval}}$  [ms]: evaluation time for evaluating the LU integrand for all Cutkosky cuts.
- $t_{\text{eval}}^{(\text{f128})}$  [ms]: evaluation time for evaluating the LU integrand in quadruple precision.



SG	proc.	order	$t_{\text{gen}}$ [s]	$M_{\text{disk}}$ [MB]	$N_{\text{sg}}$ [-]	$N_{\text{cuts}}$ [-]	$t_{\text{eval}}$ [ms]	$t_{\text{eval}}^{(\text{f128})}$ [ms]
G.1	1 → 2	NLO	0.1	0.13	2	4	0.004	0.13
G.2	1 → 2	NNLO	4.7	3.0	17	9	0.04	2.1
G.3	1 → 2	N3LO	36K	509	220	16	17.6	281
H.1	1 → 2	NLO	0.07	0.12	2	2	0.006	0.14
H.2	1 → 2	NNLO	1.5	1.3	17	3	0.056	1.9
H.3	1 → 2	N3LO	255	43	220	4	2.35	56
I.1	1 → 3	NNLO	126	22	266	9	0.32	12.4
I.2	1 → 4	NNLO	1.9K	120	4492	9	4.4	67
I.3	1 → 5	NNLO	36K	20K	$\mathcal{O}(100\text{K})$	9	3.6K	17.3K

**Table 7.** Performance for characteristic supergraphs of figure 15 corresponding to  $N^k\text{LO}$  corrections for  $1 \rightarrow N \times X$  processes, with  $k = 1, 2, 3$  and  $N = 1, 2, 3$ . See text for details.

Note that the timings  $t_{\text{eval}}$  and  $t_{\text{eval}}^{(\text{f128})}$  include numerical stability tests, which at least double the evaluation time. Also note that statistics provided here have qualitative merits only, so we do not specify the hardware that ran the tests.

Despite the minimal sample size in the progression in the perturbative order  $k$  and process multiplicity  $N$ , we see that as expected the complexity growth in these parameters is rather steep. Similarly, the growth in the number of unique supergraphs is factorial despite the grouping into isomorphic sets. For these reasons, a rough rule of thumbs for what our current implementation of LU can accommodate is any contribution with  $k + N \leq 6$ , that is 5-loop supergraphs.

For instance, I.3 is a single 6-loop supergraph whose generation proved challenging to complete, even though it requires no UV counterterm. This is because it contains a two-loop six-point integral with a rank-7 numerator for which the cLTD representation involves many terms. Note that for such a supergraph, and in general for higher multiplicity processes, the original LTD representation can be superior, also because in that case stability in the UV regime is not as important. In the future we plan on using a combination of both representation to improve on run time. We stress that this current *practical* limitation  $k + N \leq 6$  is specific to our implementation in  $\alpha\text{Loop}$  and should not be considered as a limitation inherent to LU. Our aim with this work is to establish the complete generality of LU and demonstrate it with a first implementation already capable of computing cross-sections at or beyond the state-of-the-art. Conceptually, LU is now a mature approach for processes with final-state IR singularities. Its practical application to the fully numerical computation of (differential) cross-sections is now ready to be incrementally improved by future work, starting from the baseline performance presented here.

We developed an automated testing framework in  $\alpha\text{Loop}$  of the LU representation of individual supergraphs. These tests involve the exhaustive enumeration of all UV and IR limits, followed by successive numerical evaluations of the LU integrand for sample points progressively approaching each limit so as to test the expected local cancellation pattern. In particular, investigating the scaling of the various terms with the approach parameter  $\lambda$  allows one to numerically reconstruct the power of their asymptotic  $\lambda^\xi$  behaviour and

thus verify their integrability. We note that the LU integrand is ultimately expressed with inputs in the unit hypercube, so that a conformal map  $x \in [0, 1] \rightarrow r \in [0, \infty]$  must be used. The logarithmic map  $r = -Qx \log(1 - x)$  is convenient because its Jacobian scales like the measure  $dr$  for *both*  $r \rightarrow 0$  (soft) and  $r \rightarrow \infty$  (UV). For production runs however, we instead currently use the map  $Q \frac{x}{1-x}$ , which can yield unbounded integrable singularities, but that we found to be converging better<sup>2</sup> when using a naive independent spherical parameterisation for each of the spatial momenta integrated over.

We have already presented explicit results for the cancellation of UV limits in section 6.4, and we show in the next section an analogous investigation of the cancellation of IR limits between various Cutkosky cuts.

### B.1 Numerical tests of local LU cancellations on IR limits

The enumeration of all IR limits of a supergraph is a bit more involved than for UV limits. One possible approach is to investigate each contributing Cutkosky cut (some may be excluded by the observable definition) and consider all IR limits involving the massless particles in that cut. Each limit constructed in this way is identified by a unordered set of ordered sets of collinear edges, together with a list of edges going soft. For instance an IR limit denoted  $\mathcal{C}[1, 2, 3] \mathcal{C}[4, \mathcal{S}(5)] \mathcal{S}(6) \mathcal{S}(7)$  corresponds to two sets of momenta collinear to two different normalised collinear directions  $\vec{d}_c^{(1)}$  and  $\vec{d}_c^{(2)}$ , as well as two momenta approaching each of the two non-nested soft configurations. More specifically, this particular limit would be approached using the following parametric scaling involving seven normalised random directions  $\vec{d}_i$ :

$$\begin{aligned} \vec{p}_1 &= Q \left( x_1^{(1)} \vec{d}_c^{(1)} + \lambda \vec{d}_1^{(\perp 1)} \right), & \vec{p}_2 &= Q \left( x_2^{(1)} \vec{d}_c^{(1)} + \lambda \vec{d}_2^{(\perp 1)} \right), \\ \vec{p}_3 &= Q \left( x_3^{(1)} \vec{d}_c^{(1)} + \lambda \vec{d}_3^{(\perp 1)} \right), & \vec{p}_4 &= Q \left( x_1^{(2)} \vec{d}_c^{(2)} + \lambda \vec{d}_4^{(\perp 2)} \right), \\ \vec{p}_5 &= Q \lambda \left( x_2^{(2)} \vec{d}_c^{(2)} + \lambda \vec{d}_5^{(\perp 2)} \right), & \vec{p}_6 &= Q \lambda \vec{d}_6, & \vec{p}_7 &= Q \lambda \vec{d}_7, \end{aligned} \quad (\text{B.1})$$

where we used the short-hand:

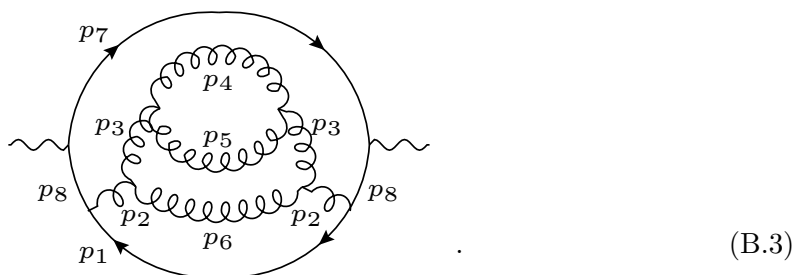
$$\vec{d}_j^{(\perp i)} = \frac{\vec{d}_j - (\vec{d}_j \cdot \vec{d}_c^{(i)}) \vec{d}_j}{|\vec{d}_j - (\vec{d}_j \cdot \vec{d}_c^{(i)}) \vec{d}_j|}, \quad (\text{B.2})$$

and  $Q$  is the scattering energy and within each set the collinear fractions  $x_j^{(i)} \in [0, 1]$  are forced to be in descending order ( $x_j^{(i)} > x_{j+1}^{(i)}$ ). For soft-collinear configurations, the scaling choice of eq. (B.1) implies that the transverse component of soft-collinear momenta scales like  $\lambda^2$ ; this is however not a problem for interpreting the asymptotic scaling  $\lambda^\xi$  of the LU integrand because, as we will discuss later, it always goes to a constant ( $\xi = 0$ )

---

<sup>2</sup>This is likely because the logarithmic map makes it difficult for the adaptive algorithm to adjust to the correct typical contributing region of interest for the radii of the spatial parts integrated over. Indeed the overall normalising scale  $Q$  is just a rough estimate, and using the rational polynomial map  $Q \frac{x}{1-x}$  makes it easier for the adaptive algorithm to adjust to the region of interest compared to the logarithm map. In the future, this issue can be solved by considering more complicated conformal maps.

on any collinear limit. Notice that when applied to a massive propagator, the soft approach  $\vec{p}_i = Q\lambda\vec{d}_i$  also allows us to probe the implementation of our local analogue of the mass renormalisation counterterm in the OS scheme. In that case, only the spatial part of the momentum will approach zero while the energy component will approach the mass of the propagator, and IR subtraction of repeated propagators is not mandatory for convergence. Approaching IR limits in the context of the LU expression is considerably simpler than in the traditional context of real-emission phase-space subtraction where complicated mappings are necessary (e.g. see [119]). Indeed, within LU, momentum conservation and on-shellness of external particles is automatically enforced by the causal flow. We now present in figure 16 a curated list of interesting soft, collinear and soft-collinear limits of the supergraph H.3 of eq. (6.6) which we repeat here for convenience:



Note that contrary to what our automated test would do, we choose here to study limits not directly involving sets of momenta appearing in Cutkosky cuts, but instead we choose a basis involving the repeated propagators so as to make it easier to study their soft limit.

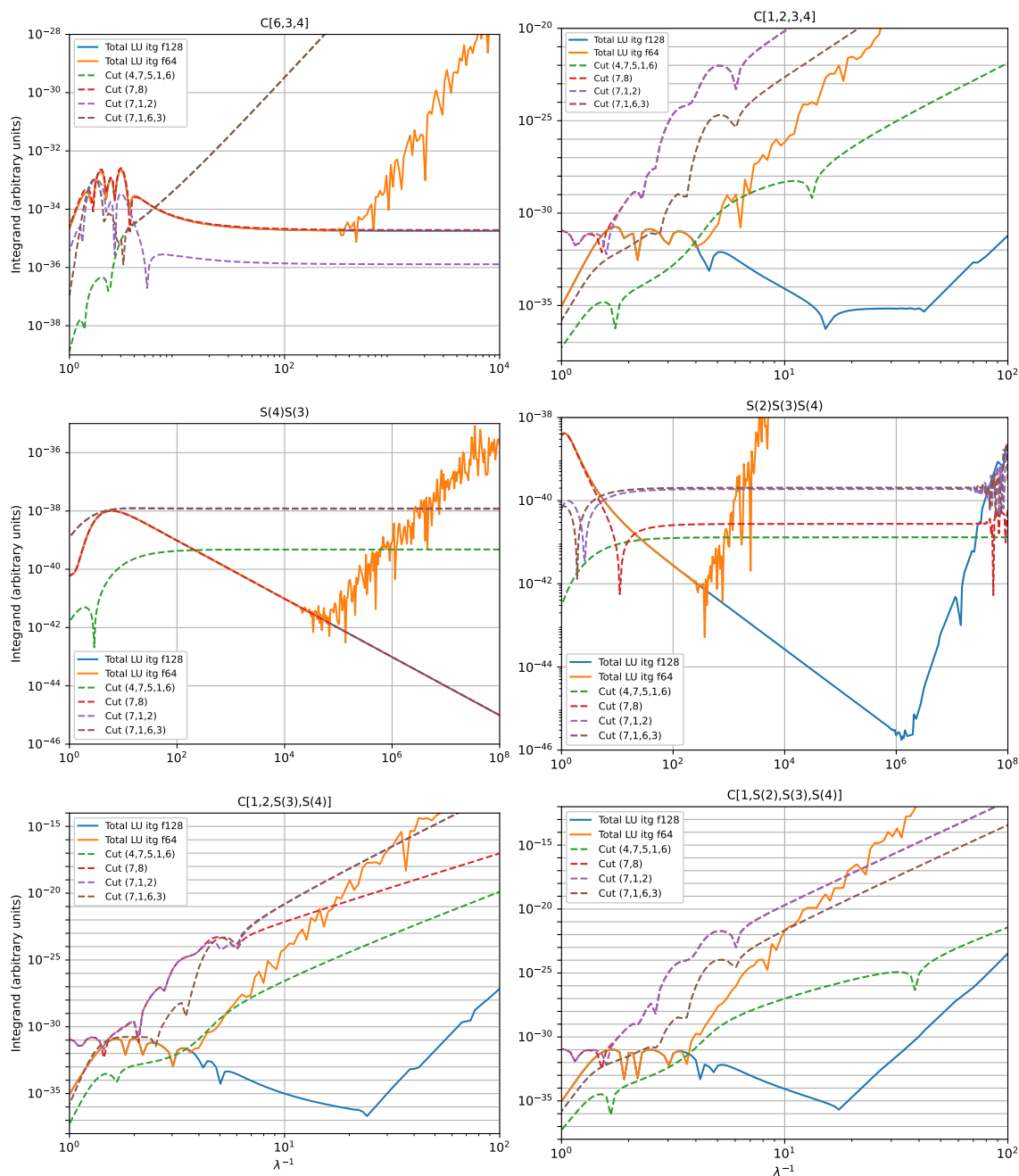


**Figure 16.** Behaviour of the LU integrand of supergraph H.3 of eq. (6.6) for various collinear, soft and soft-collinear limits approached using a rescaling parameter  $\lambda$  as shown in eq. (B.1). The soft scaling of the measure, i.e.  $d\vec{p}_i \rightarrow \lambda^3 d\vec{p}_i$ , is included in the lines shown for each momentum approaching a soft limit, but our parameterisation does not reflect the collinear suppression in the measure proportional to  $\cos(\theta_{ij})$ . Dashed lines correspond to the LU integrand for each of the four Cutkosky cuts of supergraph H.3, whereas the solid blue, resp. orange, line corresponds to the sum of all cut contributions evaluated using quadruple precision (f128) arithmetics, resp. double precision (f64) arithmetics.

IR finiteness in LU involves (multiple) pair-wise cancellations among Cutkosky cuts, so that we find it useful to show in figure 16 results for both the four individual cuts (dashed lines) of supergraph H.3 as well as for their sum, evaluated using double precision (orange lines) and quadruple precision arithmetics (blue lines). Our choice of parameterisation explicitly shows the soft-scaling of the measure, i.e.  $d\vec{p}_i \rightarrow \lambda^3 d\vec{p}_i$ , which is included in the results shown. However, our chosen parameterisation does not manifestly exhibit the collinear suppression  $\propto \cos(\theta_{ij})$  it contains, meaning that we did not align the polar axis with the collinear directions. While it may be beneficial to do so for convergence purposes, we see that it is not strictly necessary to do so in order to demonstrate that the LU integrand is bounded. Indeed, thanks to the LU cancellation pattern, we expect that the LU integrand goes to a **constant** for any collinear limit of any process and at any perturbative order! This highlights a crucial difference w.r.t. traditional phase-space subtraction strategies based on the factorisation of IR singularities of amplitude, namely the fact that within LU there remains no integrable singularities even without aligning the integration measure with collinear directions. This overzealous cancellation of IR singularities within LU contributes to facilitating an efficient numerical integration since it leaves ample freedom in the choice of parameterisations that leave no integrable singularities.

As already discussed at length in this work, cancellation of soft configurations is intricate. In the absence of raised propagators, like for supergraphs of the G.x series in figure 15, soft finiteness is directly inherited from the pair-wise collinear cancellation pattern of LU (since soft configurations are end-point of collinear ones, see discussion in section 3.2.6 of ref. [46]). However, for supergraphs featuring raised propagators, like in the case of H.3 investigated here where both  $p_2$  and  $p_3$  are raised, the soft finiteness also involves amplitude-level cancellations with the soft counterterms part of our implementation of the  $R$ -operator. These cancellations have nothing to do with the KLN theorem, and it is for example what guarantees that the cuts (7, 1, 2) and (7, 1, 6, 3) go to a constant by themselves for the double-soft limit  $\mathcal{S}(3)\mathcal{S}(4)$  and the triple-soft limit  $\mathcal{S}(2)\mathcal{S}(3)\mathcal{S}(4)$ . Then, the usual pair-wise LU cancellation mechanism offers a further suppression so that the asymptotic scaling  $\lambda^\xi$  of the complete LU integrand scales with  $\xi \geq 1$ . We see in the triple-soft limit  $\mathcal{S}(2)\mathcal{S}(3)\mathcal{S}(4)$  that the evaluation of individual cuts can themselves become numerically unstable, demonstrating that alike for UV cancellations, the amplitude-level soft cancellations can themselves be subject to numerical instabilities. These numerical instabilities however happens considerably deeper than those stemming from cancellations across Cutkosky cuts, so that they are not of concern. We note again, how strikingly different the cancellation of soft singularities within LU is compared to the traditional phase-space subtraction analogue based on the Eikonal approximation. More specifically, within LU soft cancellations happens essentially solely due to kinematics and in virtue of these configurations being endpoints of collinear limits. And in particular, LU soft cancellations do not rely on any details of the SU(3) colour structure of amplitudes.

We note that for the deeper limits like the quadruple collinear  $\mathcal{C}(1, 2, 3, 4)$ , the cancellations between cuts are especially severe, spanning seventeen orders of magnitude at the breakdown point  $\lambda_{f128}^*$  of quadruple-precision evaluations. This leaves barely enough room for observing the constant asymptotic regime in quadruple precision and clearly shows that

double-precision is not sufficient for capturing the complete non-trivial dynamics appearing in the bulk of the phase-space. Still, up to N3LO at least, quadruple precision arithmetics appears sufficient in the sense that the results shown suggest that cutting off the integrand at  $\lambda_{\text{f128}}^*$  is unlikely to have any noticeable impact in the cross-section computed.

In  $\alpha$ Loop, IR cancellation tests such as presented here are performed automatically on the exhaustive set of IR limits relevant to each supergraph. The plots are not rendered, but instead analyzed so as to extract the asymptotic scaling power  $\xi$  and confront it with the theoretical expectation discussed in this section. These tests are essential for assessing the validity of the LU construction, both conceptually and of its implementation in  $\alpha$ Loop. They are analogous to the well-known consistency checks of phase-space subtraction approaches, except that in the case of LU they also probe the IR behaviour of the loop integrals involved.

### C Dual number representations and efficient computation of derivatives

We saw in the previous sections that the application of the LU representation of differential cross-section to supergraphs with repeated edges requires taking derivatives of amplitudes. While the derivatives could be computed symbolically at the time of generating the code for the LU integrands, this would come at the cost of a significant overhead of both generation and run time. A far more elegant and efficient solution is to compute these derivatives using a numerical implementation of them based on the chain-rule, which can be achieved by using multivariate dual numbers (e.g. see survey of auto-differentiation tools and method in ref. [69]). This procedure is both *exact* and *numerically stable*. Note that such dual numbers were already used in the context of ref. [32] for efficiently computing the Jacobian of complicated contour deformations and are also commonly used in the context of machine learning when implementing the *automatic differentiation* necessary for back-propagation algorithms. Given that the generalisation of this numerical technique necessary for an efficient implementation of the LU representation is to the best of our knowledge not clearly presented anywhere, we set ourselves to describing it in details in this appendix. We first recall here the formal construction of dual numbers. We start by considering a nilpotent object with degree  $n + 1$

$$\varepsilon^{n+1} = 0. \tag{C.1}$$

We then consider all polynomials that can be obtained from such a nilpotent element. We let  $\mathcal{D}(n)$  be the set of all such polynomials. Its explicit definition reads

$$\mathcal{D}(n) = \left\{ \sum_{k=0}^n \frac{c_k}{k!} \varepsilon^k \mid c_i \in \mathbb{C}, \forall i = 0, \dots, n \right\}. \tag{C.2}$$

An element  $\bar{x} \in \mathcal{D}(n)$  is called a dual. As we will see, duals can be used to compute up to the  $n$ -th derivative of  $f$ . In particular, the truncation rule established by eq. (C.1) allows to implement duals in  $\mathcal{D}(n)$  on a computer by simply storing the  $n$  coefficients  $c_i$  in an array. The action of a function  $f$  originally defined on complex numbers is extended to an

action on a generic dual number  $\bar{x}$  through the Taylor expansion of  $f$  around  $\bar{x}|_{\varepsilon=0}$ :

$$f(\bar{x}) = \sum_{k=0}^{\infty} \frac{(\bar{x} - \bar{x}|_{\varepsilon=0})^k}{k!} f^{(k)}(\bar{x}|_{\varepsilon=0}) = \sum_{k=0}^{\infty} \frac{1}{k!} f^{(k)}(c_0) \left( \sum_{i=1}^{\infty} \frac{c_i}{i!} \varepsilon^i \right)^k. \quad (\text{C.3})$$

When applying the nilpotency condition of eq. (C.1), we can truncate the expansion explicitly as follows:

$$f(\bar{x} \in \mathcal{D}(n)) = \sum_{k=0}^n \frac{1}{k!} \left( \sum_{i=0}^k B_{n,k}(c_1, \dots, c_{n-k+1}) f^{(k)}(c_0) \right) \varepsilon^k, \quad (\text{C.4})$$

where  $B_{n,k}$  is a Bell polynomial. The two key properties of this definition of the application of functions to dual numbers is that it follows the composition rule and satisfies:

$$f(c_0 + \varepsilon) = \sum_{k=0}^n \frac{1}{k!} f^{(k)}(c_0) \varepsilon^k, \quad (\text{C.5})$$

thus allowing one to read the  $j$ -th derivative of the function  $f$  evaluated at  $c_0$  directly from the coefficient multiplying the  $j$ -th power of the dual  $\varepsilon$ .

So far, dual numbers do not seem especially useful, since at first glance it seems like implementing the action of an arbitrary function  $f$  on duals in  $\mathcal{D}(n)$  would anyway require the prior symbolic computation of all the  $n$ -th first derivatives of  $f$  in order to construct the coefficients of eq. (C.4). However, a much more efficient implementation can be obtained by realising that most complicated functions typically implemented on a computer are composites of simple elementary ones. One can then use eq. (C.4) to construct the implementation of all elementary arithmetic and intrinsic operations  $f$  (e.g.  $\sin x$ ,  $\cos x$ ,  $\sqrt{x}$ , etc.) from their trivial derivatives. Since this construction satisfies the composition rule, dual numbers provide a fast, exact and automated numerical computation of up to the  $n$ -th derivative of any complicated function that corresponds to iterated compositions of elementary ones. In that case it is useful to extend eq. (C.3) to a function with  $v > 1$  arguments that are functions of  $x$ . Multiplication is a prime example of a 2-ary elementary function necessary for implementing useful function compositions. Applying a  $v$ -ary function to  $v$  duals can be obtained using Taylor expansions again:

$$f(\bar{x}_1, \dots, \bar{x}_v) = \sum_{k_1, \dots, k_v=0}^{\infty} \left( \prod_{j=1, v} \frac{(\bar{x}_j - \bar{x}_j|_{\varepsilon=0})^{k_j}}{k_j!} \right) f^{(k_1, \dots, k_v)}(\bar{x}_1|_{\varepsilon=0}, \dots, \bar{x}_v|_{\varepsilon=0}), \quad (\text{C.6})$$

where  $f^{(k_1, \dots, k_m)}$  denotes the partial derivative with  $k_i$  derivatives in the variable  $x_i$ . The infinite sum of eq. (C.6) is truncated once the powers of dual numbers  $(\bar{x}_j - \bar{x}_j|_{\varepsilon=0})^{k_j}$  are expanded and the truncation rule  $\varepsilon^{n+1} = 0$  is imposed. Let us stress again the two fundamental steps required to successfully apply dual numbers to the numerical computation of derivatives of a function  $f$ :

- Hardcode the action of all elementary ( $v$ -ary) functions on a  $v$ -uplet of dual numbers, according to eq. (C.4) and eq. (C.6).
- Write  $f$  as a composition of elementary functions, and evaluate  $f(x + \varepsilon)$ .

This straightforward two-step procedure summarises the discussion on the use of dual numbers to compute derivatives of a single-variable function. To conclude we propose a simple example of the application of this technology to the computation of first and second derivative of a function.

**Example.** Let  $f(x) = x \sin(x)$ , and write  $f(x) = g_{\times}(x, s(x))$  with  $g_{\times}(x, y) = xy$  and  $s(x) = \sin(x)$ . In order to compute the derivative of  $f$ , we consider the following two rules for the dual evaluations of the sine function and the product function at dual numbers  $\bar{x} = c_0 + c_1\varepsilon + c_2\varepsilon^2/2$  and  $\bar{x}' = c'_0 + c'_1\varepsilon + c'_2\varepsilon^2/2$ :

$$s(\bar{x}) = \sin(c_0) + c_1 \cos(c_0)\varepsilon + \frac{1}{2}(c_2 \cos(c_0) - c_1 \sin(c_0))\varepsilon^2, \quad (\text{C.7})$$

$$g_{\times}(\bar{x}, \bar{x}') = c_0c'_0 + (c_0c'_1 + c'_0c_1)\varepsilon + \left(c_1c'_1 + \frac{c_0c'_2}{2} + \frac{c'_0c_2}{2}\right)\varepsilon^2. \quad (\text{C.8})$$

This allows us to compute the full derivative of  $f$  knowing the expansion of the elementary functions  $s$  and  $g_{\times}$ . In particular, this yields

$$\begin{aligned} f(x + \varepsilon) &= g_{\times}(x + \varepsilon, s(x + \varepsilon)) = g_{\times}\left(x + \varepsilon, \sin(x) + \cos(x)\varepsilon - \frac{1}{2}\sin(x)\varepsilon^2\right) \\ &= x \sin(x) + (\sin(x) + x \cos(x))\varepsilon + \frac{1}{2}(2 \cos(x) - x \sin(x))\varepsilon^2. \end{aligned} \quad (\text{C.9})$$

We see that the coefficients of the power series reproduce the derivatives of  $f$  divided by  $1/n!$ . In other words, it is the Taylor expansion of  $f(x + \varepsilon)$  around  $\varepsilon = 0$ .

This construction thus far only allows us to compute derivatives in a single variable, but its generalisation to what we call multivariate duals is straightforward. Given a vector of positive integers  $\vec{n} \in \mathbb{N}^m$ , we consider  $m$  objects  $\varepsilon_i$ ,  $i = 1, \dots, m$  with the following truncation rules:

$$\varepsilon_i^{n_i+1} = 0, \quad (\text{C.10})$$

and we will write  $\vec{\varepsilon} = \{\varepsilon_1, \dots, \varepsilon_m\}$ . These  $m$ -variate duals will be used to support the computation of up to  $n_i$  derivative in each of the  $m$  variables  $x_i$ . For this purpose, we must consider all multivariate polynomials in the  $\varepsilon_i$  objects

$$\mathcal{D}(\vec{n}) = \left\{ \sum_{k_1=0}^{n_1} \dots \sum_{k_m=0}^{n_m} \frac{c_{k_1 \dots k_m}}{k_1! \dots k_m!} \prod_{i=1}^m \varepsilon_i^{k_i} \mid c_{k_1 \dots k_m} \in \mathbb{C}, \forall k_i = 0, \dots, n_i, \forall i = 1, \dots, m \right\}. \quad (\text{C.11})$$

An element  $\bar{\mathbf{x}} \in \mathcal{D}(\vec{n})$  is then a  $m$ -variate dual number. Given a  $v$ -ary function  $f$ , its action on  $v$   $m$ -variate dual numbers  $\bar{\mathbf{x}}_i \in \mathcal{D}(\vec{n})$  is obtained in complete analogy w.r.t. the monovariate case of eq. (C.6):

$$f(\bar{\mathbf{x}}_1, \dots, \bar{\mathbf{x}}_v) = \sum_{k_1, \dots, k_v=0}^{\infty} \left( \prod_{j=1, v} \frac{(\bar{\mathbf{x}}_j - \bar{\mathbf{x}}_j|_{\vec{\varepsilon}=\vec{0}})^{k_j}}{k_j!} \right) f^{(k_1, \dots, k_v)}(\bar{x}_1|_{\vec{\varepsilon}=\vec{0}}, \dots, \bar{x}_v|_{\vec{\varepsilon}=\vec{0}}). \quad (\text{C.12})$$

Upon application of the truncation rules of eq. (C.10),  $f$  will thus evaluate to an element of  $\mathcal{D}(\vec{n})$ . With these definitions, the partial derivatives of any  $m$ -ary function  $f$  can be



easily obtained by evaluating it at  $(x_1 + \varepsilon_1, \dots, x_m + \varepsilon_m)$ , and then reading the coefficient of each monomial in the result. We show in appendix C.2 an example of the application of multi-variate duals to the computation of partial derivatives of a multi-variate function.

Finally, on top of the truncation rules given in eq. (C.10), one may wish to also add the following rule for optimisation purposes:

$$\prod_{i=1}^m \varepsilon_i^{k_i} = 0 \quad \forall \{k_1, \dots, k_m\} \text{ s.t. } \sum_{i=1}^m k_i > N. \quad (\text{C.13})$$

We call  $\mathcal{D}(N; \vec{n})$  the polynomials obtained from multivariate dual numbers that satisfy both eq. (C.10) and eq. (C.13).

Note that the implementation of dual numbers supporting more than one derivative is often performed through a nested formulation, that is by writing  $\bar{x} = c'_n + \bar{x}' \varepsilon_x$ , with  $\bar{x} \in \mathcal{D}(n)$  and  $\bar{x}' \in \mathcal{D}(n-1)$ , instead of the flattened version of eq. (C.4). The obvious advantage of this more common formulation is that it only requires implementing the elementary operations for the single-derivative duals in  $\mathcal{D}(1)$ , after which all deeper derivatives can easily be obtained at an arbitrary depth from properly templated data structures. However, this formulation is less efficient and very inconvenient for implementing the complicated truncation rules in the multivariate case for anything other than  $\mathcal{D}(N \times m; N, \dots, N)$ . In the context of the LU implementation in the presence of raised propagators, we can easily know a priori the derivative structure required for each term, i.e. what  $N$  and  $\vec{n}$  should minimally be. We therefore opted to explicitly implement the few dedicated dual structures necessary for the computation of cross-sections up to a given perturbative order, which we shall discuss next.

### C.1 Solving the distributional rules

Up to  $N^m \text{LO}$ , there can be at most  $m$  self-energy insertions and therefore at most  $m$ -raised cut propagators. We sort the propagators crossed by a Cutkosky cut  $\mathbf{c}_s$  of multiplicity  $n = |\mathbf{c}_s|$  based on their power in ascending order and write the  $n$ -tuple  $\vec{r} = (r_1, \dots, r_n)$  that specifies the power of each raised cut propagator *minus* one, and write  $(\mathbf{0}, x_1, \dots, x_k)$  for a tuple that can have an arbitrary number of zeros at the start and has non-zero  $x_i$ . At  $N^m \text{LO}$  the number of powers has an upper bound, and specifically one has  $\sum_{i=1}^n r_i \leq m$ . The onshellness condition of each of the first  $n - 1$  raised cut propagators will be solved in the energy component  $p_i^0$  of its independent momentum, whereas the onshellness condition of the last  $n$ -th propagator will be solved in the causal flow parameter  $t$ . Irrespective of the ordering, the derivative in  $t$  always has to be performed to the order equal to the sum of all raised powers of the Cutkosky cut edges, i.e.  $\sum_i r_i$ .

We denote with  $\mathbf{x} = (p_1^0, \dots, p_{n-1}^0, t)$  these variables in which we will solve the on-shell conditions of the Cutkosky cuts, and thus possibly compute derivatives of the LU integrand. Equipped with this notation, we can now write the generic structure of the integrand for any Cutkosky cut  $\mathbf{s}^{(\vec{r})}$  crossing  $n$  edges, as follows:

$$I_{\mathbf{s}^{(\vec{r})}} = \int \prod_{i=1}^{n-1} \left( dp_i^0 \delta^{(r_i+1)} [p_i^0 - E_i] \right) \delta^{(r_n+1)} \left[ q^0 - p_1^0 - \dots - p_{n-1}^0 - E_n \right] \mathcal{M}(\{p_i\}), \quad (\text{C.14})$$

$\vec{r}$	(0, 1)	(0, 2)	(0, 1, 1)	(0, 3)	(0, 1, 2)	(0, 1, 1, 1)
order	NLO	NNLO		N3LO		
dual	$\mathcal{D}(1; 1)$	$\mathcal{D}(2; 2)$	$\mathcal{D}(2; 1, 2)$	$\mathcal{D}(3; 3)$	$\mathcal{D}(3; 1, 3)$	$\mathcal{D}(3; 1, 1, 3)$

**Table 8.** Multivariate dual structures  $\mathcal{D}$  for the variables  $(\dots, p_{n-1}^0, t)$  required for implementing a Cutkosky cut  $\mathbf{s}^{(\vec{r})}$  of the LU representation up to N3LO, with a specific configuration  $\vec{r}$  of the raised propagators crossed by the cut and its first order of appearance. We refer to the text for details.

where  $\mathcal{M}(\{p_i\})$  is a function that contains, among all other LU factors (cutting rule factors  $1/(p_i^0 + E_i)^{r_i+1}$ , observable, Jacobians, etc...), the (c)LTD representation of the original amplitude graphs together with their UV counterterms obtained from applying the  $R$ -operator to them (as will be discussed in section 3). The quantity  $\mathcal{M}$  also contains the observable-dependent final-state density  $f(\mathcal{O})$ .

One key observation is that the first  $n - 1$  distributions, when solved and turned into derivatives, do not act on each other since they depend on the independent variables  $p_i^0$ . This means that, for a given Cutkosky cut  $\mathbf{s}^{(\vec{r})}$ , we find that the necessary multivariate dual structure is simply  $\mathcal{D}(\sum_{i=1}^n r_i; r_1, \dots, r_{n-1}, \sum_{i=1}^n r_i)$  for the variables  $(p_1^0, \dots, p_{n-1}^0, t)$ . We stress that even though eq. (C.14) contains many terms once fully expanded, a *single* evaluation of  $\mathcal{M}$  with dual arguments in the appropriate structure is sufficient to evaluate *all* necessary derivatives, as all the different combinations of derivatives needed are present in the various dual components of that single evaluation. For completeness, we report the exhaustive list of dual structures required up to N3LO in table (8).

The dedicated implementation of all dual structures listed in table 8 is then sufficient for the implementation of the LU representation of the differential cross-section of arbitrary processes up to N3LO. Notice that for perturbative orders up to N3LO, second-order derivatives w.r.t. one energy component are never needed (it only first becomes necessary at N4LO, and only for the  $\vec{r} = (0, 2, 2)$  configuration). Moreover, for QCD corrections up to N3LO of processes with only two external colour-charged particles, at most one derivative in any energy component is needed, together with at most three in the  $t$  parameter. We stress that the use of dual numbers for computing derivatives yields no extra steps during the generation of the integrand (since it is merely a type-redefinition of the integrand arguments) and it slows down run-time evaluations by a factor roughly given by the number of terms generated by the multiplication operator of two truncated dual numbers.

### C.2 Example use of multi-variate duals to compute partial derivatives

Let  $f(x, y) = e^{x+y} \sin(xy)$ ; we rewrite  $f$  as a composition of elementary functions by defining, on top of  $s(x) = \sin(x)$  and  $g_{\times}(x, y) = xy$ , the functions  $g_{+}(x, y) = x + y$  and  $e(x) = e^x$ . Let us now determine the value of  $g_{+}$ ,  $g_{\times}$ ,  $s$  and  $e$  when evaluated at multi-variate dual numbers  $\bar{\mathbf{x}} = c_{00} + c_{10}\varepsilon_1 + c_{01}\varepsilon_2 + c_{11}\varepsilon_1\varepsilon_2$  and  $\bar{\mathbf{x}}' = c'_{00} + c'_{10}\varepsilon_1 + c'_{01}\varepsilon_2 + c'_{11}\varepsilon_1\varepsilon_2$

(so  $\bar{x}, \bar{x}' \in \mathcal{D}(2; (1, 1))$ ):

$$\begin{aligned}
 s(\bar{x}) &= \sin(c_{00}) + \cos(c_{00})(c_{10}\varepsilon_1 + c_{01}\varepsilon_2) - \varepsilon_1\varepsilon_2(c_{10}c_{01}\sin(c_{00}) - c_{11}\cos(c_{00})) , \\
 g_+(\bar{x}, \bar{x}') &= c_{00} + c'_{00} + (c'_{10} + c_{10})\varepsilon_1 + (c'_{01} + c_{01})\varepsilon_2 + (c_{11} + c'_{11})\varepsilon_1\varepsilon_2 , \\
 g_\times(\bar{x}, \bar{x}') &= c_{00}c'_{00} + (c_{00}c'_{10} + c'_{00}c_{10})\varepsilon_1 + (c_{00}c'_{01} + c'_{00}c_{01})\varepsilon_2 \\
 &\quad + (c_{10}c'_{01} + c'_{10}c_{01} + c_{00}c'_{11} + c'_{00}c_{11})\varepsilon_1\varepsilon_2 , \\
 e(\bar{x}) &= e^{c_{00}} + e^{c'_{00}}(c_{10}\varepsilon_1 + c_{01}\varepsilon_2) + \varepsilon_1\varepsilon_2 e^{c_{00}}(c_{10}c_{01} - c_{11}) .
 \end{aligned} \tag{C.15}$$

This allows us to compute the full derivative of  $f$  knowing the expansion of the elementary functions. In particular, this yields

$$\begin{aligned}
 f(x + \varepsilon_1, y + \varepsilon_2) &= g_\times(e(g_+(x + \varepsilon_1, y + \varepsilon_2)), s(g_\times(x + \varepsilon_1, y + \varepsilon_2))) \\
 &= g_\times(e(x + y + \varepsilon_1 + \varepsilon_2), s(xy + x\varepsilon_2 + y\varepsilon_1 + \varepsilon_1\varepsilon_2)) .
 \end{aligned} \tag{C.16}$$

We have

$$\begin{aligned}
 e(x + y + \varepsilon_1 + \varepsilon_2) &= e^{x+y}(1 + \varepsilon_1 + \varepsilon_2 + \varepsilon_1\varepsilon_2), \\
 s(xy + x\varepsilon_2 + y\varepsilon_1 + \varepsilon_1\varepsilon_2) &= \sin(xy) + \cos(xy)(x\varepsilon_2 + y\varepsilon_1) - \varepsilon_1\varepsilon_2(xy \sin(xy) - \cos(xy)),
 \end{aligned} \tag{C.17}$$

from which we finally obtain

$$\begin{aligned}
 f(x + \varepsilon_1, y + \varepsilon_2) &= e^{x+y} \sin(xy) \\
 &\quad + e^{x+y}(\sin(xy) + y \cos(xy))\varepsilon_1 \\
 &\quad + e^{x+y}(\sin(xy) + x \cos(xy))\varepsilon_2 \\
 &\quad + e^{x+y}(\sin(xy) + (x + y) \cos(xy) - xy \sin(xy) + \cos(xy))\varepsilon_1\varepsilon_2 .
 \end{aligned} \tag{C.18}$$

We see that the coefficients of the power series reproduce the partial derivatives of  $f$ .

**Open Access.** This article is distributed under the terms of the Creative Commons Attribution License ([CC-BY 4.0](https://creativecommons.org/licenses/by/4.0/)), which permits any use, distribution and reproduction in any medium, provided the original author(s) and source are credited. SCOAP<sup>3</sup> supports the goals of the International Year of Basic Sciences for Sustainable Development.

## References

- [1] M. Czakon and D. Heymes, *Four-dimensional formulation of the sector-improved residue subtraction scheme*, *Nucl. Phys. B* **890** (2014) 152 [[arXiv:1408.2500](https://arxiv.org/abs/1408.2500)] [[INSPIRE](#)].
- [2] J.M. Campbell, R.K. Ellis and S. Seth, *Non-local slicing approaches for NNLO QCD in MCFM*, *JHEP* **06** (2022) 002 [[arXiv:2202.07738](https://arxiv.org/abs/2202.07738)] [[INSPIRE](#)].
- [3] K. Asteriadis, F. Caola, K. Melnikov and R. Röntsch, *Analytic results for deep-inelastic scattering at NNLO QCD with the nested soft-collinear subtraction scheme*, *Eur. Phys. J. C* **80** (2020) 8 [[arXiv:1910.13761](https://arxiv.org/abs/1910.13761)] [[INSPIRE](#)].
- [4] A. Gehrmann-De Ridder, T. Gehrmann and E.W.N. Glover, *Antenna subtraction at NNLO*, *JHEP* **09** (2005) 056 [[hep-ph/0505111](https://arxiv.org/abs/hep-ph/0505111)] [[INSPIRE](#)].

- [5] J. Currie, E.W.N. Glover and S. Wells, *Infrared structure at NNLO using antenna subtraction*, *JHEP* **04** (2013) 066 [[arXiv:1301.4693](#)] [[INSPIRE](#)].
- [6] G. Somogyi and Z. Trócsányi, *A new subtraction scheme for computing QCD jet cross sections at next-to-leading order accuracy*, [hep-ph/0609041](#) [[INSPIRE](#)].
- [7] G. Somogyi, *Subtraction with hadronic initial states at NLO: an NNLO-compatible scheme*, *JHEP* **05** (2009) 016 [[arXiv:0903.1218](#)] [[INSPIRE](#)].
- [8] F. Caola, K. Melnikov and R. Röntsch, *Nested soft-collinear subtractions in NNLO QCD computations*, *Eur. Phys. J. C* **77** (2017) 248 [[arXiv:1702.01352](#)] [[INSPIRE](#)].
- [9] S. Catani and M. Grazzini, *An NNLO subtraction formalism in hadron collisions and its application to Higgs boson production at the LHC*, *Phys. Rev. Lett.* **98** (2007) 222002 [[hep-ph/0703012](#)] [[INSPIRE](#)].
- [10] R. Boughezal, C. Focke, X. Liu and F. Petriello, *W-boson production in association with a jet at next-to-next-to-leading order in perturbative QCD*, *Phys. Rev. Lett.* **115** (2015) 062002 [[arXiv:1504.02131](#)] [[INSPIRE](#)].
- [11] W.J. Torres Bobadilla et al., *May the four be with you: novel IR-subtraction methods to tackle NNLO calculations*, *Eur. Phys. J. C* **81** (2021) 250 [[arXiv:2012.02567](#)] [[INSPIRE](#)].
- [12] G. Ossola, C.G. Papadopoulos and R. Pittau, *CutTools: a program implementing the OPP reduction method to compute one-loop amplitudes*, *JHEP* **03** (2008) 042 [[arXiv:0711.3596](#)] [[INSPIRE](#)].
- [13] A. Denner, S. Dittmaier and L. Hofer, *Collier: a fortran-based Complex One-Loop Library in Extended Regularizations*, *Comput. Phys. Commun.* **212** (2017) 220 [[arXiv:1604.06792](#)] [[INSPIRE](#)].
- [14] T. Peraro, *Ninja: automated integrand reduction via Laurent expansion for one-loop amplitudes*, *Comput. Phys. Commun.* **185** (2014) 2771 [[arXiv:1403.1229](#)] [[INSPIRE](#)].
- [15] V. Hirschi and T. Peraro, *Tensor integrand reduction via Laurent expansion*, *JHEP* **06** (2016) 060 [[arXiv:1604.01363](#)] [[INSPIRE](#)].
- [16] A. von Manteuffel and R.M. Schabinger, *A novel approach to integration by parts reduction*, *Phys. Lett. B* **744** (2015) 101 [[arXiv:1406.4513](#)] [[INSPIRE](#)].
- [17] T. Peraro, *FiniteFlow: multivariate functional reconstruction using finite fields and dataflow graphs*, *JHEP* **07** (2019) 031 [[arXiv:1905.08019](#)] [[INSPIRE](#)].
- [18] J. Klappert and F. Lange, *Reconstructing rational functions with FireFly*, *Comput. Phys. Commun.* **247** (2020) 106951 [[arXiv:1904.00009](#)] [[INSPIRE](#)].
- [19] J. Klappert, F. Lange, P. Maierhöfer and J. Usovitsch, *Integral reduction with Kira 2.0 and finite field methods*, *Comput. Phys. Commun.* **266** (2021) 108024 [[arXiv:2008.06494](#)] [[INSPIRE](#)].
- [20] M. Heller and A. von Manteuffel, *MultivariateApart: generalized partial fractions*, *Comput. Phys. Commun.* **271** (2022) 108174 [[arXiv:2101.08283](#)] [[INSPIRE](#)].
- [21] M. Caffo, H. Czyz, S. Laporta and E. Remiddi, *The master differential equations for the two loop sunrise selfmass amplitudes*, *Nuovo Cim. A* **111** (1998) 365 [[hep-th/9805118](#)] [[INSPIRE](#)].
- [22] M.L. Czakon and M. Niggetiedt, *Exact quark-mass dependence of the Higgs-gluon form factor at three loops in QCD*, *JHEP* **05** (2020) 149 [[arXiv:2001.03008](#)] [[INSPIRE](#)].

- [23] M. Hidding, *DiffExp, a Mathematica package for computing Feynman integrals in terms of one-dimensional series expansions*, *Comput. Phys. Commun.* **269** (2021) 108125 [[arXiv:2006.05510](#)] [[INSPIRE](#)].
- [24] F. Moriello, *Generalised power series expansions for the elliptic planar families of Higgs + jet production at two loops*, *JHEP* **01** (2020) 150 [[arXiv:1907.13234](#)] [[INSPIRE](#)].
- [25] X. Liu and Y.-Q. Ma, *AMFlow: a Mathematica package for Feynman integrals computation via auxiliary mass flow*, [arXiv:2201.11669](#) [[INSPIRE](#)].
- [26] C. Anastasiou and G. Sterman, *Removing infrared divergences from two-loop integrals*, *JHEP* **07** (2019) 056 [[arXiv:1812.03753](#)] [[INSPIRE](#)].
- [27] C. Anastasiou, R. Haindl, G. Sterman, Z. Yang and M. Zeng, *Locally finite two-loop amplitudes for off-shell multi-photon production in electron-positron annihilation*, *JHEP* **04** (2021) 222 [[arXiv:2008.12293](#)] [[INSPIRE](#)].
- [28] W. Gong, Z. Nagy and D.E. Soper, *Direct numerical integration of one-loop Feynman diagrams for N-photon amplitudes*, *Phys. Rev. D* **79** (2009) 033005 [[arXiv:0812.3686](#)] [[INSPIRE](#)].
- [29] S. Becker and S. Weinzierl, *Direct numerical integration for multi-loop integrals*, *Eur. Phys. J. C* **73** (2013) 2321 [[arXiv:1211.0509](#)] [[INSPIRE](#)].
- [30] S. Buchta, G. Chachamis, P. Draggiotis and G. Rodrigo, *Numerical implementation of the loop-tree duality method*, *Eur. Phys. J. C* **77** (2017) 274 [[arXiv:1510.00187](#)] [[INSPIRE](#)].
- [31] Z. Capatti, V. Hirschi, D. Kermanschah, A. Pelloni and B. Ruijl, *Manifestly causal loop-tree duality*, [arXiv:2009.05509](#) [[INSPIRE](#)].
- [32] Z. Capatti, V. Hirschi, D. Kermanschah, A. Pelloni and B. Ruijl, *Numerical loop-tree duality: contour deformation and subtraction*, *JHEP* **04** (2020) 096 [[arXiv:1912.09291](#)] [[INSPIRE](#)].
- [33] C. Anastasiou and K. Melnikov, *Higgs boson production at hadron colliders in NNLO QCD*, *Nucl. Phys. B* **646** (2002) 220 [[hep-ph/0207004](#)] [[INSPIRE](#)].
- [34] C. Anastasiou and K. Melnikov, *Pseudoscalar Higgs boson production at hadron colliders in NNLO QCD*, *Phys. Rev. D* **67** (2003) 037501 [[hep-ph/0208115](#)] [[INSPIRE](#)].
- [35] C. Anastasiou, C. Duhr, F. Dulat, F. Herzog and B. Mistlberger, *Higgs boson gluon-fusion production in QCD at three loops*, *Phys. Rev. Lett.* **114** (2015) 212001 [[arXiv:1503.06056](#)] [[INSPIRE](#)].
- [36] C. Duhr, F. Dulat and B. Mistlberger, *Higgs boson production in bottom-quark fusion to third order in the strong coupling*, *Phys. Rev. Lett.* **125** (2020) 051804 [[arXiv:1904.09990](#)] [[INSPIRE](#)].
- [37] C. Anastasiou et al., *High precision determination of the gluon fusion Higgs boson cross-section at the LHC*, *JHEP* **05** (2016) 058 [[arXiv:1602.00695](#)] [[INSPIRE](#)].
- [38] B. Mistlberger, *Higgs boson production at hadron colliders at N<sup>3</sup>LO in QCD*, *JHEP* **05** (2018) 028 [[arXiv:1802.00833](#)] [[INSPIRE](#)].
- [39] L.-B. Chen, H.T. Li, H.-S. Shao and J. Wang, *Higgs boson pair production via gluon fusion at N<sup>3</sup>LO in QCD*, *Phys. Lett. B* **803** (2020) 135292 [[arXiv:1909.06808](#)] [[INSPIRE](#)].
- [40] C. Duhr, F. Dulat and B. Mistlberger, *Charged current Drell-Yan production at N<sup>3</sup>LO*, *JHEP* **11** (2020) 143 [[arXiv:2007.13313](#)] [[INSPIRE](#)].

- [41] C. Duhr and B. Mistlberger, *Lepton-pair production at hadron colliders at  $N^3LO$  in QCD*, *JHEP* **03** (2022) 116 [[arXiv:2111.10379](#)] [[INSPIRE](#)].
- [42] X. Chen, T. Gehrmann, E.W.N. Glover, A. Huss, B. Mistlberger and A. Pelloni, *Fully differential Higgs boson production to third order in QCD*, *Phys. Rev. Lett.* **127** (2021) 072002 [[arXiv:2102.07607](#)] [[INSPIRE](#)].
- [43] T. Kinoshita, *Mass singularities of Feynman amplitudes*, *J. Math. Phys.* **3** (1962) 650 [[INSPIRE](#)].
- [44] T.D. Lee and M. Nauenberg, *Degenerate systems and mass singularities*, *Phys. Rev.* **133** (1964) B1549 [[INSPIRE](#)].
- [45] F. Bloch and A. Nordsieck, *Note on the radiation field of the electron*, *Phys. Rev.* **52** (1937) 54 [[INSPIRE](#)].
- [46] Z. Capatti, V. Hirschi, A. Pelloni and B. Ruijl, *Local unitarity: a representation of differential cross-sections that is locally free of infrared singularities at any order*, *JHEP* **04** (2021) 104 [[arXiv:2010.01068](#)] [[INSPIRE](#)].
- [47] Z. Capatti, *Local unitarity*, *SciPost Phys. Proc.* **7** (2022) 024 [[arXiv:2110.15662](#)] [[INSPIRE](#)].
- [48] I. Bierenbaum, S. Buchta, P. Draggiotis, I. Malamos and G. Rodrigo, *Tree-loop duality relation beyond simple poles*, *JHEP* **03** (2013) 025 [[arXiv:1211.5048](#)] [[INSPIRE](#)].
- [49] R. Baumeister, D. Mediger, J. Pečovnik and S. Weinzierl, *Vanishing of certain cuts or residues of loop integrals with higher powers of the propagators*, *Phys. Rev. D* **99** (2019) 096023 [[arXiv:1903.02286](#)] [[INSPIRE](#)].
- [50] N. Agarwal, L. Magnea, C. Signorile-Signorile and A. Tripathi, *The infrared structure of perturbative gauge theories*, [arXiv:2112.07099](#) [[INSPIRE](#)].
- [51] D. Kreimer, *Outer space as a combinatorial backbone for Cutkosky rules and coactions*, Springer (2021) [[arXiv:2010.11781](#)] [[INSPIRE](#)].
- [52] D. Kreimer and K. Yeats, *Algebraic interplay between renormalization and monodromy*, [arXiv:2105.05948](#) [[INSPIRE](#)].
- [53] M. Berghoff and D. Kreimer, *Graph complexes and Feynman rules*, [arXiv:2008.09540](#) [[INSPIRE](#)].
- [54] S. Catani, T. Gleisberg, F. Krauss, G. Rodrigo and J.-C. Winter, *From loops to trees by-passing Feynman's theorem*, *JHEP* **09** (2008) 065 [[arXiv:0804.3170](#)] [[INSPIRE](#)].
- [55] I. Bierenbaum, S. Catani, P. Draggiotis and G. Rodrigo, *A tree-loop duality relation at two loops and beyond*, *JHEP* **10** (2010) 073 [[arXiv:1007.0194](#)] [[INSPIRE](#)].
- [56] Z. Capatti, V. Hirschi, D. Kermanschah and B. Ruijl, *Loop-tree duality for multiloop numerical integration*, *Phys. Rev. Lett.* **123** (2019) 151602 [[arXiv:1906.06138](#)] [[INSPIRE](#)].
- [57] R. Runkel, Z. Ször, J.P. Vesga and S. Weinzierl, *Causality and loop-tree duality at higher loops*, *Phys. Rev. Lett.* **122** (2019) 111603 [*Erratum ibid.* **123** (2019) 059902] [[arXiv:1902.02135](#)] [[INSPIRE](#)].
- [58] J. Jesús Aguilera-Verdugo, R.J. Hernández-Pinto, G. Rodrigo, G.F.R. Sborlini and W.J. Torres Bobadilla, *Mathematical properties of nested residues and their application to multi-loop scattering amplitudes*, *JHEP* **02** (2021) 112 [[arXiv:2010.12971](#)] [[INSPIRE](#)].



- [59] J.J. Aguilera-Verdugo et al., *Open loop amplitudes and causality to all orders and powers from the loop-tree duality*, *Phys. Rev. Lett.* **124** (2020) 211602 [[arXiv:2001.03564](#)] [[INSPIRE](#)].
- [60] G. Sterman, *An introduction to quantum field theory*, Cambridge University Press (1993).
- [61] M.D. Schwartz, *Quantum field theory and the Standard Model*, Cambridge University Press (2014).
- [62] L. Mantovani, B. Pasquini, X. Xiong and A. Bacchetta, *Revisiting the equivalence of light-front and covariant QED in the light-cone gauge*, *Phys. Rev. D* **94** (2016) 116005 [[arXiv:1609.00746](#)] [[INSPIRE](#)].
- [63] J.L. Bourjaily, H. Hannesdottir, A.J. McLeod, M.D. Schwartz and C. Vergu, *Sequential discontinuities of Feynman integrals and the monodromy group*, *JHEP* **01** (2021) 205 [[arXiv:2007.13747](#)] [[INSPIRE](#)].
- [64] R.P. Feynman, *Quantum theory of gravitation*, *Acta Phys. Polon.* **24** (1963) 697 [[INSPIRE](#)].
- [65] S. Catani, T. Gleisberg, F. Krauss, G. Rodrigo and J.-C. Winter, *From loops to trees by-passing Feynman's theorem*, *JHEP* **09** (2008) 065 [[arXiv:0804.3170](#)] [[INSPIRE](#)].
- [66] S. Plätzer and I. Ruffa, *Towards colour flow evolution at two loops*, *JHEP* **06** (2021) 007 [[arXiv:2012.15215](#)] [[INSPIRE](#)].
- [67] Z. Capatti, V. Hirschi and B. Ruijl, *Local unitarity: a KLN-based approach to hadronic cross-sections*, to appear.
- [68] R.E. Cutkosky, *Singularities and discontinuities of Feynman amplitudes*, *J. Math. Phys.* **1** (1960) 429 [[INSPIRE](#)].
- [69] A.G. Baydin, B.A. Pearlmutter, A.A. Radul and J.M. Siskind, *Automatic differentiation in machine learning: a survey*, *J. Mach. Learn. Res.* **18** (2018) 1.
- [70] N.N. Bogoliubov and O.S. Parasiuk, *On the multiplication of the causal function in the quantum theory of fields*, *Acta Math.* **97** (1957) 227 [[INSPIRE](#)].
- [71] W.E. Caswell and A.D. Kennedy, *A simple approach to renormalization theory*, *Phys. Rev. D* **25** (1982) 392 [[INSPIRE](#)].
- [72] W. Zimmermann, *Convergence of Bogolyubov's method of renormalization in momentum space*, *Commun. Math. Phys.* **15** (1969) 208 [*Lect. Notes Phys.* **558** (2000) 217] [[INSPIRE](#)].
- [73] K. Hepp, *Proof of the Bogolyubov-Parasiuk theorem on renormalization*, *Commun. Math. Phys.* **2** (1966) 301 [[INSPIRE](#)].
- [74] F. Herzog, *Zimmermann's forest formula, infrared divergences and the QCD  $\beta$ -function*, *Nucl. Phys. B* **926** (2018) 370 [[arXiv:1711.06121](#)] [[INSPIRE](#)].
- [75] K.G. Chetyrkin and F.V. Tkachov, *Infrared R operation and ultraviolet counterterms in the MS scheme*, *Phys. Lett. B* **114** (1982) 340 [[INSPIRE](#)].
- [76] K.G. Chetyrkin and V.A. Smirnov, *R\* operation corrected*, *Phys. Lett. B* **144** (1984) 419 [[INSPIRE](#)].
- [77] V.A. Smirnov and K.G. Chetyrkin, *R\* operation in the minimal subtraction scheme*, *Theor. Math. Phys.* **63** (1985) 462 [*Teor. Mat. Fiz.* **63** (1985) 208] [[INSPIRE](#)].
- [78] F. Herzog and B. Ruijl, *The R\*-operation for Feynman graphs with generic numerators*, *JHEP* **05** (2017) 037 [[arXiv:1703.03776](#)] [[INSPIRE](#)].

- [79] K.G. Chetyrkin, *Combinatorics of  $R$ -,  $R^{-1}$ -, and  $R^*$ -operations and asymptotic expansions of Feynman integrals in the limit of large momenta and masses*, [arXiv:1701.08627](#) [[INSPIRE](#)].
- [80] J.H. Lowenstein and W. Zimmermann, *On the formulation of theories with zero mass propagators*, *Nucl. Phys. B* **86** (1975) 77 [[INSPIRE](#)].
- [81] A.A. Vladimirov, *Method for computing renormalization group functions in dimensional renormalization scheme*, *Theor. Math. Phys.* **43** (1980) 417 [*Teor. Mat. Fiz.* **43** (1980) 210] [[INSPIRE](#)].
- [82] M. Gomes, J.H. Lowenstein and W. Zimmermann, *Generalization of the momentum-space subtraction procedure for renormalized perturbation theory*, *Commun. Math. Phys.* **39** (1974) 81 [[INSPIRE](#)].
- [83] J.H. Lowenstein, *Convergence theorems for renormalized Feynman integrals with zero-mass propagators*, *Commun. Math. Phys.* **47** (1976) 53 [[INSPIRE](#)].
- [84] A. Pikelner, *FMFT: Fully Massive Four-loop Tadpoles*, *Comput. Phys. Commun.* **224** (2018) 282 [[arXiv:1707.01710](#)] [[INSPIRE](#)].
- [85] B. Ruijl, F. Herzog, T. Ueda, J.A.M. Vermaseren and A. Vogt, *The  $R^*$ -operation and five-loop calculations*, *PoS RADCOR2017* (2018) 011 [*J. Phys. Conf. Ser.* **1085** (2018) 052006] [[arXiv:1801.06084](#)] [[INSPIRE](#)].
- [86] K.G. Chetyrkin and F.V. Tkachov, *Integration by parts: the algorithm to calculate  $\beta$ -functions in 4 loops*, *Nucl. Phys. B* **192** (1981) 159 [[INSPIRE](#)].
- [87] R.N. Lee, *Presenting LiteRed: a tool for the Loop InTEgrals REDuction*, [arXiv:1212.2685](#) [[INSPIRE](#)].
- [88] R.N. Lee, *LiteRed 1.4: a powerful tool for reduction of multiloop integrals*, *J. Phys. Conf. Ser.* **523** (2014) 012059 [[arXiv:1310.1145](#)] [[INSPIRE](#)].
- [89] B.A. Kniehl, A.F. Pikelner and O.L. Veretin, *Three-loop massive tadpoles and polylogarithms through weight six*, *JHEP* **08** (2017) 024 [[arXiv:1705.05136](#)] [[INSPIRE](#)].
- [90] S.P. Martin and D.G. Robertson, *Evaluation of the general 3-loop vacuum Feynman integral*, *Phys. Rev. D* **95** (2017) 016008 [[arXiv:1610.07720](#)] [[INSPIRE](#)].
- [91] S. Borowka et al., *pySecDec: a toolbox for the numerical evaluation of multi-scale integrals*, *Comput. Phys. Commun.* **222** (2018) 313 [[arXiv:1703.09692](#)] [[INSPIRE](#)].
- [92] A. Denner, *Techniques for calculation of electroweak radiative corrections at the one loop level and results for  $W$  physics at LEP-200*, *Fortsch. Phys.* **41** (1993) 307 [[arXiv:0709.1075](#)] [[INSPIRE](#)].
- [93] J.-N. Lang, S. Pozzorini, H. Zhang and M.F. Zoller, *Two-loop rational terms in Yang-Mills theories*, *JHEP* **10** (2020) 016 [[arXiv:2007.03713](#)] [[INSPIRE](#)].
- [94] S. Pozzorini, H. Zhang and M.F. Zoller, *Rational terms of UV origin at two loops*, *JHEP* **05** (2020) 077 [[arXiv:2001.11388](#)] [[INSPIRE](#)].
- [95] G. Ossola, C.G. Papadopoulos and R. Pittau, *On the rational terms of the one-loop amplitudes*, *JHEP* **05** (2008) 004 [[arXiv:0802.1876](#)] [[INSPIRE](#)].
- [96] D.N. Blaschke, F. Gieres, F. Heindl, M. Schweda and M. Wohlgenannt, *BPHZ renormalization and its application to non-commutative field theory*, *Eur. Phys. J. C* **73** (2013) 2566 [[arXiv:1307.4650](#)] [[INSPIRE](#)].



- [97] S. Weinzierl, *Review on loop integrals which need regularization but yield finite results*, *Mod. Phys. Lett. A* **29** (2014) 1430015 [[arXiv:1402.4407](#)] [[INSPIRE](#)].
- [98] A. Signer and D. Stöckinger, *Using dimensional reduction for hadronic collisions*, *Nucl. Phys. B* **808** (2009) 88 [[arXiv:0807.4424](#)] [[INSPIRE](#)].
- [99] J. Alwall et al., *The automated computation of tree-level and next-to-leading order differential cross sections, and their matching to parton shower simulations*, *JHEP* **07** (2014) 079 [[arXiv:1405.0301](#)] [[INSPIRE](#)].
- [100] J.C. Collins, F. Wilczek and A. Zee, *Low-energy manifestations of heavy particles: application to the neutral current*, *Phys. Rev. D* **18** (1978) 242 [[INSPIRE](#)].
- [101] W. Bernreuther and W. Wetzel, *Decoupling of heavy quarks in the minimal subtraction scheme*, *Nucl. Phys. B* **197** (1982) 228 [*Erratum ibid.* **513** (1998) 758] [[INSPIRE](#)].
- [102] G.M. Prosperini, M. Raciti and C. Simolo, *On the running coupling constant in QCD*, *Prog. Part. Nucl. Phys.* **58** (2007) 387 [[hep-ph/0607209](#)] [[INSPIRE](#)].
- [103] I.V. Tyutin, *Gauge invariance in field theory and statistical physics in operator formalism*, [arXiv:0812.0580](#) [[INSPIRE](#)].
- [104] C. Becchi, A. Rouet and R. Stora, *Renormalization of gauge theories*, *Annals Phys.* **98** (1976) 287 [[INSPIRE](#)].
- [105] T. Kugo and I. Ojima, *Local covariant operator formalism of non-Abelian gauge theories and quark confinement problem*, *Prog. Theor. Phys. Suppl.* **66** (1979) 1 [[INSPIRE](#)].
- [106] F. Herzog, B. Ruijl, T. Ueda, J.A.M. Vermaseren and A. Vogt, *On Higgs decays to hadrons and the R-ratio at N<sup>4</sup>LO*, *JHEP* **08** (2017) 113 [[arXiv:1707.01044](#)] [[INSPIRE](#)].
- [107] K.G. Chetyrkin, J.H. Kühn and M. Steinhauser, *Three loop polarization function and O( $\alpha_s^2$ ) corrections to the production of heavy quarks*, *Nucl. Phys. B* **482** (1996) 213 [[hep-ph/9606230](#)] [[INSPIRE](#)].
- [108] K.G. Chetyrkin, A.H. Hoang, J.H. Kühn, M. Steinhauser and T. Teubner, *Double bubble corrections to heavy quark production*, *Phys. Lett. B* **384** (1996) 233 [[hep-ph/9603313](#)] [[INSPIRE](#)].
- [109] Y. Kiyo, A. Maier, P. Maierhofer and P. Marquard, *Reconstruction of heavy quark current correlators at O( $\alpha_s^3$ )*, *Nucl. Phys. B* **823** (2009) 269 [[arXiv:0907.2120](#)] [[INSPIRE](#)].
- [110] L. Chen, O. Dekkers, D. Heisler, W. Bernreuther and Z.-G. Si, *Top-quark pair production at next-to-next-to-leading order QCD in electron positron collisions*, *JHEP* **12** (2016) 098 [[arXiv:1610.07897](#)] [[INSPIRE](#)].
- [111] W. Bernreuther, L. Chen, O. Dekkers, T. Gehrmann and D. Heisler, *The forward-backward asymmetry for massive bottom quarks at the Z peak at next-to-next-to-leading order QCD*, *JHEP* **01** (2017) 053 [[arXiv:1611.07942](#)] [[INSPIRE](#)].
- [112] S.-Q. Wang, R.-Q. Meng, X.-G. Wu, L. Chen and J.-M. Shen, *Revisiting the bottom quark forward-backward asymmetry  $A_{FB}$  in electron-positron collisions*, *Eur. Phys. J. C* **80** (2020) 649 [[arXiv:2003.13941](#)] [[INSPIRE](#)].
- [113] L. Chen, *Forward-backward asymmetries of the heavy quark pair production in  $e^+e^-$  collisions at O( $\alpha_s^2$ )*, in *International workshop on future linear colliders*, (2021) [[arXiv:2105.06213](#)] [[INSPIRE](#)].

- [114] D.E. Soper, *QCD calculations by numerical integration*, *Phys. Rev. Lett.* **81** (1998) 2638 [[hep-ph/9804454](#)] [[INSPIRE](#)].
- [115] D.E. Soper, *Techniques for QCD calculations by numerical integration*, *Phys. Rev. D* **62** (2000) 014009 [[hep-ph/9910292](#)] [[INSPIRE](#)].
- [116] S.D. Ellis and D.E. Soper, *Successive combination jet algorithm for hadron collisions*, *Phys. Rev. D* **48** (1993) 3160 [[hep-ph/9305266](#)] [[INSPIRE](#)].
- [117] M. Cacciari, *FastJet: a code for fast  $k_t$  clustering, and more*, in 41<sup>st</sup> rencontres de Moriond: *QCD and hadronic interactions*, (2006), p. 487 [[hep-ph/0607071](#)] [[INSPIRE](#)].
- [118] D. Kermanschah, *Numerical integration of loop integrals through local cancellation of threshold singularities*, *JHEP* **01** (2022) 151 [[arXiv:2110.06869](#)] [[INSPIRE](#)].
- [119] V. Del Duca, N. Deuschmann and S. Lionetti, *Momentum mappings for subtractions at higher orders in QCD*, *JHEP* **12** (2019) 129 [[arXiv:1910.01024](#)] [[INSPIRE](#)].